RIGA TECHNICAL UNIVERSITY

Pauls Pāvils Ārgalis

RECYCLING OF WOOD-CEMENT MANUFACTURING WASTE INTO INNOVATIVE BUILDING MATERIALS

Doctoral Thesis

RTU Press
Riga 2025

RIGA TECHNICAL UNIVERSITY
Faculty of Civil and Mechanical Engineering
Institute of Sustainable Building Materials and Engineering Systems

Pauls Pāvils Ārgalis
Doctoral study programme „Civil Engineering" doctoral student

RECYCLING OF WOOD-CEMENT MANUFACTURING WASTE INTO INNOVATIVE BUILDING MATERIALS

Doctoral Thesis

Scientific supervisors:
Professor *Dr. sc. ing.*
DIĀNA BAJĀRE
Senior Researcher *Dr. sc. ing.*
MĀRIS ŠINKA

Riga 2025

FOREWORD

The thesis was developed at the Institute of Sustainable Building Materials and Engineering Systems, Faculty of Civil and Mechanical Engineering, Riga Technical University. The thesis includes studies on the European Green Deal, the sustainability of the Latvian construction sector, the development of a suitable cementitious binder from industrial waste, its properties, its potential application in the production of biocomposites, and the life cycle assessment of the produced biocomposites.

Firstly, thanks go to Cewood Ltd. for showing me how their products are manufactured and supplying the waste materials for me to experiment with—special thanks to Janis, Rudolfs, Kristaps, and Ingars for answering all my questions.

Secondly, I would like to thank Ph.D. Laura Vitola, thank you for the tremendous help you have given me. Starting with a change of thinking about civil engineering as a science (my previous major was material science), consulting about experiments in the laboratory, and proofreading some of the sections in the thesis. I would also like to thank Dr.sc.ing. Girts Bumanis, for his expertise in the experimental part of the thesis and Mg.sc.ing. Liga Puzule for calculating the LCA data and proofreading the analysis and discussion of it. I would also like to thank my supervisors for all the hard discussions I have put them through and all the other colleagues who helped me through this journey.

Thirdly, my biggest gratitude is to my family, who have been close to me, motivating and cheering me on during this process. Thank you, and as once a great man said:

“Labāk kā būs, nebūs!”

ANNOTATION

This thesis explores recycling wood-wool cement panel (WWCP) waste into innovative building materials, addressing the construction sector's sustainability challenges within the European Green Deal and the EU's 2050 climate neutrality goals. The study analyses waste management, develops sustainable cementitious binders from by-products, creates and characterises bio-composites, and performs a life cycle assessment (LCA) to validate material benefits. This approach provides a pathway for transforming WWCP waste into a valuable resource, promoting circular economy principles.

Much of the research is dedicated to developing a method for effectively separating and reactivating hardened cement paste from WWCP waste. The study investigates various mechanical and thermal treatment methods to optimise the recovery of cementitious binders. Mechanical activation is explored through different milling techniques, including collision milling (at 25 and 50 Hz), planetary ball milling (at 300 RPM for 1-30 minutes), and vibration milling (for 5-20 minutes). These methods aim to fragment the hydrated cement conglomerates and release unhydrated cement minerals. For example, vibration milling for 20 minutes achieved a compressive strength of 1.6 MPa at 28 days. Thermal treatment methods are analysed to assess their impact on binder reactivation using a muffle furnace (from 300 to 1200 °C) and a rotary kiln (at 450 °C and 900 °C). The research evaluates the influence of processing parameters, such as milling duration and heat treatment temperature, on the properties of the reactivated binders, with muffle furnace treatment at 900 °C yielding the highest compressive strength of 19.6 MPa on the 28th day.

The reactivated binders and recovered wood-wool are then utilised to develop and characterise bio-based composites for potential application in multilayered building panels. The research explores the relationship between material composition, mechanical properties, and thermal performance of the composites. Different formulations, incorporating alternative fillers like hemp shives (up to 75 %) and production line waste (PLW), are investigated to optimise the composites' properties for specific building applications. For instance, biocomposites with hemp shives demonstrated thermal conductivity as low as 0.052 W/(m·K) and densities from 170 to 780 kg/m^3. The feasibility of producing self-bearing multilayered panels with enhanced hydrothermal performance is demonstrated, achieving compressive strengths up to 1.4 MPa.

A comprehensive life cycle assessment (LCA) is conducted using the SimaPro platform and the NE 15804 + A2 V1.03 method to evaluate the environmental viability of the developed binders and the produced biocomposites. The LCA compares the environmental impact of the recycled materials with that of commercially available alternatives, such as rock wool and EPS, based on a functional unit of 1 m³ and a U-value of 0.18 W/(m²K). The analysis revealed that incorporating PLW can reduce the overall emission of 1 m^3 of biocomposite by 26-58% compared to cement-based alternatives.

Overall, this research provides valuable insights into the effective recycling of WWCP waste and its transformation into sustainable building materials. The findings demonstrate the potential of reactivated binders, achieving compressive strengths from 0.5 to 19.6 MPa, and biocomposites with thermal conductivities ranging from 0.052 to 0.139 W/(m·K) to contribute to a more circular and environmentally responsible construction industry. By optimising waste separation and binder reactivation methods and carefully characterising the properties of the developed materials, this study offers a foundation for future research and practical applications, potentially transforming approximately 450 000 m³ of waste annually into raw materials for sustainable construction.

ANOTĀCIJA

Šajā promocijas darbā tiek pētīta koksnes vilnas cementa paneļu (WWCP) atkritumu pārstrāde inovatīvos būvmateriālos, risinot būvniecības nozares ilgtspējības problēmas saistībā ar Eiropas Zaļo kursu un ES 2050. gada klimata neitralitātes mērķiem. Pētījumā analizēta atkritumu apsaimniekošana, izstrādātas ilgtspējīgas cementa saistvielas no blakusproduktiem, izveidoti un raksturoti biokompozīti, kā arī veikts dzīves cikla novērtējums (LCA), lai apstiprinātu materiālu ekoloģiskumu. Šī pieeja nodrošina ceļu, kā pārveidot WWCP atkritumus par vērtīgu resursu, veicinot aprites ekonomikas principus.

Liela daļa pētījumu ir veltīta metodes izstrādei, lai efektīvi atdalītu un reaktivizētu sacietējušo cementa pastu no WWCP atkritumiem. Pētījumā tiek pētītas dažādas mehāniskās un termiskās apstrādes metodes, lai optimizētu cementa saistvielu reģenerāciju. Mehāniskā aktivizācija tiek pētīta, izmantojot dažādas malšanas metodes, tostarp dezintegratoru (ar 25 un 50 Hz), planetāro bumbu dzirnavas (ar 300 apgriezieniem minūtē 1-30 minūtes) un vibrāciju dzirnavas (5-20 minūtes). Šo metožu mērķis ir sadrumstalot hidratētos cementa konglomerātus un atbrīvot nehidratētos cementa minerālus. Piemēram, ar 20 minūšu vibrācijas malšanu slīpputekļiem, javas paraugiem tika iegūta 1,6 MPa spiedes stiprība 28.dienā pēc to izveides. Termiskās apstrādes metodes ir analizētas, lai novērtētu to ietekmi uz saistvielas reaktivāciju, izmantojot mufeļkrāsni (no 300 līdz 1200 °C) un rotācijas krāsni (450 °C un 900 °C). Pētījumā novērtēta apstrādes parametru, piemēram, malšanas ilguma un termiskās apstrādes temperatūras, ietekme uz reaktivēto saistvielu īpašībām, un, veicot apstrādi mufeļkrāsnī pie 900 °C, 28. dienā tika iegūta visaugstākā spiedes stiprība 19,6 MPa.

Reaktivētās saistvielas un reģenerētā koksnes vate pēc tam tiek izmantotas, lai izstrādātu un raksturotu bioloģiskos kompozītmateriālus potenciālajam pielietojumam daudzslāņu celtniecības paneļos. Pētījumā tiek pētīta saistība starp materiālu sastāvu, mehāniskajām īpašībām un kompozītu termisko veiktspēju. Lai optimizētu kompozītu īpašības konkrētiem būvniecības lietojumiem, tiek pētīti dažādi sastāvi, iekļaujot alternatīvus pildvielas, piemēram, kaņepju spaļus (līdz 75 %) un ražošanas līnijas atkritumus (PLW). Piemēram, biokompozīti ar kaņepju spaļiem uzrādīja siltumvadītspēju tikai 0,052 W/(m·K) un blīvumu no 170 līdz 780 kg/m^3. Pierādīta iespēja izgatavot pašnesošus daudzslāņu paneļus ar uzlabotām hidrotermiskajām īpašībām, sasniedzot spiedes stiprību līdz 1,4 MPa.

Lai novērtētu izstrādāto saistvielu un izgatavoto biokompozītu ekoloģiskumu, izmantojot SimaPro platformu un NE 15804 + A2 V1.03 metodi, tiek veikts visaptverošs dzīves cikla novērtējums (LCA). LCA salīdzina pārstrādāto materiālu ietekmi uz vidi ar komerciāli pieejamām alternatīvām, piemēram, minerālvati un EPS, pamatojoties uz 1 m³ funkcionālo vienību un U vērtību 0,18 W/(m²K). Analīzē atklājās, ka šādu materiālu izmantošana var samazināt kopējo emisiju no 1 m^3 biokompozīta par 26-58 %, salīdzinot ar cementa alternatīvām.

Kopumā šis pētījums sniedz vērtīgu ieskatu par efektīvu WWCP atkritumu pārstrādi un to pārveidi ilgtspējīgos būvmateriālos. Iegūtie rezultāti liecina, ka reaktivētās saistvielas, sasniedzot spiedes stiprību no 0,5 līdz 19,6 MPa, un biokompozīti ar siltumvadītspēju no 0,052 līdz 0,139 W/(m·K) var veicināt aprites un vides ziņā atbildīgāku būvniecības nozari. Optimizējot atkritumu šķirošanas un saistvielu reaktivācijas metodes un rūpīgi raksturojot izstrādāto materiālu īpašības, šis pētījums piedāvā pamatu turpmākajiem pētījumiem un praktiskiem pielietojumiem, potenciāli pārveidojot aptuveni 450 000 m³ atkritumu gadā par ilgtspējīgas būvniecības izejvielām.

TABLE OF CONTENTS

ABBREVIATIONS USED IN THE THESIS

CDW – Construction and Demolition Waste
LEGMC – Latvian Environment, Geology and Meteorology Centre
EU – European Union
NECP – National Energy and Climate Plan
nZEB – nearly Zero Emission Buildings
GPP – Green Public Procurement
WMP – Waste Management Plan
URC – Urban Recycling Centre
LCA – Life Cycle Assessment
WWCP – Wood-Wool Cement Panels
CEM I -> 95 % cement clinker binder ≥ 52.5 MPa on the 28th day.
CEM II/A-LL 42.5 N – Cement clinker and limestone binder ≥ 42.5 MPa on the 28th day.
PLW – Production Line Waste
TG – Thermogravimetry
DTA – Differential Thermal Analysis
XRF – X-Ray Fluorescence
XRD – X-Ray Diffraction
C-S-H - Calcium Silicate Hydrate
C_2S – Belite phase
C_3S – Alite phase
AFm - Monosulfoaluminate phase
AFt - Ettringite phase
CEM II/A-LL 42.5 N - CEM II type cement with a 42.5 MPa compressive strength on the 28^{th} day.
W/B ratio – Water-to-Binder ratio
W/F ratio – Water-to-Filler ratio
W/C ratio – Water-to-Cement ratio
AAC – Autoclaved Aerated Concrete
ECCB – Expanded Clay Cement Block
CBB – Ceramic Building Block
EPS – Expanded Polystyrene
SW – Stone Wool

GENERAL DESCRIPTION OF THE THESIS

Research topicality and problem statement

The construction sector significantly contributes to environmental challenges in Latvia and globally, particularly in the context of the European Union's ambitious climate neutrality goals for 2050 [1,2]. While essential for economic development, the world's construction sector faces mounting pressure to reduce its environmental footprint, especially concerning waste management and resource efficiency. The existing construction and demolition waste (CDW) management practices in Latvia [3], coupled with the sector's substantial carbon footprint, underscores the urgent need for innovative sustainable solutions that align with both national environmental policies [4] and EU directives for the circular economy transition [5].

One tonne of Portland cement is estimated to produce around 0.8 tonnes of CO_2 GHG emissions. Around 8 % of global energy consumption is directly related to the Portland cement production process [6,7]. Consequently, introducing new alternative binder materials in the construction sector is vital for sustainability. Construction and demolition waste are great precursors to introducing new recycling methods and alternative materials to the market. The reactivation of Portland cement-based binders represents a crucial technological frontier in construction material recycling, offering promising pathways for waste reduction and resource optimisation. Current technologies, including mechanical [8], thermal [9], and chemical activation methods [10], demonstrate varying degrees of effectiveness in cement recovery and reuse. However, these processes often remain energy-intensive and economically challenging, highlighting the need for more efficient and sustainable approaches to binder recycling and reactivation [11].

Public perception and market scepticism of recycled building materials regarding their performance and reliability are significant barriers to widespread adoption [3]. Despite testing protocols and quality assurance measures that can validate the mechanical, physical, and durability properties of materials manufactured from secondary resources, these products often face unwarranted stigma in the construction market. This resistance highlights the need for technical innovation and systematic demonstration of performance metrics that meet or exceed industry standards.

The recovery of hardened cement binder from construction and demolition waste streams primarily focuses on concrete and mortar recycling, where effectiveness largely depends on separation methods from aggregates through mechanical, thermal, or chemical processes [12,13]. However, these traditional sources are not the only potential feedstock. Wood-wool cement panels, which typically contain 25-40 % cement binder by weight [14], represent another significant source for cement recovery. Since their introduction in the 1920s, these materials have been widely used throughout Europe for their thermal insulation and acoustic properties. Approximately 174 million m^2 of wood-wool cement panels are expected to be manufactured globally, of which 25 % are manufactured in Europe [15]. This substantial production volume generates considerable manufacturing waste and defective and end-of-life products suitable for cement recovery.

Wood and cement-containing production waste is generated by various processes in their manufacturing stages, such as forming, cutting, processing, and final sorting, where lower-quality materials are separated from higher-quality ones. Recycling end-of-life products is also feasible with the same processing methods as processing production waste. Traditionally, manufacturing waste and end-of-life products are sent to landfills. They can cause pollution, so optimal technologies are being

sought to efficiently recycle these wastes into raw materials (wood-wool and reactivated cement binder) that can be used to produce new building products.

Considering the growing market demand for sustainable construction materials, there remains a critical gap in research regarding the effective recycling and reuse of wood-wool cement panel (WWCP) manufacturing wastes. Often, manufacturing companies do not realise the value of their waste or do not have access to optimal recycling technologies, and the waste is taken to landfills. This research addresses this gap by investigating innovative methods to transform manufacturing and end-of-life waste into viable raw materials usable for producing building materials with lower environmental impact, thereby contributing to waste reduction and resource efficiency in the construction sector.

The aim of the thesis

This thesis aims to develop a method for partial separation and recycling of wood-wool cement panel manufacturing and demol**i**tion waste into new raw materials for innovative multilayered building panels with a decreased environmental footprint.

Objectives of the thesis

To achieve the aim, the following objectives for the thesis are set:

1. **Define** requirements and develop a method for the most effective wood-wool cement board's manufacturing and demolition waste separation into wood and hardened cement paste;
2. **Develop** and **optimise** the method for reactivation of separated hardened cement paste;
3. **Determine** properties of reactivated binder and define the application in the building industry;
4. **Develop** and **characterise** properties of biobased composites for multilayer panels using reactivated binders and waste wood-wool;
5. **Demonstrate** application of multilayered panels in an industrial setting (TRL6);
6. **Validate** the environmental viability of the developed materials by conducting a life cycle assessment and comparison with commercially available products.

The scientific novelty of the research

This research contributes to the circularity of building materials, Green Deal initiatives, and construction industry sustainability. The thesis aims to develop a method for recycling wood-wool cement panel manufacturing and demolition waste into new raw materials for innovative multilayered building panels with a reduced environmental footprint.

The waste from wood-wool cement panel manufacturing and end-of-life products was collected and analysed. The separation process for hydrated cement pastes and wood-wool was optimised. The reactivation of hydrated cement paste through milling and heat treatment techniques was investigated, and a more efficient reactivation method was applied to restore the binding properties of the cement binder.

For the first time, the reactivated Portland-cement-based binders were developed using wood-wool cement panel manufacturing waste and end-of-life products. The separated wood-wool and reactivated

cement binder were utilised to develop novel biocomposites. These biocomposites, formulated from the recovered raw materials, demonstrated diverse mechanical and thermal properties. The application of biocomposites (produced from recovered materials) in producing self-bearing multilayered building panels with excellent hydrothermal performance and a reduced environmental impact was demonstrated.

The optimised milling parameters for processing hydrated cement paste effectively fragmented the hydrated cement conglomerates, releasing unhydrated cement minerals. The efficiency, characteristics, and effect of the hydrated cement paste's collision, planetary, and vibration mills were examined. Different reactivated binders were developed by changing the mills' parameters, which allowed obtaining samples with compressive strengths from 0.5 to 15.4 MPa on day 28.

The heat treatment methods proved the reactivation of the cement binder by dehydrating the hydrated minerals. The heat treatment started at around 450 °C when the portlandite started dehydrating. At 600 °C, calcium silicate hydrates (C-S-H) started dehydrating, introducing dehydrated C-S-H products into the reactivated binder, which affected the physical and mechanical properties of the binder.

Cement used in wood-wool cement panel manufacturing typically contains a certain amount of fine limestone. The free lime in the cement clinker and $Ca(OH)_2$, which may form as hydration products in the binder structure, can undergo carbonation over the long service life of recycled wood-wool cement panels. The heat treatment of hydrated cement paste at 900 °C resulted in the decarbonization of $CaCO_3$, but it proved inefficient as it released CO_2 into the atmosphere, which was not the intended outcome. With heating energy emissions and the release of CO_2 from the reaction, the high-temperature heat treatment method is not a sustainable method of reactivation of the cement binder. However, heating below 900 °C proved to be a more sustainable method, scalable to an industrial scale. The reactivated binders proved effective and could be used as a secondary cementitious binder in blended cement, achieving 1.6 to 19.6 MPa compressive strength on the 28th day and lowering the environmental impact of said materials.

The innovation related to improving biocomposites' thermal conductivity involves incorporating a certain amount of hemp shives into the composition. Based on the knowledge gained from the research, novel biocomposites have been developed mainly using production line waste, adding up to 75 % of hemp shives as filler material. Based on their microstructure, hemp shives have proven to be an effective thermal insulator, and their addition to the mix has been proven to decrease the thermal conductivity coefficient.

Developed biocomposites resulted in a self-bearing, low-to-mid density (170-780 kg/m^3) thermal insulation material with a compressive strength of up to 1.4 MPa and a thermal conductivity of 0.052-0.139 W/(m·K). The developed biocomposites have been subjected to an environmental impact assessment and have been found to comply with the EU Green Deal guidelines, lowering the overall emission of 1 m^3 of biocomposite by 26-58 % compared to cement-based alternatives.

Practical relevance of the thesis

The reactivation of cement binders has been considered a complex, energy-intensive, inefficient process, and many countries do not have standards governing the production and use of reactivated cement in construction. From the perspective of the EU Green Deal, reactivated cementitious binders are an ideal solution to ensure the sustainability of construction processes: reactivated cementitious

binders can use industrial by-products and waste as precursors, reducing the consumption of non-renewable resources and can be produced with reduced environmental impact compared to raw Portland-cement-based binders.

A deeper understanding of the possibilities and advantages of using recycled binders can increase the popularity of the circular approach among professionals in the construction sector. The thesis describes the results of studies on alternative binders produced from local industrial wastes using either milling or heat treatment, which allows for the efficient disposal of waste products. The results obtained in the thesis can also be used for pedagogical purposes related to civil engineering, material science, and chemistry. By transforming approximately 450 000 m^3 of waste into potential raw materials annually, the research offers a tangible solution to industrial waste management. It demonstrates a clear pathway for converting what was once considered waste into valuable, eco-friendly construction materials with potential applications across the construction and manufacturing sectors.

The production of a reactivated binder from industrial by-products allows obtaining a binder with a 28-day compressive strength of up to 20 MPa. Using the developed binders and wood waste as filler, a self-bearing, low-to-mid density (170-780 kg/m^3) thermal insulation material with a compressive strength of up to 1.4 MPa and a thermal conductivity of 0.052-0.139 W/(m·K) was obtained.

Research Methodology

Characterising the binder and biocomposites involved several standardised techniques to ensure accurate and reproducible results. For the binder, **granulometry** of sanding dust (waste stream from wood-wool cement panel manufacturing) was performed according to the ASTM C136 standard, using mesh sizes ranging from 0.125 mm to 8 mm. Post-mixing, the developed mortars were placed in a moistened cone on an ASTM C143 impact table, and the **workability** of the mortars was tested.

Material density was calculated mathematically from the dimensions and weight of the samples. **Compressive strength** tests were conducted using a Zwick Z100 universal testing system at a 0.5 mm/min speed. Cubic specimens were measured and weighed to calculate density, which was derived by dividing the mass by the volume. Compressive strength was calculated based on the force applied to the specimen's area. Specimens were dried at 45 °C for 16 hours before testing on days 7, 14, and 28 to remove excess moisture.

Cumulative particle size distribution was analysed using laser diffraction (CILAS 1090), ranging from 0.10 μm to 500.00 μm. **X-ray fluorescence** (XRF) was employed to determine the elemental composition of the samples using a Rigaku ZXS PrimusIV, providing a detailed chemical analysis. **X-ray diffractometric analysis** was performed with a BRUKER-AXS D8 ADVANCE X-ray diffractometer, utilising CuKα1 and CuKα2 radiation in the 2θ range from 10° to 70°. **Thermal properties** were assessed using a Mettler Toledo TGA1/SF thermogravimetric analysis machine, with analyses conducted from 25 °C to 900 °C at 10 °C/min in an air environment.

For biocomposites, **macrostructure and appearance** were evaluated using a Veho HDMI Dual Vision Digital microscope. **Thermal conductivity** was measured with a LaserComp FOX600 heat flow meter according to LVS EN 12667 guidelines, with test settings of 0 °C for the upper plate and 20 °C for the lower plate. The **flexural and compressive strength** tests were conducted using a Zwick Z100 universal testing machine at 0.5 mm/min, following BS EN 12390-3 standards. Compressive strength was measured in both parallel and perpendicular directions to the forming direction, with tests performed until 10 % and 20 % relative deformations in the casting direction and a load of 10 % of the

sample's height for the perpendicular direction. Flexural strength was measured perpendicular to the forming direction for three parallel samples.

Life Cycle Analysis (LCA) principles were applied to assess the sustainability of binders and biocomposites. The analysis compared 1 kg of binder (developed binders and Portland cement) and biocomposites against commercially available alternatives like rock wool and EPS, maintaining a U-value of 0.18 W/(m²K). Calculations were performed using the SimaPro platform, employing the NE 15804 + A2 V1.03 method as per Product Category Rules (PCR) for building materials.

Limits of research

The research limits can be characterised by the following:

- To obtain a technologically usable sanding dust fraction (**<0.25 mm**) for reactivation experiments;
- To obtain a reactivated binder with compressive strength of **up to 20 MPa** on day 28 by using the following reactivation methods:
    - Collision milling at rotational frequencies of **25** and **50 Hz** for **1 to 5 times**;
    - Planetary ball milling with **300 RPM** for the duration of **1 to 30 minutes**;
    - Vibration milling for the duration of **5 to 20 minutes**;
    - Heating in a muffle furnace **from 300 to 1200 °C** for **1 to 5 hours** at the heating rate of **10 °C/min**;
    - Heating in a rotary kiln at a speed of **25 RPM** with a **5 ° inclination** at **450 and 900 °C**.
- To obtain biocomposites **as filler using production line waste or a mix of up to 75 % hemp shives**, with a material density of **150 to 800 kg/m^3**, thermal conductivity coefficient of **0.05 to 0.15 W/(m·K)**, and compressive strength of up **to 1.5 MPa** on the 28th day after formation.

Theses for defence

- Mechanical activation through optimised milling processes can effectively reactivate partially hydrated cement from wood-wool cement panel manufacturing wastes, producing a low-strength binder of up to 10 MPa on the 28th day, suitable for specific construction applications.
- Heat treatment reactivation at controlled temperatures significantly enhances the binding properties of already hydrated cement-based materials, achieving up to 20 MPa compressive strength compared to mechanical activation.
- Integrating reactivated cement binders with production line waste and hemp shives creates biocomposites that demonstrate comparable thermal insulation and mechanical properties to conventional construction materials while maintaining a low environmental impact.
- The environmental impact assessment of the developed biocomposites confirms their alignment with EU Green Deal objectives, demonstrating a reduced carbon footprint of 26-58 % (47-82 kg CO_2 eq./m^3 of biocomposite). Compared to traditional cement-based products (111 kg CO_2 eq./m^3 of biocomposite).

Composition and scope of the thesis

The thesis comprises an annotation in two languages, a general description of the thesis, nine main chapters divided into subsections, conclusions, and a list of references. Chapters 1-3 review the literature and formulate the thesis's aim and objectives. Chapters 4-7 outline the research methods and materials used and the results obtained through experimental analysis to achieve the objective. Chapter 8 compares the LCA results of the developed materials, and the chapter before references concludes the thesis.

The thesis comprises 139 pages, 99 figures, 28 tables, and a reference list with 245 references. The thesis is written in English.

Approbation of the thesis results

- Participation in conferences: The key findings and methodological innovations have been shared and reviewed at international scientific conferences, allowing for expert opinion and feedback:

1. Riga Technical University 62nd International Scientific Conference, Section "Civil Engineering," Riga, Latvia, 28.10.2021.
2. 5th International Conference "Innovative Materials, Structures and Technologies" IMST 2022, Riga, Latvia, 28.–30.09.2022.
3. Riga Technical University 63rd International Scientific Conference, Section "Civil Engineering," Riga, Latvia, 10.11.2022.
4. XVI International Scientific conference of environmental and climate technologies "Conect 23", Riga, Latvia, 10.-12.05.2023.
5. 5th International Conference on Bio-Based Building Materials "ICBBM 2023", Austria, Vienna, 21.-23.06.2023.
6. Riga Technical University 64th International Scientific Conference, Section "Civil Engineering," Riga, Latvia, 19.10.2023.
7. XVII International Scientific Conference of Environmental and Climate Technologies "Conect 2024", Riga, Latvia, 15.-17.05.2024.
8. The 4th International Conference on Sustainable Development in Civil, Urban and Transportation Engineering "CUTE 2024", Wroclaw, Poland, 14.-16.10.2024.
9. 6th International Conference on Bio-Based Building Materials "ICBBM 2025", Rio de Janeiro, Brazil, 17.-20.06.2025.

- Academic Publications: The research has been presented in 4 publications of conference proceedings and 5 publications of scientific journals, indexed in the SCOPUS database; in total, they have been cited 83 times, h_5-index – 5 (h-index – 6). Research has been published in international journals, such as *Recycling*, *Environmental and Climate Technologies*, and *Materials*.
- Industrial Collaboration: The research was conducted in close collaboration with Cewood®, a leading producer of wood-wool cement panels, ensuring practical relevance and real-world applicability of the developed methods and materials.

List of publications

1. **Argalis, P.P.**; Sinka, M.; Bajare, D. Recycling of Cement–Wood Board Production Waste into a Low-Strength Cementitious Binder. *Recycling* 2022, *7*, 76, doi:10.3390/recycling7050076.
2. **Argalis, P.P.**; Sinka, M.; Bajare, D. A Preliminary Study of Mechanical Treatments' Effect on the Reactivation of Hydrated Cement Paste. *J Phys Conf Ser* 2023, *2423*, 012008, doi:10.1088/1742-6596/2423/1/012008.
3. Bumanis, G.; **Argalis, P.P.**; Sahmenko, G.; Mironovs, D.; Rucevskis, S.; Korjakins, A.; Bajare, D. Thermal and Sound Insulation Properties of Recycled Expanded Polystyrene Granule and Gypsum Composites. *Recycling* 2023, *8*, 19, doi:10.3390/recycling8010019.
4. **Argalis, P.P.**; Bumanis, G.; Bajare, D. Gypsum Composites with Modified Waste Expanded Polystyrene. *Journal of Composites Science* 2023, *7*, 203, doi:10.3390/jcs7050203.
5. **Argalis, P.P.**; Sinka, M.; Andzs, M.; Korjakins, A.; Bajare, D. Development of New Bio-Based Building Materials by Utilising Manufacturing Waste. *Environmental and Climate Technologies* 2024, *28*, 58–70, doi:10.2478/rtuect-2024-0006.
6. Bumanis, G.; **Argalis, P.P.**; Sinka, M.; Korjakins, A.; Bajare, D. The Use of Recycled Cement-Bonded Particle Board Waste in the Development of Lightweight Biocomposites. *Materials* 2024, *17*, 5890, doi:10.3390/ma17235890.
7. **Argalis, P.P.**; Sinka, M.; Bumanis, G.; Bajare, D. Application of a Recovered Low-Strength Binder from Wood–Cement Particleboard Production. *In Proceedings of the 4th International Conference on Sustainable Development in Civil, Urban and Transportation Engineering*; Springer, 2025; Vol. 418, pp. 245–253.
8. Hajj Obeid, M.; **Argalis, P.P.**; Sinka, M.; Bajare, D.; Pailha, M.; Woloszyn, M. Advancing Sustainable Building Technologies: A Focus on Bio-Based Multi-Layer Panels and Real-Scale Hygrothermal Analysis. In *Proceedings of the 4th International Conference on Sustainable Development in Civil, Urban and Transportation Engineering*; Springer Nature, 2025; Vol. 418, pp. 323–332.
9. **Argalis, P.P.**; Puzule, L.; Sinka, M.; Bajare, D. Transforming Cement-Wood Fiber Industrial Byproducts into Hybrid Binder. In *Bio-Based Building Materials - Proceedings of ICBBM 2025*; Springer Nature, 2025; pp. 738–751, doi:10.1007/978-3-031-92874-1_58.
10. Balina, K.; Gailitis, R.; Sinka, M.; **Argalis, P.P.**; Radina, L.; Sprince, A. Prospective LCA for 3D-Printed Foamed Geopolymer Composites Using Construction Waste as Additives. Sustainability 2025, 17, 6459, doi:10.3390/su17146459.

1. ENVIRONMENTAL IMPACT AND CLIMATE STRATEGIES IN LATVIA

1.1. Environmental Impact of the Construction Materials Sector

Global Context

The construction materials sector is a major contributor to global resource consumption and environmental impact, with significant implications for sustainability. According to the International Energy Agency's global status report for buildings and construction [16], the sector is responsible for 33 % of energy-related CO_2 emissions. This figure includes operational emissions (26 %) and embodied carbon emissions from materials and construction processes (7 %), underscoring the sector's critical role in climate change mitigation efforts [17].

Material consumption patterns in construction are particularly concerning in terms of sustainability challenges. The United Nations Environment Programme's resource efficiency and climate change report indicates that construction materials account for approximately 50 % of all raw materials extracted globally [18]. Concrete production is a critical environmental concern in this context, contributing to about 8 % of global CO_2 emissions (Fig. 1.1), with annual cement production exceeding 4 billion tonnes [19,20].

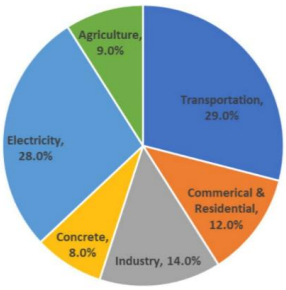

Figure 1.1. Concrete production global CO_2 emissions [20].

The steel industry, intrinsically linked to construction, compounds these environmental impacts, accounting for approximately 9 % of global CO_2 emissions [21]. The construction sector's demand drives approximately half of global steel production, creating a significant environmental burden beyond immediate construction activities [22].

Water consumption in construction materials represents another significant environmental challenge that often receives less attention than emissions. The World Business Council for Sustainable Development has documented that concrete production alone consumes approximately 10 % of the world's industrial water [23]. This considerable water footprint primarily stems from the extraction and processing of raw materials, particularly in cement production and aggregate washing processes. The impact extends beyond mere consumption, as these processes often affect local water quality and ecosystem health through industrial runoff and altered hydrogeological patterns [24].

Latvia's Construction Sector Overview

Latvia's construction sector has demonstrated remarkable dynamism over the past decade, establishing itself as a crucial component of the national economy. Between 2022 and 2024, the sector's contribution to the national GDP fluctuated between 200 000 € and 514 000 € quarterly, reflecting its significance and sensitivity to economic cycles [25] (Fig. 1.2).

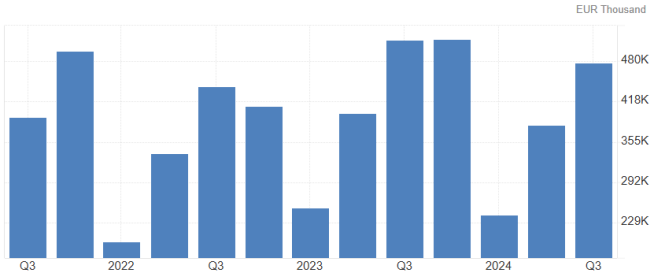

Figure 1.2. Latvia's GDP from the construction sector (last 3 years) [25].

According to Eurostat, the sector employed 62 380 people as of December 2024, representing approximately 7 % of the total workforce [26]. This employment figure underscores the sector's role in economic output, social stability, and workforce development.

The environmental footprint of Latvia's construction sector must be understood within the context of the country's unique geographical and economic characteristics. Latvia's extensive forest coverage, encompassing 53 % of the total land area [27], positions timber as a crucial construction material while raising important sustainability considerations. The Central Statistical Bureau Forest Service's annual report reveals that timber harvesting reached 15 million cubic meters in 2023, an increase of 15 % since 2022 [28]. This significant utilisation of forest resources has sparked ongoing debates about sustainable forest management practices and the long-term viability of current harvesting rates.

Material consumption patterns in Latvia's construction sector reveal intensifying environmental pressures. The Latvian Environment, Geology, and Meteorology Centre (LEGMC) reports that the annual extraction of construction minerals has reached the lowest levels in the last few years. Sand and gravel extraction dropped to 5.4 million m^3 in 2023, limestone extraction reached 730 610 m^3, and clay extraction for brick production approached 228 040 m^3 [29]. The energy intensity of Latvia's construction sector remains significant, although lower than the EU average, accounting for approximately 12 % of the country's industrial energy consumption.

Specific Environmental Concerns in Latvia

Latvia faces distinct environmental challenges related to its construction materials sector, with impacts manifesting differently across regions and ecosystems. The Latvian State Environmental Service has identified several critical areas requiring immediate attention and long-term strategic planning. The challenges present a complex interplay between economic development needs and environmental preservation imperatives.

Forest resource management is a primary concern within Latvia's construction materials sector. While the country maintains one of the highest forest coverage rates in the EU, the intensity of timber harvesting for construction has raised significant sustainability concerns. The State Forest Service's

monitoring data reveals a complex picture of forest resource utilisation. Annual timber harvest rates for construction have increased by 15 % between 2018 and 2022 [28] (Fig. 1.3). This imbalance has led to a gradual shift in the age structure of managed forests, with an increasing predominance of younger trees. Younger trees have decreased mechanical properties, affecting the materials' performance [30]. The long-term implications of this trend extend beyond timber availability to impact biodiversity, carbon sequestration capacity, and ecosystem resilience.

Figure 1.3. Wood growth 100 years apart [31].

The extraction of mineral resources for construction has precipitated substantial changes in Latvia's landscape and ecological systems. According to the LEGMC's subsoil information system, the country currently maintains 2794 active quarries for construction materials [32] (Fig. 1.4). The environmental impact extends beyond the immediate extraction sites, affecting groundwater dynamics and local ecosystems.

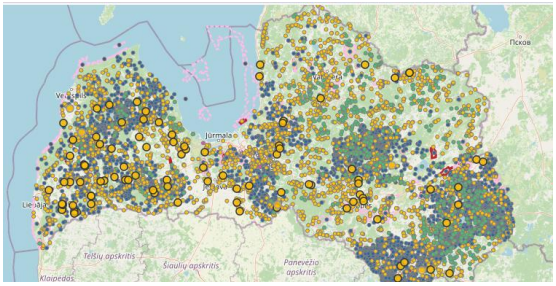

Figure 1.4. Active queries for construction materials in Latvia [32].

The State Audit Office of the Republic of Latvia documented that in 2021, secondary materials were only 6 % of the total material consumption, while the EU's average was 12 %. The ongoing operation and development of different industries, including construction, may be complex due to the lack of governmental policy, a strategic long-term vision, and thorough monitoring of mineral resource extraction [33].

Water quality impacts from construction activities and material processing facilities represent another significant environmental challenge (Fig. 1.5). The 2024 report by the European Investment Bank details a concerning pattern of water quality degradation near construction-related activities [34]. The program has documented increased suspended solids concentrations in water bodies adjacent to

major construction sites, alongside elevated pH levels in drainage from concrete production facilities [35], underscoring the need for more effective site management and water protection measures.

Figure 1.5. Water pollution from construction activities [36].

1.2. Latvia's Role in the European Climate Neutrality Plan

European Climate Neutrality Goals

The European Union's commitment to climate neutrality, formalised through the European Green Deal (Fig. 1.6), represents one of the world's most ambitious climate action frameworks. The significance of this initiative extends far beyond mere emissions reduction targets, encompassing a fundamental transformation of the European economy and society. At its core, the Green Deal sets forth a comprehensive roadmap to achieve net-zero greenhouse gas emissions by 2050 [37], with the construction sector playing a pivotal role in this transition. The European Commission's "Renovation Wave" strategy, launched in 2020, particularly emphasises the transformative potential of the built environment, targeting the renovation of 35 million buildings by 2030 [38].

Figure 1.6. European Green Deal objectives [2].

The EU's climate neutrality objectives translate into interconnected targets and requirements for the construction sector. The most immediate goal is a 55 % reduction in embodied carbon emissions by 2030 and 100 % by 2050 [39]. This ambitious target acknowledges the sector's substantial contribution to Europe's carbon footprint while recognising the technical and economic challenges inherent in such a transformation. The EU's construction products regulation revision, published in

December 2024 [40], further strengthens these requirements by introducing mandatory carbon assessment and reporting for construction materials, marking a significant shift toward carbon-conscious construction practices [41].

The European framework also addresses the broader environmental impacts of construction activities through initiatives such as the circular economy action plan. This plan explicitly targets construction and demolition waste (CDW), which accounts for approximately 35 % of total waste generation in the EU [5]. Implementing these objectives has catalysed innovation in sustainable construction technologies and practices across member states, though progress remains uneven.

Latvia's Commitments and Progress

Latvia's response to European climate neutrality objectives reflects ambition and pragmatism, shaped by the country's unique economic and environmental context. The nation has slightly increased its climate objectives with EU targets, committing to a 65 % reduction in greenhouse gas emissions by 2030 compared to 1990 levels [42]. This commitment, formalised through the National Energy and Climate Plan (NECP) 2021-2030, represents a significant acceleration of Latvia's climate action efforts, particularly in the construction sector [43].

The NECP outlines specific targets for the construction sector beyond simple emissions reduction. Central to these objectives is the mandate for a 30 % reduction in energy consumption in new buildings by 2030, complemented by the implementation of nearly zero-energy building (nZEB) standards for all new construction [42]. These targets are supported by a comprehensive renovation strategy that aims to upgrade 3 % of public buildings annually to improve energy efficiency [44]. The Ministry of Economics' progress reports indicate varying degrees of success in achieving these objectives, with energy efficiency improvements showing promising results. In contrast, progress in reducing embodied carbon in construction materials lags behind targets [45].

Latvia's progress toward these goals presents a complex picture of achievements and challenges (Fig. 1.7). Recent monitoring data from the Ministry of Environmental Protection and Regional Development indicate that while Latvia has achieved a 15 % reduction in building-related emissions since 2018, this progress falls short of the trajectory needed to meet 2030 targets [45].

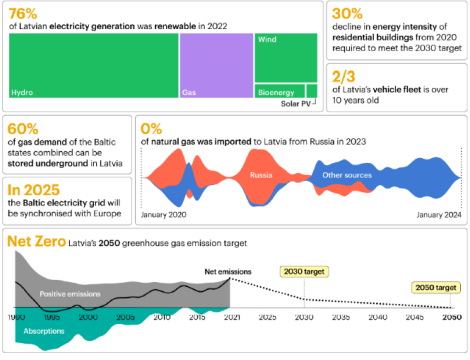

Figure 1.7. Latvia’s progress towards NECP goals [45].

Implementing nZEB standards has been particularly challenging for smaller construction projects, with compliance rates varying significantly between urban and rural areas. The ministry's analysis

suggests that while technical solutions exist, economic challenges and skill gaps impede faster progress [46].

Policy and Regulatory Framework in Latvia

The evolution of Latvia's regulatory environment for sustainable construction reveals the complexities of implementing ambitious climate goals within existing institutional frameworks. The current policy landscape combines national legislation with EU directives, creating a multi-layered approach to sustainable construction governance. The construction law, last amended in 2025 [47], is the primary legislative framework, incorporating sustainability requirements into building permits and inspections. However, implementation challenges and enforcement inconsistencies greatly affect the effectiveness of the lawn-driving sustainable practice [44].

The energy efficiency of buildings law [30] represents another crucial component of Latvia's regulatory framework, translating EU requirements for energy efficiency into a national context. This legislation has introduced mandatory energy performance certificates for buildings and established minimum energy performance requirements for new construction and major renovations [48]. The law's impact has been significant in the commercial sector but less pronounced in residential construction, where cost considerations often dominate decision-making [49].

Latvia's Green Public Procurement (GPP) regulations (Fig. 1.8) have emerged as a powerful tool for promoting sustainable construction practices [50]. These regulations mandate environmental criteria in public construction projects, leveraging government purchasing power to drive market transformation. According to the Procurement Monitoring Bureau's 2023 report, GPP requirements have led to a 12 % increase in the use of sustainable construction materials in public projects since 2020 [51]. However, the effectiveness of these requirements varies significantly across different regions and project types.

Figure 1.8. GPP sustainability development goals [52].

The implementation of these policies faces several structural challenges that merit careful consideration. The fragmentation of responsibilities between national and municipal authorities has created coordination difficulties and inconsistent requirements application. The State Construction Control Bureau's assessment identifies significant variations in enforcement capacity across different municipalities, with smaller jurisdictions particularly struggling to provide adequate oversight [44]. This situation is further complicated by the overlapping mandates of different regulatory bodies and the absence of a unified database for monitoring compliance [53].

Moreover, the interaction between different policy instruments sometimes creates unintended consequences. For instance, strict energy efficiency requirements can inadvertently lead to increased use of carbon-intensive materials [54], highlighting the need for a more holistic approach to sustainability in construction regulations. The recent introduction of the circular economy framework for building materials attempts to address these policy conflicts, but its effectiveness remains to be thoroughly evaluated [55].

1.3. Waste Management Practices in Latvia's Construction Sector

Waste Generation and Composition

Construction and demolition waste is often separated into three categories: roadwork demolition, building construction, and building demolition and renovation (Fig. 1.9). The categories then divide further into material categories such as construction materials, waste from road and street repair operations, and waste from building demolition, etc.

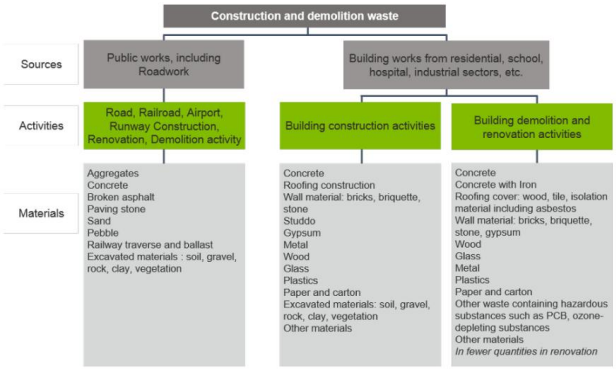

Figure 1.9. Diversity of construction and demolition waste by activity [56].

The scale and composition of construction waste in Latvia present a complex picture that reflects the sector's economic dynamics and its material use patterns. According to the LSM+ review, the construction sector generated roughly 15 % of the country's total waste stream in 2022 [57], which, compared to the 2019 data of 380 000 tonnes of CDW generated, is a slight decrease in the amount [58]. In 2020, the CDW generated 368 000 tonnes, 15.7 % of all waste [59]. Detailed waste composition analysis reveals patterns that challenge and inform management strategies [1]. In 2023, the collected CDW was 585 000 tonnes, out of which 33 343 tonnes were pure concrete waste, and 120 787 tonnes were mixed concrete with tiles and ceramics. This predominance reflects the widespread use of these materials in Latvian construction and the significant volumes generated during construction and demolition activities.

Wood and timber waste, comprising about 2 % of the total CDW mass [60], presents unique management challenges and opportunities within Latvia's context. Although 2 % seems low, 11 011 tonnes of wood materials can be recycled or repurposed. Environmental monitoring data from processing facilities indicates that while wood waste offers significant potential for resource recovery, contamination with preservatives and treatments often complicates recycling efforts [61]. Kiesnere et

al. [62] estimate that around 40 % of construction wood waste does not currently undergo proper recycling or energy recovery.

Current CDW Management Situation

Latvia's approach to CDW management reflects a growing recognition of waste as both an environmental challenge and a potential resource. The country's waste management framework [63], fundamentally shaped by EU waste framework directive requirements, establishes a clear waste hierarchy prioritising prevention, reuse, recycling, and recovery over disposal (Fig. 1.10). However, the practical implementation of this hierarchy within Latvia's construction sector reveals significant complexities and challenges unique to the country's economic and geographic context [58].

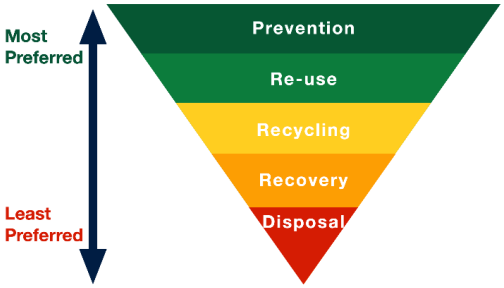

Figure 1.10. Waste prevention hierarchy scheme [64].

The regulatory framework for construction waste management in Latvia has evolved significantly since the country's EU accession. The Waste Management Law, amended in 2021, mandates specific requirements for construction waste handling [65]. These plans must detail expected waste volumes, management methods, and final disposal routes. A noteworthy aspect of the current strategy is the requirement for on-site waste sorting, detailed in the “Life waste to resources” report [66] about the differences in materials and why everything cannot be stored together.

A Waste Management Plan (WMP) was initially adopted in Latvia in 2006, but has been updated and changed following the new trends. Now, it is up to its current version with a plan for 2021-2028. The WMP has 4 main objectives [3]:

- Expand the current system for the separation and collection of waste;
- Develop the institutional framework for waste management;
- Create more substantial waste management regions;
- Implement CE principles that will lead to increased waste recycling.

With these four goals in mind, the State WMP aims to assist:

- Reusing building materials during construction (inclusion in GPP and standards);
- Making as little waste as possible during construction (training, adding criteria for the best construction in tenders, awarding the most environmentally friendly construction);
- Helping to reuse asphalt and soil surfaces (inclusion in GPP and standards);
- Encouraging the economy to use compost made from biodegradable waste.

Latvia's CDW management system follows a structured process involving multiple stakeholders and processes (Fig. 1.11). Construction activities requiring building permits mandate shared responsibility for waste management between construction companies and their clients. Construction companies must acquire appropriate waste containers from authorised waste management companies. The collected waste undergoes assessment at sorting facilities unless pre-sorted at the construction location.

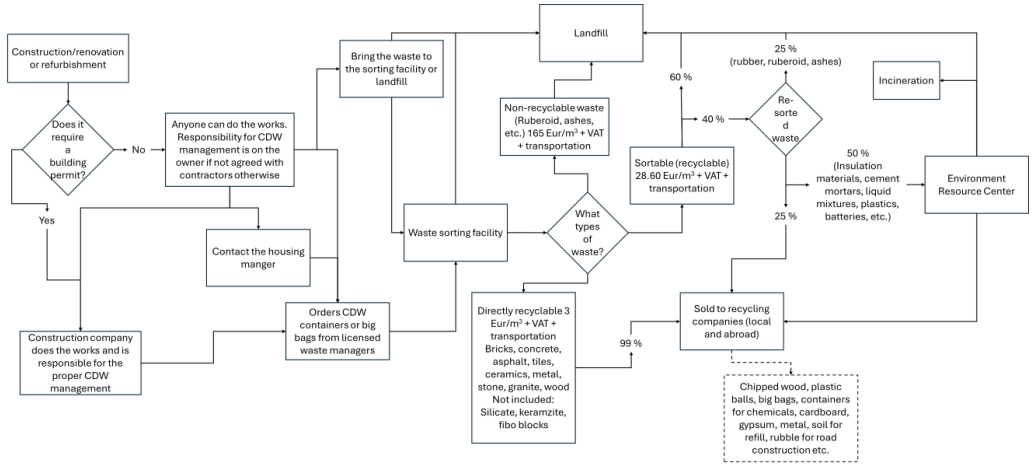

Figure 1.11. Latvia's CDW management system [3].

The waste management system categorises CDW into three primary classifications. The first category comprises non-recyclable materials, with disposal costs of 165 €/m³ (excluding VAT and transport), destined for landfills. The second category includes potentially recyclable materials, charged at 28.60 €/m³ (excluding VAT and transport). Of this category, 60 % is sent directly to landfills, while the remaining 40 % undergoes further sorting:

- 25 % is designated for recycling companies;
- 25 % (including materials like rubber and rubberoid) goes to landfills;
- 50 % (insulation, cement, mortars, and other materials) is directed to the Environment Resource Centre for further assessment and processing.

The third category encompasses directly recyclable materials, priced at 3 €/m³, sent straight to recycling facilities. Landfill disposal fees vary significantly between private and commercial entities: private individuals face charges of 181.50 €/t (a substantial increase from the previous 85 €), while business entities pay between 2.5 € and 7 €/t [3].

When construction activities do not require building permits, individual property owners are responsible for CDW management unless they establish specific contractor agreements. These individuals have three available methods for handling their construction waste:

- They may transport the waste directly to sorting facilities or landfills themselves;
- Arrange for waste container delivery through their housing management company;
- Independently order and transport waste containers to sorting facilities.

Once the waste reaches the sorting facility, it follows the same processing pathway as contractor-managed waste, undergoing identical classification and disposal procedures.

Challenges and Future Directions

The transition to more circular management of CDW in Latvia is hindered by several key challenges (Annex II). These obstacles can be grouped into three main categories. On the one hand, market and business-related challenges prevail, including a scarcity of suitable waste materials, complex product requirements, and prohibitively high costs associated with upcycling and logistics. Additionally, regulatory shortcomings, such as the lack of material passport regulations and insufficient financial support from the national government, pose significant hurdles. Furthermore, the behaviour of citizens, marked by rampant illegal dumping and a general lack of awareness regarding proper CDW disposal, exacerbates the issue [3].

Conversely, several factors have been identified as solutions that could facilitate a more circular approach to CDW management (Annex III). Government initiatives, such as subsidies for recycled materials, green procurement practices, and increased landfill fees, can be pivotal in driving the change.

The market also holds potential, with opportunities for niche markets, the availability of advanced separation technologies, and the emergence of sustainable financing options from banks. Moreover, the active engagement of citizens, as evidenced by their participation in social media platforms focused on CDW management and their willingness to pay for recycling services, including Urban Recycling Centres (URCs), can significantly contribute to a more circular waste management system [3]. This experimental centre operates as a materials exchange hub, enabling residents to trade construction materials, tools, and renovation supplies, including unused and reclaimed materials. The pilot served as a testing ground to evaluate public engagement, identify potential challenges, and assess various operational aspects of such a resource-sharing facility. Possible designs and their functions have been illustrated in Figure 1.12.

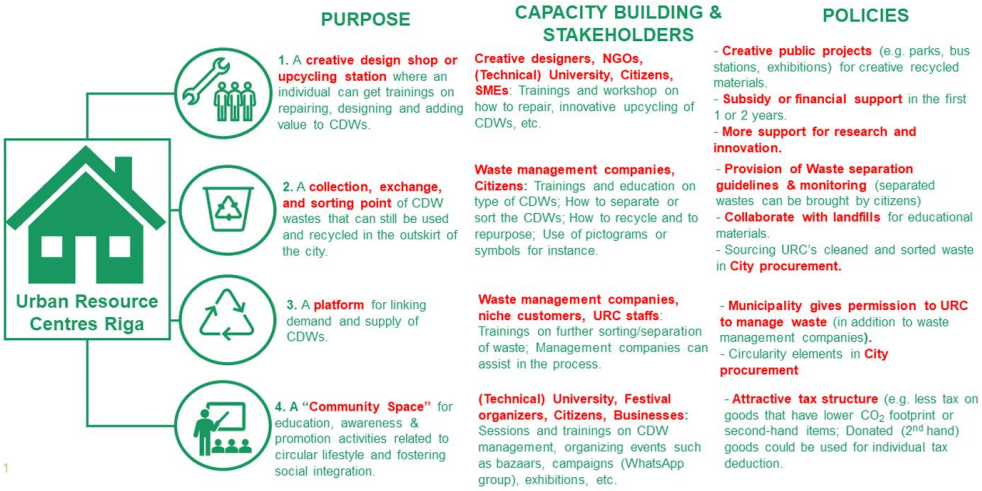

Figure 1.12. Designs and function of a URC [3].

Stakeholder interviews revealed multiple innovative approaches to CDW management, which can be organised into six distinct categories, with the first category encompassing practices aligned with the Circular Economy's 10R principles for material utilisation. Three subsequent categories relate to

community-driven initiatives, while the final two focus on technological implementation and adoption. The categories are as follows [3]:

Reuse of materials – Material reuse initiatives have emerged among construction material manufacturers in Riga. One notable example involves a local producer experimenting with recycled glass as a sand substitute in plaster and concrete mixtures. Despite promising thermal and acoustic properties, with potential energy savings of 50-70% through improved insulation, widespread adoption faces challenges. These include the high costs of processing recycled materials, rigorous testing requirements for regulatory compliance, and a lack of subsidies. Additionally, some construction elements, such as windows, hold potential for reuse, particularly those with architectural significance. However, the higher cost of recycled materials than virgin resources remains a significant barrier to implementing them.

A community-based resource centre and/or material exchange points - Riga's Material exchange initiatives operate through temporary events and permanent community spaces. The NGO Free Riga implemented A notable pilot program, establishing a temporary exchange hub for affordable material trading. The organisation also maintains several permanent exchange locations, primarily focusing on general consumer goods. While these facilities do not specifically target construction materials, their operational model offers valuable insights for the planned Urban Resource Centre (URC). Key lessons learned include the importance of developing a sustainable business model with professional staff rather than relying solely on volunteers and the necessity of establishing strong community connections and local engagement.

Sustainable building usage – an NGO, Free Riga, driven by circular economy principles, specialises in transforming vacant buildings into affordable spaces for communities, artists, and refugees. The organisation converts unused structures into creative and social hubs while emphasising sustainability through reclaimed building materials in their renovation projects.

Grassroots system - A new community-based initiative is being tested in a Riga neighbourhood, creating a network of residents with various maintenance and renovation skills. This pilot program combines a skills database with access to a workshop space provided by Free Riga, where community members can use tools and equipment for woodworking and metalworking. This grassroots approach facilitates circular practices through community resource sharing and skill exchange.

Waste sorting centres - Riga's CDW management infrastructure includes specialised waste sorting facilities operated by private companies. Currently, two sorting centres are operational (11 total in Latvia), with municipal plans to expand this network to eight facilities. These centres specialise in waste segregation to facilitate material recycling and reuse.

CleanR app - CleanR's mobile application enables residents to schedule waste collection services within their designated service areas. The platform implements a household-specific payment system based on individual waste generation.

1.4. Sustainability Assessment of Construction Materials

The development of sustainability assessment methods in Latvia's construction sector reflects the increasing complexity of sustainability considerations in the built environment. The adoption of international assessment frameworks, particularly the European Commission's Level(s) framework (Fig. 1.13) [67], has established a foundation for systematic sustainability evaluation. However,

implementation patterns reveal significant adaptation challenges within Latvia's context, particularly regarding integrating local construction practices.

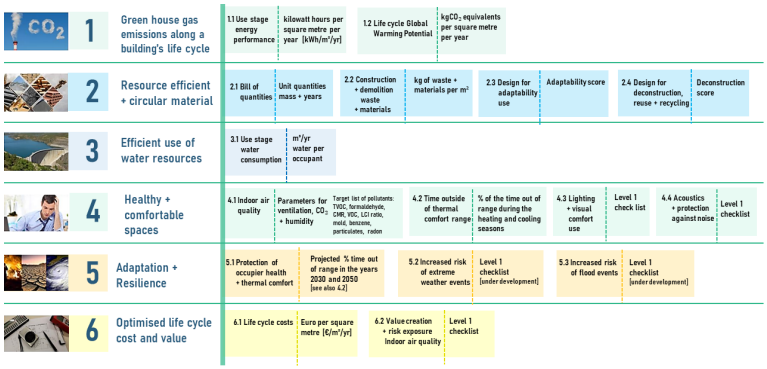

Figure 1.13. Key indicators of Level(s)[67].

Implementing multi-criteria assessment systems in Latvia demonstrates varying levels of adoption and effectiveness across different construction sectors. While gaining traction in commercial construction, BREEAM and LEED certifications (Fig. 1.14) represent only one aspect of sustainability assessment [68]. The Latvian Sustainable Building Council indicates that these international certification systems, while comprehensive, sometimes fail to address local priorities and conditions adequately.

Figure 1.14. BREEAM and LEED certification logos [69].

Sustainability assessment consists of many aspects, the most popular being economic, social, and environmental.

Economic Sustainability Metrics

Economic sustainability assessment in Latvia's construction sector has expanded beyond traditional cost-benefit analysis to incorporate lifecycle costing and circular economy principles. The sustainable governance indicators in the context of Latvia introduced standardised methods for evaluating long-term economic sustainability, including maintenance costs, adaptation potential, and end-of-life value recovery [70]. Their analysis indicates that buildings designed using comprehensive economic sustainability criteria demonstrate 24-28 % lower lifecycle costs than conventional approaches [71].

Social Impact Assessment

Social sustainability assessment has emerged as a crucial component of comprehensive evaluation frameworks. Established methodologies for evaluating social impacts (Fig. 1.15), including risk assessment, cultural impact, economic assessment, and hazard assessment [72]. Their findings indicate that projects incorporating robust social sustainability assessment achieve significantly higher occupant satisfaction rates and better community integration.

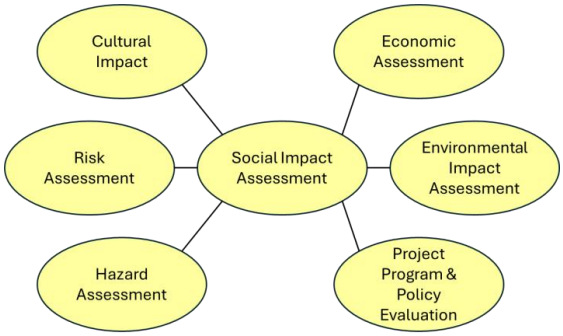

Figure 1.15. Aspects of social impact assessment [73].

Environmental Impact Evaluation

Environmental impact assessment methodologies in Latvia's construction sector have evolved beyond simple carbon accounting to encompass broader ecological considerations. The Ministry for Climate and Energy's report introduces comprehensive evaluation criteria covering biodiversity impact, water resource management, and local ecosystem services. Their analysis reveals that projects utilising this expanded assessment framework achieve 35 % better environmental outcomes than those focused solely on energy efficiency and carbon emissions [4]. The primary method of evaluating environmental impact is life cycle assessment (LCA).

Life Cycle Assessment represents a crucial quantitative tool within Latvia's broader sustainability assessment framework. Following ISO 14 040 and 14 044 standards, LCA implementation in Latvia's construction sector has evolved to address specific regional challenges. The Energy Systems and Environment Institute's study demonstrates that LCA applications in Latvia typically focus on four key impact categories: global warming potential, resource depletion, acidification, and eutrophication [74]. Their analysis reveals significant variations in environmental impacts between different construction approaches, with traditional wooden buildings showing 30 % lower lifetime carbon emissions than conventional concrete structures (Annex I).

However, there are limitations in current LCA practice, particularly regarding data availability for local materials and the need for better integration with other assessment methods. Recent developments in the field have focused on harmonising LCA methodologies with broader sustainability criteria [75].

The literature section of this doctoral thesis builds a compelling case for urgent innovation within the construction sector, guided by global environmental challenges to a defined research problem and its solution. This narrative begins by firmly establishing the environmental footprint of traditional construction practices and materials, providing the essential global and local context for the following research.

The construction materials sector contributes to environmental degradation, characterised by its intensive consumption of virgin resources and significant greenhouse gas emissions. This impact is particularly stark in producing conventional binders like Portland cement, which accounts for roughly 8% of global CO_2 emissions [19,20]. These challenges are not abstract; they manifest acutely in regions like Latvia, where the industry's reliance on new resources and its generation of substantial waste volumes underscore a need for sustainable transformation. This realisation frames the aim to explore alternative, more sustainable material solutions and innovative waste valorisation strategies to mitigate environmental damage and conserve finite natural resources.

This understanding of environmental impact naturally transitions into analysing Latvia's strategic positioning within the broader European climate agenda. As an EU member state, Latvia is committed to achieving climate neutrality by 2050, aligning its national policies with the ambitious goals of the European Green Deal [1,2]. This commitment translates into a regulatory and economic environment that actively champions circular economy principles, resource efficiency, and waste reduction across all sectors. Consequently, a strong political and societal impetus exists to develop and implement new, low-carbon building materials. This alignment between national priorities and European directives provides a crucial driving force for the research presented in this thesis, highlighting its direct relevance and societal value in sustainable construction.

Building on the policy and environmental imperatives, the thesis identifies a specific, pressing problem within Latvia's waste management landscape: the ineffective handling of construction and demolition waste (CDW), with a particular emphasis on the underutilised potential of wood-wool cement panel (WWCP) manufacturing and end-of-life waste. Despite the quantities of this waste, which contains valuable cementitious components (25-40% by weight) [14], it is predominantly directed to landfills. This represents an avoidable environmental burden and a significant missed opportunity for resource recovery and value creation. The lack of efficient recycling technologies and insufficient industry awareness perpetuate this practice, revealing a critical gap that the thesis aims to bridge by exploring the valorisation of this specific waste stream as a viable raw material for novel building products.

Through these arguments—from the global environmental pressures and the policy-driven mandate for sustainability to the specific shortcomings in waste management—the thesis articulates a clear and undeniable need for innovative solutions. This analysis of the existing literature, current challenges and newest reports collectively defines and justifies the central aim of this doctoral thesis: to develop a method for the partial separation and recycling of wood-wool cement panel manufacturing and demolition waste into new raw materials for innovative multilayered building panels with a decreased environmental impact. This research thus promises to deliver a tangible and environmentally beneficial pathway for transforming industrial waste into valuable building resources, directly contributing to the circular economy and fostering a more sustainable future for the construction sector.

2. WOOD-WOOL CEMENT PANELS

2.1. Wood-Wool Cement Panels

Manufacture

Cewood Ltd continues Latvia's 50-year-old wood-wool cement panel manufacturing traditions and manufactures wood-wool cement acoustic panels. Founded in 2015, the company produces high-quality building materials derived from cement and renewable wood resources. Their signature products combine sound absorption properties with aesthetic appeal, making them popular worldwide for architects and interior designers. Cewood's commitment to environmental stewardship is evident in its FSC-certified sourcing practices and energy-efficient manufacturing processes. The company stands out for its dedication to innovation, consistently developing new applications for wood-wool cement panels while maintaining quality standards that have earned it recognition as an industry leader in European acoustic solutions.

Spruce wood is used in manufacturing, as it has a relatively small heartwood, so the material remains homogeneous in cross-section. Once the wood has been peeled and pruned, it is stacked in piles to dry. The timber dries on an elevated surface to better disperse moisture migration. During the drying process, the wood's resins and sugars migrate to the wood's surface [76]. The total drying time is 6 to 12 months.

The following process is to prepare the logs into 50 cm blocks. This size was found to be the optimum size for the manufacturing process. If the diameter of the block exceeds the diameter allowed for manufacturing, a special press is used to split the block into the required diameter. The offcuts and chips are fed into the furnace for energy recovery.

The sawed blocks are stacked on racks (Fig. 2.1a), with racks with a reserve on the outside that can stand for up to 10 days. The blocks are distributed on the racks so that each block is made of a different wood, so there is not so much dispersion between the woods during manufacturing. Wood-wool can vary in colour and other characteristics, so there are 80 blocks per rack from 80 trees. At the start of a shift, 5 blocks are taken, and the moisture content is determined, from which it is assumed that all the blocks in that shift will have the specified moisture content. The moisture content of the blocks is expressed as the total wood density and is recorded on a factory board (Fig. 2.1b). The data are stored in logbooks. If there is a wide dispersion of densities, the worker manually adjusts the water added in further manufacturing. A special apparatus is shaving the blocks into the necessary length and thickness of the wood fibres.

Figure 2.1. a) Racks stacked with wood blocks, b) Density data of the wood used in the manufacturing.

The shaved wood fibres, called wood-wool, are taken further to the production line, where it is moistened. The waste shavings are burned in a furnace to recover energy. If the outside temperature is below 0 °C, part of the energy goes into heating the wool.

Wood-wool is moistened with clean water (Fig. 2.2) and passed on to be mixed with cement. This stage uses about 10 m^3 of clean industrial water per day. The cement, water, and wood-wool ratio can vary according to manufacturing needs.

Figure 2.2. Wetting of wood-wool.

Once the wood-wool has been wetted and mixed with cement, it is fed along a conveyor line to rotary dispersers. Before the mixed material reaches the dispersers, the first waste fraction is produced, consisting of wet wood-wool and cement (Fig. 2.3). At the end of the shift, the waste is taken to a waste pile, which accumulates until it is collected and transported to a landfill.

Figure 2.3. a) Production line waste (PLW) waste collection point; b) close-up of the PLW.

The mixed material is fed further into the manufacturing process. On one side of the production line, moulds are fed into the production line, which is oiled to make it easier to demould the panel (Fig. 2.4a). The material is then fed onto the moulds and smoothed by rotary dispersers inserted into the manufacturing process (Fig. 2.4b). The material is dispersed on the mould in two layers so that the material is evenly laid into the mould. At this stage, you can primarily tell whether the manufacturing process is successful. Different curing times are observed when different types of cement are used, and if it is observed that the cement does not form a good bond between the layers, it is assumed that 5 minutes of defective panels were produced. The technicians record the situation, change the manufacturing parameters, and follow up to ensure the material maintains its quality during manufacturing.

Figure 2.4. a) Preparation of the moulds; b) laying of the material.

After the material has undergone several mixing and smoothing operations, the panel is pressed and sawn into lengths 2.4 m long, where they are stacked one on top of the other and transported to a 1-day warehouse where a weight is placed on top of the mould stack (Fig. 2.5) to help the material cure to the desired thickness and their primary strength during the curing process.

The technician often lifts some of the panels to insert a temperature sensor 1 m in the middle to determine the internal temperature of the panel. Cement hydration can result in temperatures as high

as 65 °C, and as the temperature increases, the material can get scorched, changing its colour and, therefore, its quality. The temperature differences can be changed by adding water to the manufacturing process.

Figure 2.5. Mould stack on the 1st hour of manufacturing.

After day 1, the panels are taken to the demoulding station (Fig. 2.6), where they are demoulded, the moulds are inserted back into the manufacturing process, and the panel is sent for final preparation to be milled and sawn as necessary. This process produces another fraction of waste containing partially hardened cement and fine wood fibres. The final product is then stacked and taken to a second warehouse for further drying, where it sits for approximately 2-4 weeks. There is approximately 4 kg of water per panel, which must evaporate.

Figure 2.6. The demoulding and sawing stage.

Once the panels have been cured and the excess water has evaporated, the panel is transferred to the dryer for further drying. The drying process can be done with 2 methods. Initially, the panels were dried for 8 h in a 30 m long kiln with calorifiers set to dry at 75 °C. The process was optimised, reducing the time to 3.5-4 hours. A new kiln, the Orkan II project, has now been set up, where the panels are dried in 15 minutes with the help of heat pumps. Once dried, the panels are sent to quality control, where they are sawed, sanded, or milled. Another waste stream is formed in the sanding process to get the material to the correct thickness. This waste stream is sanding dust (SD) and contains wood and partially hydrated cement particles. This stream is collected at an outside storage facility (Fig. 2.7) to avoid any respiratory risks for workers.

Figure 2.7. Sanding dust extraction system; 1) panel treatment facility with cutting and sanding equipment; 2) Dust filters and separators; 3) sanding dust storage room [77].

The sanded panels are also varnished and painted if necessary. Quality control is subjective; 3 workers visually look for defects and grade them from 1 to 3, with the 1st grade being the highest quality. The defective panels are stacked in a separate pile.

Defective panels account for around 3-5 % of total production. They are mainly used as pallet material to reduce pallet indentation on qualitative panels. After sorting the panels, they go to the final warehouse (Fig. 2.8), where the finished products are stored, awaiting transport to their destination.

Figure 2.8. Warehouse for finished products.

Use and Properties

Cewood Ltd. panels are mainly divided into acoustic and construction panels. Acoustic panels are widely used in public and residential interior design; according to the manufacturer [78], they are eco-

friendly and harmless to health. Owing to their natural composition and outstanding properties, they are widely used in premises with increased acoustic load, where sound insulation and noise absorption are of the essence:

- Offices, public spaces and private homes;
- Schools, kindergartens, universities;
- Sports facilities, swimming pools, spa;
- Music halls, theatres, and cinemas;
- Recording studios, TV and radio stations;
- Industrial premises and warehouses.

Acoustic panels are manufactured using a variety of wooden fibres (length, width, thickness) and panels in different thicknesses. The manufacturing uses white cement, and the panels are coloured afterwards if necessary.

Construction panels, on the other hand, are made with grey cement and have the widest application in different building constructions:

- In the construction of buildings – walls, partitions, coverings, roof construction, etc.
- In building insulation – especially in wooden frame buildings, renovation of old buildings, and increasing building thermal inertia;
- Sound insulation solutions and permanent shuttering in monolithic buildings.

Construction panels are offered in 4 different thicknesses, but with a fixed wood fibre thickness of 3 mm. The comparison of both categories for 3 mm wood-wool cement panel properties can be found in Table 2.1.

Table 2.1

Comparison of acoustic and construction panel properties [78]

Property	Unit of measurement	Acoustic panels			Construction panels			
Thickness	mm	25	35	50	25	50	75	100
Size (standard panel)	mm	2400x600; 1200x600; 600x600			2400x600			
Size (for suspended ceilings)	mm	1195x595; 595x595			Not applicable			
Dimensional tolerance (EN 13168)		L4; W2; T2; S2; P2			L3; W1; T2; S2; P2			
Weight	kg/m^2	10.5	14.5	19.5	11.5	19.5	28	35
Density	kg/m^3	420	410	390	460	390	370	360
Thermal resistance	m^{2}K/W	0.35	0.5	0.75	0.35	0.75	1.1	1.5
Thermal conductivity	W/(m·K)	0.066			0.066			
Specific heat	J/(kgK)	Not applicable			1300			
Flexural strength (EN 12089)	kPa	≥ 1300	≥ 1000	≥ 700	≥ 1300	≥ 700	≥ 500	≥ 300
Compressive strength (EN 826)	kPa	≥ 300	≥ 200	≥ 200	≥ 300	≥ 200	≥ 150	≥ 100
Chloride content (EN 13168)	%	≤ 0.06 class C3			≤ 0.15			
Reaction to fire (EN 13501-1:2007)		B-s1, d0			B-s1, d0			

The wood-wool cement panel (WWCP) manufacturing uses just a few materials without special additives or chemicals. The binder material is either white cement or alternative grey cement of type CEM I 52.5R. The water for the binders' reaction is regular industrial water. Only spruce wood is used as a bio-based aggregate, with a 14-22 cm diameter at the short end. Varnishes and colours are water-based and selected based on the customer's preferences.

2.2. Waste from WWCP Manufacturing

A few waste streams can be identified in the manufacturing process of wood-wool cement panels (fig. 2.9). Wood-wool may fall over the line after wetting. However, the volumes are small and can be added back without compromising the quality of the final product. Once the wet wool is mixed with cement, it is conveyed through a conveyor system. The material accumulates on the conveyor belts and falls to the floor, where it is collected as 1. fraction waste (Fig. 2.9a) and denoted production line waste (PLW) for further research. This fraction can be pressed into blocks or, after curing, broken down and used as a filler to produce biocomposites. The mixture is then passed along the production line to be smoothed, compacted, and cut into 2.4 m-long panels. This sawing process produces a second stream of waste, which is drier but can also be pressed into blocks (Fig. 2.9b). This fraction contains shorter wood fibres with cement. After sawing, the panels are left to cure for 1 day in storage; then, they are demoulded, sawed and milled to the required dimensions. At this stage, a third and fourth stream of wastes are produced (Fig. 2.9c and d), and the material is taken to the curing warehouse for further curing for 2-4 weeks. After curing, the panel is taken to the quality control department, where it is sanded and milled for the correct thickness and prepared for painting or varnishing. This stage generates sanding dust (SD) (Fig. 2.9e). Fig. 2.9c and 2.9e fractions are discharged through filters to a storage facility outside the factory.

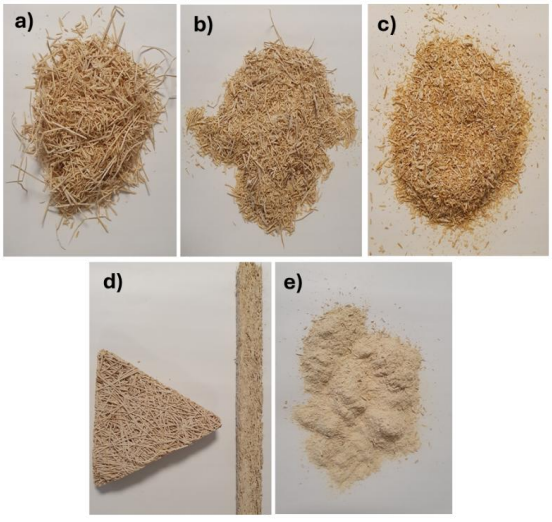

Figure 2.9. Different waste streams from the manufacturing plant.

2.3. Possible Application of the Waste

The wood-wool cement panel (WWCP) manufacturing process generates waste with promising potential for biocomposite development. This research focuses on an innovative approach using coarse wood-wool waste (Production Line Waste) as a bio-based aggregate, while modified sanding dust is a binder.

Using longer wood-wool fibres as bio-based aggregate marks a shift from their traditional application as reinforcement in composites. These fibres' irregular shape and size suggest they could create effective mechanical interlocking within the composite structure. Their natural arrangement is likely to create micro-voids throughout the material, potentially enhancing the final product's acoustic and thermal insulation properties.

Applying modified sanding dust as a binder takes advantage of its fine particle size and unique composition. This dust fraction contains both wood and cement particles from the original manufacturing process, which, after modification, could create an effective binder. Combining modified wood components and residual cement particles is expected to contribute to an overall composite performance.

This approach efficiently utilises both extremes of the waste stream - the coarsest and finest fractions - to create a potentially sustainable and economically viable biocomposite. Further research will optimise the sanding dust modification process and determine ideal binder-to-filler ratios to develop biocomposites from this industrial waste. The potential prototype schematic is represented in Figure 2.10.

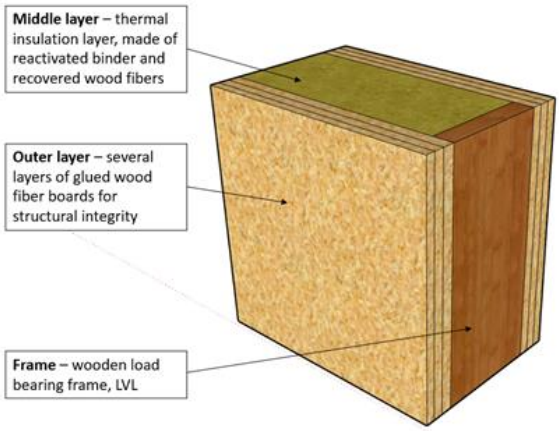

Figure 2.10. Prototype schematic.

3. REACTIVATION OF PORTLAND CEMENT-BASED BINDERS

As the demand for sustainable materials grows, researchers increasingly focus on the reactivation and recycling of Portland cement-based binders, particularly from cement-based production waste [19,79]. This multifaceted technological approach aims to revive the binding properties of partially hydrated cementitious materials, transforming waste into valuable construction resources [80,81]. By implementing advanced reactivation technologies, the industry can address significant environmental concerns such as waste generation, resource depletion, and carbon emissions [6]. The reactivation technologies involve complex processes like recycling, crushing, milling and processing waste materials to create innovative building solutions that conserve natural resources, reduce energy consumption, and minimise environmental impacts [82]. This approach represents a promising pathway to mitigate the environmental degradation associated with traditional cement production, offering a more sustainable alternative to conventional material extraction and manufacturing processes [83].

3.1. Reactivation by Milling

Mechanical activation through various milling processes has emerged as a promising strategy for enhancing the reactivity of cement-based binders. Research by Seghir et al. [84] demonstrated that ball milling can decrease cement particle sizes from 10-50 μm to less than 5 μm, significantly increasing specific surface area and reactivity. The mechanical energy applied during milling introduces lattice strain and creates structural defects, accelerating chemical interactions during hydration. However, these processes are not without challenges. Energy consumption, equipment wear, and potential particle agglomeration represent critical considerations researchers must address to optimise milling-based reactivation strategies [85]. Collision, planetary ball milling, and vibratory milling have demonstrated remarkable capabilities in modifying material characteristics at the microscopic level. These techniques primarily work by reducing particle size, breaking up conglomerates, increasing surface area, and inducing structural modifications that promote more rapid and extensive hydration reactions [86,87].

Planetary ball mills are well known and have been used to reduce particle size in laboratory and pilot experiments for decades. The processes in planetary ball mills are complex and highly dependent on the material being processed, so the optimum grinding conditions must be considered for each system [88]. Planetary ball mills have the same design as other ball mills - a grinding vessel filled with material and rotated on its axis (Fig. 3.1).

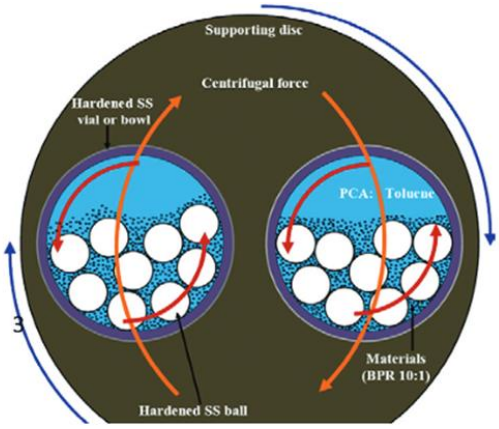

Figure 3.1. Operating principle of planetary mills [89].

However, their unique design uses centrifugal force and the Coriolis effect to grind materials very fine or even micron size [90]. When the grinding bowl in a planetary ball mill rotates on its axis opposite the disc (usually called the sun wheel) attached to it, these forces play. These opposing motions and the differences in rotational speed produce a strong combination of frictional and impact forces necessary for a fine grinding level. Planetary ball milling would lead to a reduction in the size of particles due to the high impact forces generated by the grinding balls inside the rotating jars. As a result, larger particles would be broken down into smaller sizes.

This method increases the surface area of the particles due to the intense grinding action and can produce finer particles. It may also lead to a more uniform particle size distribution [91]. Planetary ball mills are well-suited for grinding samples in laboratory conditions. However, the high costs involved in scaling up to industrial production have led to the high use of planetary mills at an industrial scale [92].

Collision milling, also known as impact milling or impact grinding, is a particle size reduction technique that employs a high-speed rotor or impeller to create impacts between particles and against stationary surfaces [93]. In this process, the material is fed into the path of the rotating impeller (Fig. 3.2), where the high velocity imparts kinetic energy to the particles, causing them to collide with each other or with impact surfaces, making it particularly suitable for grinding friable or crystalline materials [94]. While various equipment types, including hammer mills and fluid energy mills, can be utilised for this method, the high-speed impact forces can efficiently break down particles into smaller sizes. However, they may result in a more heterogeneous particle size distribution than other milling methods, with the final particle size range dependent on factors such as rotor speed, impact force, and feed rate [94].

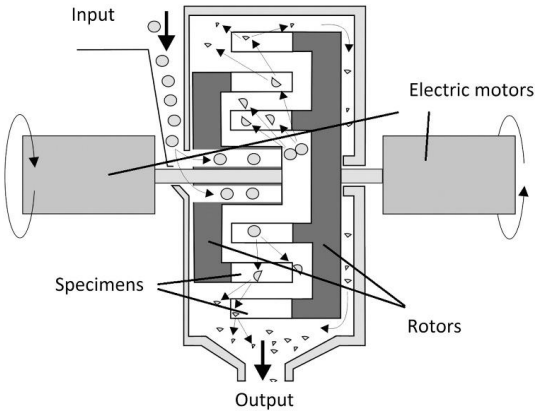

Figure 3.2. Schematic representation of the collision milling process [95].

A vibrating mechanism in a vibration ball mill sets the grinding chamber into oscillatory motion. A schematic of the vibratory mill is given in Figure 3.3. This motion causes the grinding media (usually balls) and the material to impact and rub against each other, leading to the size reduction of the material. Vibration mills operate at relatively low frequencies but at high amplitudes. The impact and friction generated by the vibrating motion facilitate efficient grinding of various materials. Vibration ball mills are often used for the synthesis of complex materials. They can also be used for wet grinding.

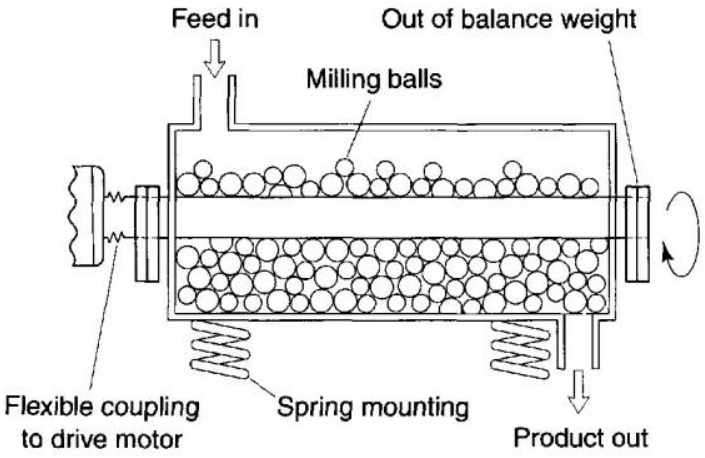

Figure 3.3. Vibratory mill schematic diagram [96].

Vibration ball milling would also reduce particle size, albeit through a mechanism different from planetary ball milling. In vibration ball milling, the oscillatory motion of the grinding chamber causes the grinding media and particles to impact and rub against each other, leading to size reduction. The amplitude and frequency of the vibrations can influence the extent of particle size reduction and the resulting particle size distribution. Vibration milling may produce particles with different shapes and surface characteristics compared to other milling methods, potentially affecting the reactivity and performance of the material.

Each milling method would impart specific particle changes, influencing their size, shape, surface properties, and reactivity. The choice of milling method would depend on factors such as the desired particle size distribution, the specific properties required for the cement application, and the equipment available for milling.

3.2. Reactivation by Heat Treatment

Cement recycling has also focused on the reactivation of the binder through heat treatment. Heat treatment techniques aim to change the cement stone's physical and chemical properties and restore the cement's activity, thereby reducing the need to use newly manufactured cement [97].

The opportunities offered by heat treatment are significant in terms of sustainability and resource-saving. The recovery and reuse of cement stone can reduce the demand for raw materials, thereby reducing energy consumption, greenhouse gas emissions, and the overall environmental impact of cement production [98]. In addition, it can potentially reduce construction and demolition waste by diverting it from landfills and using a circular economy approach [99].

Different heat treatment methods are being explored in cement recycling to reactivate the binder. Pyrolysis, a process involving applying high temperatures without oxygen, can break down organic matter and remove contaminants, thus recovering a clean cement paste [100]. Calcination, conversely, involves heating cementitious materials at high temperatures to induce chemical changes that release carbon dioxide and recover reactive calcium compounds [101]. Incineration, a more extreme heat treatment, removes organic matter and impurities and uses the energy released during combustion [102].

The reactivation of cement binders has gained significant attention in recent years as a promising approach to reducing environmental impact and resource consumption in the construction industry [103,104]. Among various thermal treatment technologies, muffle furnaces and rotary kilns have emerged as promising options due to their versatility, precise temperature control capabilities, and scalability potential [105]. While muffle furnaces are widely used in laboratory-scale investigations due to their excellent temperature uniformity and controlled atmosphere, rotary kilns offer advantages in continuous operation and industrial-scale processing, making them suitable for large-scale cement reactivation applications [106]. Microwave heating has attracted significant attention due to its unique ability to heat material components selectively. Choi et al. [107] demonstrated that microwave treatment could effectively reactivate hydrated cement paste, increasing compressive strength by up to 30 % compared to untreated samples. The mechanism involves selective molecular vibration and dielectric heating, which can more efficiently redistribute moisture and activate chemical bonds than traditional heating methods.

Muffle furnaces are characterised by their enclosed heating chamber surrounded by electrical heating elements and thermal insulation materials. They are typically capable of operating at temperatures between ambient and 1200 °C, with some specialised models reaching up to 2000 °C [108]. The chamber design ensures uniform heat distribution and prevents direct contact between the sample and heating elements or combustion gases, enabling precise control of the thermal treatment conditions. Modern muffle furnaces often incorporate advanced features such as programmable temperature profiles, multiple heating zones, and sophisticated proportional-integral-derivative control systems, facilitating detailed studies of cement reactivation kinetics and optimisation of treatment parameters [109]. In cement reactivation applications, muffle furnaces play a vital role in studying

various cement types' thermal behaviour and reactivation potential, where controlled heating environments are essential for investigating phase transformations and chemical reactions [9]. Research has shown that cement materials subjected to thermal treatment in muffle furnaces at temperatures ranging from 400 ℃ to 900 ℃ exhibit significant changes in their mineralogical composition and reactivity, with optimal reactivation temperatures varying depending on the cement composition and initial conditions [9,110]. The precise temperature control and uniform heat distribution characteristics of muffle furnaces make them particularly suitable for studying the dehydration and rehydration processes in cement materials and investigating the formation of new phases during thermal treatment [111].

Rotary kilns, in contrast, consist of a rotating cylindrical vessel slightly inclined to the horizontal, with the material moving through the kiln due to rotation and gravity [112]. These systems typically operate at temperatures ranging from 400 ℃ to 1000 ℃, with the duration controlled through kiln rotation speed and inclination angle [113]. The continuous operation capability and efficient heat transfer characteristics of rotary kilns make them suitable for industrial-scale cement reactivation processes. At the same time, their design allows for good mixing and uniform heating of the material [114]. Advanced rotary kiln systems often feature variable speed drives, automated feed systems, and temperature monitoring and control systems to ensure optimal processing conditions [115].

3.3. Chemical Reactivation Methods

The recycling of hydrated cement presents a significant challenge in sustainable construction materials management. As cement-based materials age and degrade, their original binding properties diminish, necessitating innovative chemical approaches to restore their functional characteristics. The primary objective of chemical reactivation is to recover and revitalise the binders within hydrated cement, transforming waste materials into valuable resources [116].

Chemical leaching techniques have emerged as a promising method for reactivating hydrated cement. Specific acid-based solutions, including dilute hydrochloric acid and sulfuric acid, have shown the potential to break down calcified structures and release reactive calcium ions [10,117]. These treatments partially dissolve the existing hydration products, creating new reactive sites that can potentially reform cementitious bonds [118].

Chelating agents represent another innovative approach to cement reactivation. Compounds such as ethylenediaminetetraacetic acid and citric acid have demonstrated remarkable capabilities in modifying the chemical structure of hydrated cement. A study by Popov et al. [119] revealed that these chelating agents can effectively extract and redistribute calcium compounds, potentially restoring some of the original binding capabilities of aged cement materials. The mechanism involves creating soluble metal complexes that disrupt the existing mineral structure, allowing for the potential reformation of cementitious compounds [120].

Electrochemical treatment has emerged as a sophisticated method for chemical reactivation. Research by Lizarazo-Marriaga et al. [121] explored the use of controlled electrical currents with alkaline solutions to modify the chemical composition of hydrated cement. This approach involves applying a specific electrical potential to induce ion migration and restructuring of the cement matrix. Preliminary studies suggest electrochemical methods can potentially reactivate dormant hydration products and improve some of the material's mechanical properties.

Enzymatic approaches represent a novel and environmentally friendly strategy for cement reactivation. Rosewitz et al. [122] investigated specialised enzymatic treatments that can selectively break down and restructure the mineral composition of hydrated cement. These biological catalysts show promise in creating more sustainable building methods, potentially offering lower environmental impact than traditional chemical approaches [123].

The effectiveness of chemical reactivation methods varies significantly depending on multiple factors, including the original cement composition, the age of the material, and specific chemical treatment parameters. Challenges remain in developing universally applicable reactivation strategies that can be economically and environmentally viable on a larger scale. Critical considerations include the energy consumption of chemical treatments, potential material degradation, and the ultimate performance of reactivated cement [124,125].

Future research directions focus on developing more sustainable and precise chemical reactivation techniques. Emerging studies are exploring combined approaches integrating multiple chemical and physical methods to create more comprehensive reactivation strategies. The ultimate goal is to develop technologies to transform waste cement materials into valuable, high-performance construction resources [126,127].

3.4. Environmental and Economic Considerations

Cement reactivation technologies' environmental and economic aspects present a complex of sustainability challenges and technological innovations. While effective in enhancing cement reactivity, milling technologies demonstrate additional energy consumption concerns. The carbon footprint of milling techniques is primarily associated with electricity consumption, with studies suggesting that ball and jet milling can increase CO_2 emissions by approximately 30-50 % compared to traditional cement production methods [7,128,129]. However, the potential for material recovery and reduced raw material extraction presents a counterbalancing environmental benefit [11].

Although cement recycling and binder reactivation through thermal treatment are promising, a few challenges must be addressed to exploit their potential fully. One of the main challenges is the development of efficient and cost-effective technologies capable of treating large volumes of cement waste streams. Thermal treatment methods' scalability and economic viability must be carefully assessed to ensure their practical applicability in industrial settings [101]. Heat treatment offers compelling opportunities for sustainable construction practices [130]. It was observed during the literature search that temperature can be used as a reactivation option in cement recycling. At elevated temperatures, the hydrated compounds in cement dehydrate, and with the rehydration of these compounds, it is possible to return some binding capacity [99].

By recovering and reusing cement paste, these approaches contribute to the conservation of natural resources, waste reduction, and transitioning to a circular economy [131]. The economic considerations are particularly critical, with initial equipment costs for advanced heating technologies ranging from 250 000 € to 1.5 million €, creating a significant barrier to widespread adoption [132]. Despite these challenges, the potential for improved material performance and extended lifecycle presents a compelling economic argument.

Chemical reactivation methods introduce a different set of environmental and economic considerations. Using chemical agents for cement reactivation involves complex trade-offs between material recovery and potential environmental contamination. Studies by Ho et al. [133] demonstrate

that chelating agents and specialised chemical treatments can reduce raw material consumption by 25-35 %, presenting a significant environmental advantage. However, the economic viability remains challenging, with chemical treatment costs estimated at 150-300 €/t of processed cement [134]. Environmental concerns are particularly pronounced, with potential risks of chemical waste generation and water contamination requiring comprehensive management strategies.

Further research, technological advances, and supportive policy frameworks [135] are essential to maximise the potential of cement recycling for binder reactivation. Through innovative approaches, the construction industry can move closer to achieving its sustainability goals while minimising its environmental impact [136]. While reactivation technologies offer substantial environmental benefits, their ecological footprint must be carefully assessed. Energy consumption, emissions during processing, and potential waste generation are critical factors [137]. Economic viability studies suggest that well-designed reactivation processes can generate significant cost savings, potentially reducing material procurement expenses by 20-40 % compared to traditional manufacturing approaches [138].

Despite considerable advances, substantial knowledge gaps remain in cement binder reactivation. Future research should focus on:

1. Developing more energy-efficient reactivation technologies;
2. Understanding the long-term performance of reactivated materials;
3. Scaling up laboratory-proven techniques for industrial application;
4. Exploring hybrid activation methods combining multiple approaches.

The reactivation of Portland cement-based binders represents a promising frontier in sustainable materials engineering. Researchers can transform waste materials into valuable resources by integrating mechanical, thermal, and chemical approaches, contributing to more environmentally responsible construction practices.

4. MATERIALS AND METHODS

4.1. Raw Materials

Binder

Sanding Dust (SD)

In the final manufacturing stage of wood-wool cement panels, cured and dried panels undergo cutting, edge treatment, and size calibration through sanding. To mitigate potential health risks from airborne dust exposure during sanding, a dust extraction system (Fig. 3.7) minimises dust and maintains a clean work environment. The amount of SD can vary depending on factors such as the wood fibre type, board density, sandpaper grit size, and sanding techniques employed. The manufacturing waste generated by Cewood Ltd. is shown in Figure 4.1. The continuous grinding and filter cleaning processes produce about 4 to 5 m^3 of SD daily.

Figure 4.1. SD was generated during the manufacturing of the wood-wool cement panels.

The final sanding step is critical for achieving the desired surface finish during wood-wool cement panel manufacturing. This sanding process generates dust particles, and understanding their morphology is essential for occupational health and safety and process optimisation. The SD primarily consists of two key components: wood fibre particles and partially hydrated cement particles. Wood fibre particles are typically elongated and fibrous, resembling strands or flakes. Their morphology can vary based on wood species, fibre processing, and board manufacturing methods.

In contrast, cement particles are usually much finer, appearing as small, irregularly shaped grains or fragments. Cement particle morphology is influenced by cement type, fineness, and hydration state.

The size distribution of SD particles can range widely, from larger, visible coarse particles to finer particulates that may become airborne. Coarse particles tend to settle quickly due to their size and weight. In contrast, fine particles can remain suspended in the air for longer, posing potential inhalation hazards that require mitigation measures like dust extraction systems.

Due to electrostatic forces or moisture absorption, SD particles may agglomerate or clump together, especially finer particles. These agglomerates can affect dust behaviour during handling and transport, potentially impacting the effectiveness of dust control measures.

The granulometric composition of the SD was determined by sieving according to ASTM C136 [139] prior to processing. The sizes range from 0.125 mm to 11.2 mm. Figure 4.2. summarises the average granulometric composition of the SD as a green-shaded area, with the average distribution indicated by a dashed line. The analysis shows that approximately 31 % (± 8.5 %) of the material consists of the finest fraction (0-0.125 mm). The fraction between 0.125-0.25 mm comprises about 26 % of the material, bringing the cumulative passing percentage to 57 % (± 9.2 %) for particles under 0.25 mm. Moving up in size, the 0.25-0.5 mm fraction contains roughly 18 % of the material, and the 0.5-1 mm fraction adds another 15 %, bringing the total passing to approximately 90 % (± 5.9 %) for particles under 1 mm. The remaining fractions contribute minimally to the overall distribution, with particles between 1 and 8 mm making up about 10 % of the total material. The shaded area in the graph represents the variation in particle size distribution, with the greatest spread observed in the middle range (0.125-0.5 mm). This analysis indicates that the sanding dust predominantly comprises particles smaller than 1 mm, with the majority falling below 0.5 mm.

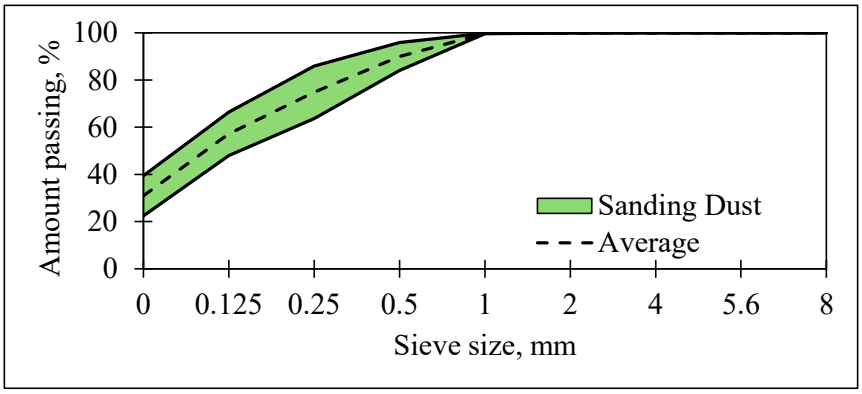

Figure 4.2. Granulometric composition of the sanding dust used for disintegration.

The sieving and the determination of the granulometric composition of the material were done in the laboratory. Figure 4.3. shows the visual appearance of each fraction of SD, where it can be observed that in figures 4.3a, b and c, large wood particles with cement hydrates can be observed. In figures 4.3g and h, a distinct powdery material can be observed, which is a mixture of fine cement and wood particles.

Figure 4.3. The appearance of sand dust by a fraction (a) 5.6-8 mm; (b) 4-5.6 mm; (c) 2-4 mm; (d) 1-2 mm; (e) 0.5-1 mm; (f) 0.25-0.5 mm; (g) 0.125-0.25 mm; (h) 0-0.125 mm.

Semi-industrial sieving was done at Cewood Ltd. to gather larger quantities of the sieved fractions of the material. The SD collected was subjected to sieving with a mesh size of 0.2 mm. A 0.2 mm mesh size was selected to remove larger wood particles, so only fine powder remains, and it is further used for mechanical activation and heat treatment in the laboratory. SD and the sieving apparatus are shown in Figure 4.4.

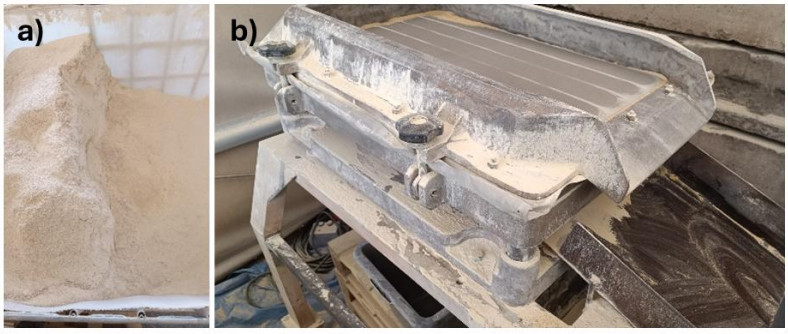

Figure 4.4. (a) Sanding dust before sieving; (b) vibration sieving apparatus.

Both fractions of the sieved material are given in Figure 4.5. Figure 4.5a shows a fraction of > 0.2 mm, while 4.5b shows a fraction of < 0.2 mm. The fraction below 0.2 mm is used as the binder precursor for further tests and experiments. Fractions above 0.2 mm can be used as bedding material.

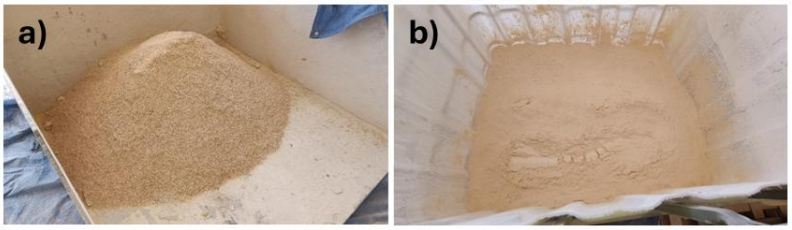

Figure 4.5. a) Fraction > 0.2 mm; b) SD particles below 0.2 mm.

Cewood Ltd. is constructing a rotary drum sieve to separate SD particles. This device will enable the separation of fractions during the filtration stage, allowing fine particles to be reused to manufacture

new panels as a supplementary cementitious material. Various mesh sizes can be applied to achieve the desired particle separation.

The SD originates from sanding the wood-wool cement panels after 3 to 4 weeks of hardening. 72 wt. % of sawing dust is smaller than 0.25 mm; therefore, hydrated cement's fine nature and high content could be used as supplementary cementitious material or as a material for reactivation and production of new binder.

The sieved and unsieved sanding dust was also subjected to Thermogravimetry/Differential Thermal Analysis (TG/DTA) to determine what decomposed and dehydrated at different temperatures. The sieved and unsieved SD were also ground for 10 minutes in a planetary mill to obtain a more homogeneous material for the TG test. Figure 4.6 shows the TG/DTA curves. The curves on the left show the percentage change in mass and the derived mass change on the right.

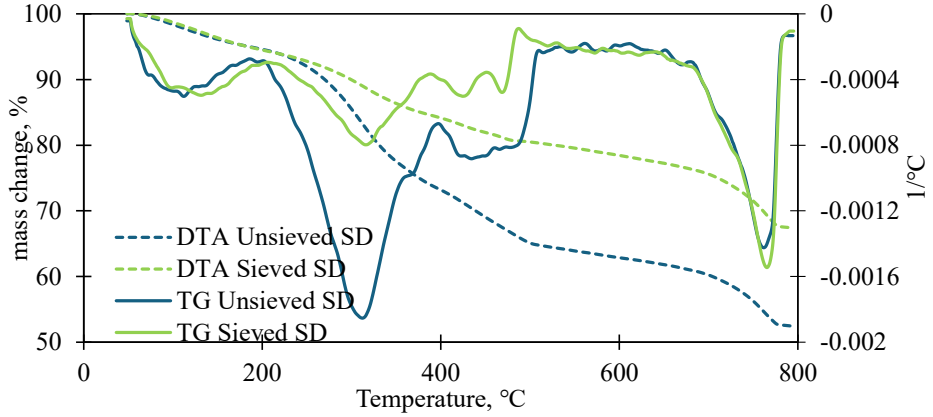

Figure 4.6. TG/DTA curves for sieved and unsieved SD.

The blue curve is the unsieved SD, where it can be observed that heating the sample to 800 °C reduces the mass by 47.5 %, of which 18 % are wood particles decomposed in the temperature range of 200-370 °C. The green curve is a sieved SD curve with a total mass loss of 32.6 %, of which 10 % comprises wood particles decomposed in the temperature range 204 to 390 °C. Table 4.1 shows the explanations of the DTA peaks.

Table 4.1

Explanation of TG/DTA peaks

Unsieved		Sieved		Reference
50-203	free water, C-S-H gel dehydration	50-215	free water, C-S-H gel dehydration	[140–149]
204-364	Pyrolysis of organics, dehydration of C-S-H	216-390	Pyrolysis of organics, dehydration of C-S-H	[142,143,145,147–149]
398-455	CH dehydration, Char combustion	391-451	CH dehydration, Char combustion	[142–144,146–152]
455-514	Portlandite dehydration	452-488	Portlandite dehydration, $Ca(OH)_2$ dehydration	[140–142,144,147–153]

514-685	C-S-H dehydration, $Ca(OH)_2$ decomposition	489-684	C-S-H dehydration dehydroxylation, $Ca(OH)_2$ decomposition	[142,150,153]
685-785	Decarbonisation of calcite ($CaCO_3$), release of CO_2	685- 788	Decarbonisation of calcite ($CaCO_3$), release of CO_2	[140,142,144,146–152,154]

Fine particles from SD are proposed as raw materials for developing binders to make biocomposites with production line waste (PLW) as filler. Binder recovery was examined through two different approaches:

1. Mechanical reactivation with different types of milling;
2. Heat treatment from 300 to 1200 ℃.

CEM II/A-LL 42.5 N

CEM II/A-LL 42.5 N is a hydraulic binder according to EN 197-1. This type of cement (Schwenk, Latvia) is produced by blending ordinary Portland cement clinker (80-94 %) with limestone as a secondary constituent. The limestone component typically comprises 6-20 % of the cement composition. The rest are minor additional constituents, resulting in 0-5 % of the total cement composition [155].

Using limestone as a supplementary cementitious material helps reduce the overall carbon footprint of the cement manufacturing process compared to traditional ordinary Portland cement. Limestone is a naturally occurring mineral ground with the OPC clinker to produce the final product [155].

The cement offers > 10 MPa of early compressive strength (2 days) and ≥ 42.5 MPa on the 28th day. The initial setting for this material is 60 minutes with soundness of ≤ 10 mm and sulphate and chloride content of ≤ 3.5 and ≤ 0.1 %, respectively.

Filler

Production line waste (PLW)

During the manufacturing of wood-wool cement panels, several types of waste are generated at different stages of the process. Firstly, in the initial stage of preparing wood-wool, waste may arise from the trimming and shaping of raw wood materials into the desired fibre lengths, resulting in sawdust and wood scraps. Secondly, during the mixing stage, where wood-wool fibres are combined with cement and water, an excess mixture or spillage may occur, leading to waste material that cannot be used in the final product (production line waste). Additionally, trimming and cutting excess material from the formed panels to achieve the desired dimensions can generate waste (sanding dust) in moulding. Any defective or rejected panels that do not meet quality standards and end-of-life products may contribute to waste generation (scraps). Overall, the waste generated while manufacturing wood-wool cement panels consists primarily of wood scraps, sawdust, excess mixture, and trim material, which can potentially be recycled or repurposed to minimise environmental impact. The manufacturing waste generated by Cewood Ltd. is given in Figure 4.7.

Production line waste

Figure 4.7. PLW generated during the manufacturing of the wood-wool cement panels.

This research used production line waste (PLW) as the bio-based aggregates for biocomposites. The material is spruce wood fibres ranging from 5 to 200 mm in length, from 1 to 1.5 mm in width and from 0.5 to 0.8 mm in thickness. The average bulk density is 250 kg/m^3. The wood fibres are coated with hydrated cement from the manufacturing process. Most of the fibres have been separated from one another, except for small patches of fibres that have clumped together. The bio-based aggregates are checked before the sample preparation to avoid these hardened patches of material for a more homogenous structure. The visual appearance of the material can be observed in Figure 4.8.

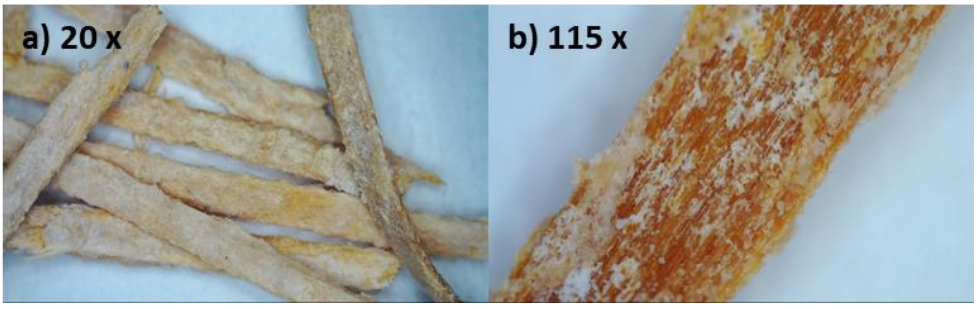

Figure 4.8. The visual appearance of PLW at different magnifications.

According to Bumanis et al. [131], two secondary raw materials can be obtained from the wood-wool cement panel manufacturing facility. A coarse waste comes from the production line, where, 24 hours after initial curing, wood-wool cement panels are demoulded, and material remains are collected as waste. It is characterised by high cement content together with wood-wool fibres. The other coarse material is from damaged, low-quality, end-of-life wood-wool cement panels. They can be crushed mechanically by a hammer mill or jaw crusher. The particle size is similar for both processed materials, but the crushing efficiency may differ. Hammer mills proved more efficient in producing bio-based aggregates from damaged panels, with 89 % of the milled material smaller than 10 mm. These findings highlight three distinct waste streams from wood-wool cement panel manufacturing: production line waste, panel scraps, and end-of-life panels that can be effectively processed into consistently sized particles. The different characteristics of these materials, like particle size distribution and cement

content, play crucial roles in determining their potential applications as secondary raw materials in future research and composite formulations.

Hemp Shives (HS)

Hemp shives produced by Natural Fibre (Natūralus Pluoštas, Lithuania) were utilised as additional bio-based aggregates. The hemp shives supplied by this regional processor are the only ones suitable for making building materials. According to Table 4.2, 64 % of the particles range from 1 to 20 mm. The shives have an 80 kg/m^3 bulk density and a 115 kg/m^3 compacted bulk density. The compacted bulk density is more pertinent to the material manufacturing process than the bulk density. When the shives are crushed, their thermal conductivity is 0.043 W/(m·K). Hemp shives were added to lower the overall thermal conductivity of the biocomposites.

Table 4.2

Hemp shive particle size distribution [156]

Fibres, %	Skins/ Leaves, %	Part. <1 mm, %	Shives							
			1-5 mm, %	5-10 mm, %	10-15 mm, %	15-20 mm, %	20-25 mm, %	25-30 mm, %	30-35 mm, %	35-40 mm, %
2.49	11.18	2.00	13.57	21.95	15.47	12.77	4.58	5.64	4.19	6.15

4.2. Modification of the Sanding Dust

Sanding dust was sieved according to the process depicted in section 4.1. The sieved fraction below 0.2 mm was used as the binder precursor and processed in three mechanical mills and two heat treatment methods (Fig. 4.9). For the investigation of the effect of milling on binder quality, sieved sanding dust was subjected to mechanical processing of:

- Planetary ball milling using Retsch PM 400 (Germany, 2007) of 1 to 30 minutes at 300 RPM;
- Collision milling using Desi Desi-16C (Estonia, 2016) at 25 and 50 Hz frequencies for 1, 3, and 5 milling cycles);
- Vibration milling using Stankomash MV-20 (Russia, 2016) for 5, 10, 15, and 20 minutes.

Assessing different reactivation mechanisms, sieved sanding dust was subjected to heat treatment using two methods:

- Heating in Uterna W-80 muffle furnace (Lithuania, 2012) for 1 to 5 hours at 300, 450, 600, 750, 900, 1050, and 1200 °C at the heating rate of 10 °C/min;
- Heating in Keramserviss KLR rotary kiln (Latvia, 2009) at 450 and 900 °C at 5° at 25 RPM.

Altogether, 37 different binders were developed using 5 processing methods. Each binder is characterised by its representing thesis chapter.

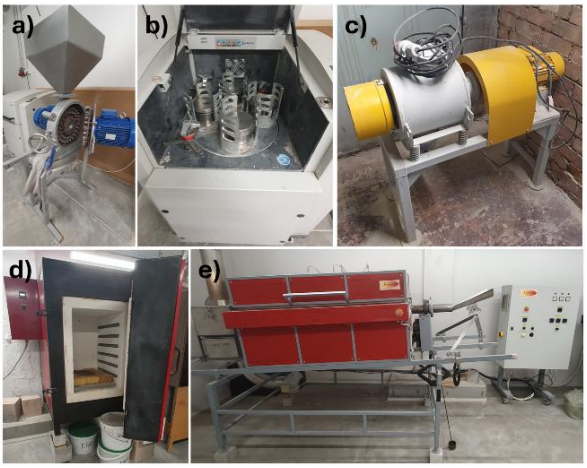

Figure 4.9. Sanding dust processing apparatus: a) disintegrator, b) planetary ball mill, c) vibration mill, d) muffle furnace, and e) rotary kiln.

4.3. Characterisation Techniques

For Binder

Granulometry of sanding dust was performed according to ASTM C136 [157] standard with a mesh size of 0.125 mm to 8 mm.

The material was mixed on an ASTM C143 impact table in a moistened cone and compacted to prevent air entrapment. Twenty jolts were performed with the impact table, and the reaction of the cone to this force was observed. The cone's diameter was measured, and the cone's viscosity was analysed.

The compressive strength was tested using a Zwick Z100 universal testing system (ZwickRoell, Kennesaw, GA, USA) at a 0.5 mm/min test speed. The specimens were dried at 45 ℃ for 16 hours before testing to remove excess water from the structure, and were tested on days 7, 14, and 28.

Cumulative particle size distribution of the materials obtained by laser diffraction (CILAS 1090, range 0.10-500.00 µm).

X-ray fluorescence (XRF) is a widely used analytical method for determining the elemental composition of a sample. The XRF was performed on a Rigaku ZXS PrimusIV.

X-ray diffractometric (XRD) analysis of the material was carried out using a BRUKER-AXS D8 ADVANCE X-ray diffractometer (Bruker, Billerica, MA, USA) using CuKα1 and CuKα2 radiation in the 2θ range from 10 to 70°.

The physical properties of the temperature effect on the raw materials were determined using a Mettler-Toledo TGA1/SF thermogravimetric analysis machine. At the same time, Mettler STARe software helps to obtain thermograms through which mass changes and release of destruction products can be determined. The mode used for the analyses is 25-900 ℃ at 10 ℃/min in an air environment.

For Biocomposites

Biocomposites were characterised using a digital microscope, Veho HDMI Dual Vision Digital, to assess the biocomposites' macrostructure and visual appearance.

Thermal conductivity was measured with a LaserComp FOX600 heat flow meter; according to the standard LVS EN 12667 guidelines, the test settings were 0 ℃ for the upper and 20 ℃ for the lower plate.

The compressive and flexural strength of the bio-based building materials was tested at 0.5 mm/min using Zwick Z100 universal testing equipment (ZwickRoell, Kennesaw, GA, USA) according to BS EN 12390-3 standard. The compressive strength was measured in two directions, and samples were tested parallel and perpendicular to the forming direction (3 samples for each direction). An ultimate load was used to calculate compressive strength for the parallel direction. The compressive strength test was performed until 10 % and 20 % relative deformations in the casting direction (according to the LVS EN 826). A load of 10 % of the sample's height was used for the perpendicular direction. The flexural strength was measured in 1 direction – perpendicular to the forming direction for 3 parallel samples to account for variability.

4.4. Life Cycle Assessment

The environmental evaluation of the developed materials was conducted using the Life Cycle Assessment (LCA) approach. Calculations were performed in SimaPro with the Ecoinvent 3.8 database. The primary goal was to compare the biocomposites made with existing insulation materials based on their thermal insulation properties. The functional unit for the base scenario was set at 1 m^3. An additional functional unit was chosen for biocomposites to compare their thermal insulation effectiveness based on the U-value of 0.18 $W/(m^2K)$ per m^2 of either biocomposite or wall assembly.

Four different manufacturing scenarios were assessed, which have been described in Table 4.3. Sanding dust (SD) was a precursor material for the first three scenarios. The fourth scenario portrays a commercial cement (CEM II/A-LL 42.5 N) for data comparison. The first three scenario materials were modified sanding dust, a waste generated during wood-wool cement panel manufacturing. In this study, the environmental impact of these waste products was assumed to be zero, meaning the impact of the developed materials stems solely from other components. The results of the climate change impact are derived from the EN 15804 + A2 Method V1.03. System boundaries included product stage - A1 to A3. The main limitation to this LCA is energy consumption for production processes - for now, this biocomposite is in a development phase and thus is produced on a laboratory scale; however, in the best-case scenario, this material would be produced on an industrial scale onsite on Cewood Ltd. Industrial-scale energy consumption data is needed to compare developed materials to traditionally used materials for comparable results.

Table 4.3

Scenarios for the manufacturing of materials

Binders Scenario	Description
Reactivation with a vibration mill (V-20min)	The SD was milled for 20 minutes (+5-minute discharge) using a vibration mill (1.5 kWh). Process losses are not considered.
SD heated at 450 ℃ (M-450-2)	The SD was heated for 4 hours at 450 ℃.
SD heated at 600 ℃ (M-600-2)	The SD was heated for 4 hours at 600 ℃.
CEM II/A-LL 42.5 N	CEM II cement was purchased and transported from *Brocēni*, Latvia.

It was assumed that all material manufacturing occurred within the Cewood Ltd. facility in *Jaunalūksne*, Latvia; therefore, transportation was only considered for CEM II. The input data for the environmental evaluation of the developed materials is provided in Table 4.4.

Table 4.4

Input data in SimaPro for environmental evaluation

Name	Water, kg	CEM II, kg	Electricity, kWh	Transport, km	Heat, kg CO_2 eq.
Vibro (0.05)	17	-	7.14	-	-
Vibro (0.15)	57	-	24.11	-	-
Vibro (0.5)	196	-	83.33	-	-
450 (0.05)	48	-	-	-	26.67
450 (0.15)	70	-	-	-	39.00
450 (0.5)	148	-	-	-	82.34
600 (0.05)	67	-	-	-	39.48
600 (0.15)	81	-	-	-	48.01
600 (0.5)	131	-	-	-	77.89
CEM (0.05)	20	5	-	299	-
CEM (0.15)	31	31	-	299	-
CEM (0.5)	70	70	-	299	-

For reactivation with a vibration mill (V-20min), the SD was milled for 20 minutes (+5 minute discharge) using a vibration mill (1.5 kWh). In 20+5 minutes, 2.1 kg of SD can be milled. Thus, to mill 1 kg of SD, 0.30 kWh of electricity is needed. The Latvian electricity mix is used from the Ecoinvent 3.8 database.

SD heating was done using a laboratory-scale oven; however, all binder production is assumed to be done onsite within the Cewood Ltd. facility. Considering that, at the time, there was no such process, it was not possible to measure the energy consumption of the heating process for industrial ovens. To use heating data, which would be more like industrial processes, data from 9 articles [158–166] was collected - significantly higher and lower values were removed, and the average value for emitted CO_2 eq. emissions during the industrial heating process were taken from the rest.

Comparisons were made with traditionally used building materials. Life cycle assessment results for these materials were taken from previous studies and adapted to match the functional unit used in this work [167], which is 1 m^2 of wall with U-value 0.18 W/(m^2K). A wall assembly with a wooden frame was made to compare developed biocomposites (0.05) with traditional building materials (see Table 4.5.). The approximate thickness of the wall assembly is 36-39 cm.

Table 4.5

Wall assembly input data

Material	Thickness, mm	Amount, kg
Wooden frame	-	6.3
Spun planks	25	17.5
Developed insulation material	257-280*	92.4-122.1*
Frontrock wool	30	1.8
Anti-wind film	-	-
Wood-wool cement panel	50	21.0

*Depending on the binder type in the biocomposite.

This chapter has documented the materials, experimental processes, and techniques adopted for developing and characterising the novel cementitious binders and the created biocomposites. The selection of wood-wool cement panel manufacturing waste and the control over mixing, curing, and testing parameters were paramount in ensuring the robustness and reproducibility of the generated data. With the methodological framework thoroughly established, the subsequent chapters (5.-7.) will present and analyse the experimental findings derived from these procedures, evaluating the performance and properties of the developed materials.

5. MILLING EFFECT ON THE REACTIVATION OF THE SANDING DUST

All the samples using milling methods followed a similar mix design, which is visualised in Figure 5.1. Their respective thesis chapters explain the differences in mix design and sample preparation.

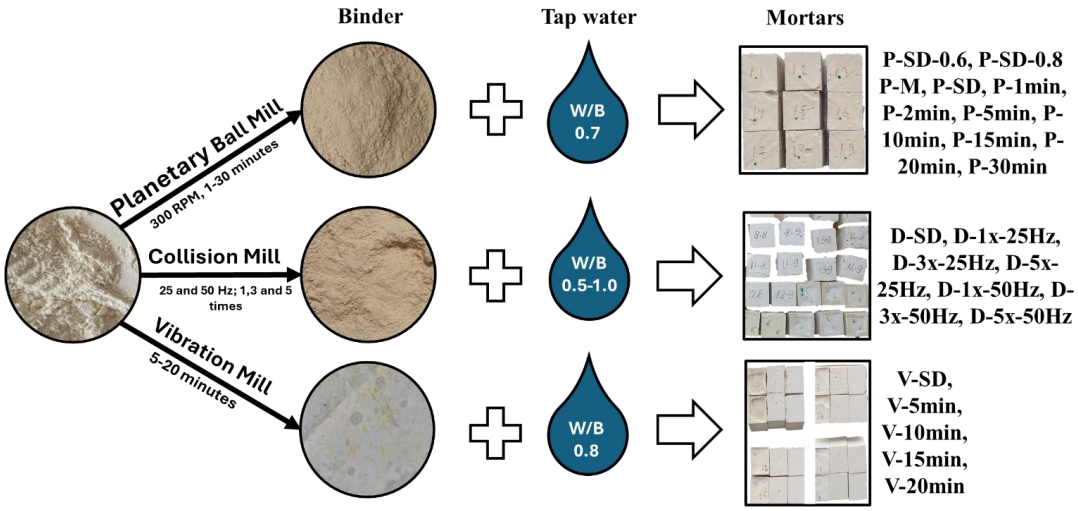

Figure 5.1. Visualisation of the mix designs of milling methods experiments.

5.1. Sanding Dust Reactivated by Planetary Ball Mill

Mix Design and Sample Preparation

Using sanding dust (SD) processed in a planetary ball mill as the binder according to the process mentioned in 4.2., 11 compositions were created, of which 2 were created as references for comparison. The compositions differed in the added W/B ratio of the sanding dust and its milling duration. The 1 to 30-minute range allowed us to observe the effects of short-term to longer-term milling on workability, setting time, and compressive strength development of the sanding dust. The 300 RPM speed represents a balance between achieving effective grinding force and preventing excessive heat buildup or damage to the SD, as optimal grinding conditions depend highly on the specific material being processed.

For all sample series, the W/B ratio was adjusted to a flowability between 15 and 20 cm after 20 jolts on the impact table. The required amount of SD was added to the mixing vessel, the appropriate mass of water was added, and the mortar was mixed for 2 minutes with a hand mixer on the slowest setting. After mixing, the flowability of the mortar was determined. If the flowability does not reach the 15-20 cm zone, additional water is added to the mortar and mixed until the water is incorporated into the mortar. The flowability is retested until the flowability falls within the required zone after 20 jolts. In parallel with the flowability, the setting time is determined using a Vicat apparatus. The mixed material was formed in moulds (20 × 20 × 20 mm), covered in plastic film and left to cure at ambient

conditions (atmospheric pressure, 20 ± 2 °C) for 2 days. The samples were demoulded, labelled, and placed in 3 curing conditions, out of which curing was done in a sealable plastic bag to ensure sufficient moisture.

The samples were tested for compressive strength on days 7, 14, and 28. For each testing time, 6 replicate samples were tested to obtain more reliable results.

Results

Effect of Curing Conditions

Curing conditions are an important factor for cement hydration and the setting of the samples. A total of 3 different curing conditions were tested:

- Curing in room conditions involves exposing samples to normal room conditions (22 ± 2 °C, RH < 50 %).
- Curing in water (22 ± 2 °C, RH = 100 %) was carried out by immersing the samples in water for the remainder of the curing period. The samples were removed from the water and dried in a drying chamber before testing.
- Curing in high humidity (22 ± 2 °C, RH > 90 %) environment consisted of placing the samples in a plastic sealable bag, where moisture desorbs from the samples, creating a microclimate inside the bag, increasing the ambient relative humidity and providing more moisture for the samples to cure.

The material properties summarised for SD are shown in Table 5.1. Both samples were made using a W/B ratio of 0.6, and different flowability was obtained. This is due to the treatment of the material by milling the SD for 10 minutes in a planetary ball mill. It can be observed that the P-SD-0.6 has a flowability of 17 cm after 20 jolts. P-SD-0.6 was tested as reference baseline data, and P-M was a 10-minute milled SD, as the milling effect is the main objective of the reactivation of SD. If SD is treated in a planetary mill, obtaining a more viscous material with a flowability of 21 cm after 20 jolts is possible compared to P-SD-0.6. The setting start time is 4 hours for P-SD-0.6 and 3 hours for P-M. The total setting time was about 15 hours for both series.

Table 5.1

Summary of W/B ratios and material properties

Sample	W/B ratio	Flowability after 20 jolts, cm	Setting time start, hours	Total setting time, hours
P-SD-0.6	0.6	17	04:00:00	15:15:00
P-M		21	03:00:00	15:00:00

Comparing the mechanical data obtained on day 28 (Fig. 5.2), the highest compressive strength was obtained for the P-M sample cured in water and in a high-humidity environment, reaching 2.2 and 1.9 MPa. Curing in room conditions resulted in lower compressive strength – 1.6 MPa. Summarising the data obtained, conclusions can be made that this type of material cures better in high-humidity environments. For samples P-SD-0.6, compressive strength showed similar tendencies but within a marginal error. In some samples, Argalis et al. [168] observed that samples cured in water experienced

dissolution due to weak binding and a loss of structural integrity, a phenomenon also seen in this study with samples undergoing deformation and eventual breakdown. To avoid this problem, the samples cannot be cured in water. As the curing in a high-humidity environment showed marginally similar results, the curing conditions for the following samples will be chosen as curing in a high-humidity environment.

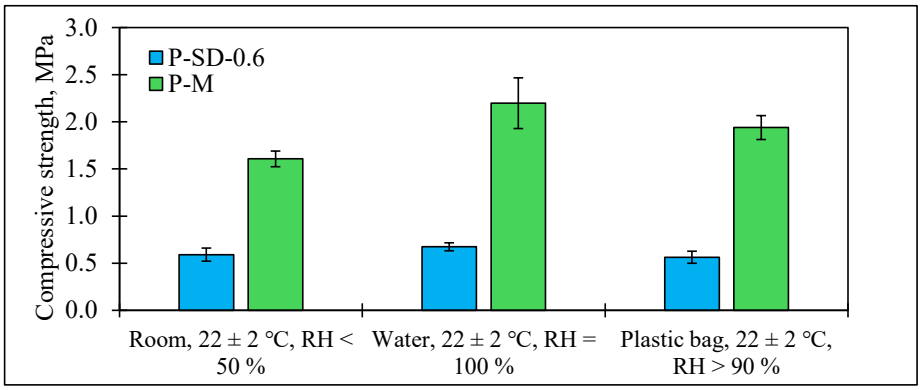

Figure 5.2. Summary of mechanical properties on day 28 under different curing conditions.

Effect of W/B Ratio

To analyse the effect of the W/B ratio of the SD, 2 mortar compositions were made. To make P-SD-0.6 and P-SD-0.8, untreated SD was used as the binder, and the values representing 0.6 and 0.8 were the tested W/B ratios. The samples were cured in a high-humidity environment (22 ± 2 °C, RH > 90 %) to induce sufficient moisture during the curing process, referring to the results of the previous section.

P-SD-0.6 was more workable as the flowability was in the optimal 15-20 cm zone after 20 jolts. For sample P-SD-0.8, the flowability was above 20 cm, making the material more on the slurry side. At the same time, segregation of SD and water was observed, indicating the upper limit of the water-to-binder (W/B) ratio for SD.

The compiled data on the compressive strength of the P-SD-0.6 and -0.8 samples are visualised in Figure 5.3. The data are similar and vary within the error margins on days 7 and 14. On day 28, the P-SD-0.8 showed a 90 % higher compressive strength than P-SD-0.6. The observations show that increasing the W/B ratio can improve the compressive strength on day 28 due to enough water, which helps the continued hydration of the cement in the samples. As the wood can absorb water, it helps the cement hydration by desorbing the needed water for the reaction. For future research, a W/B ratio of 0.6-0.8 will be used as the base reference ratio.

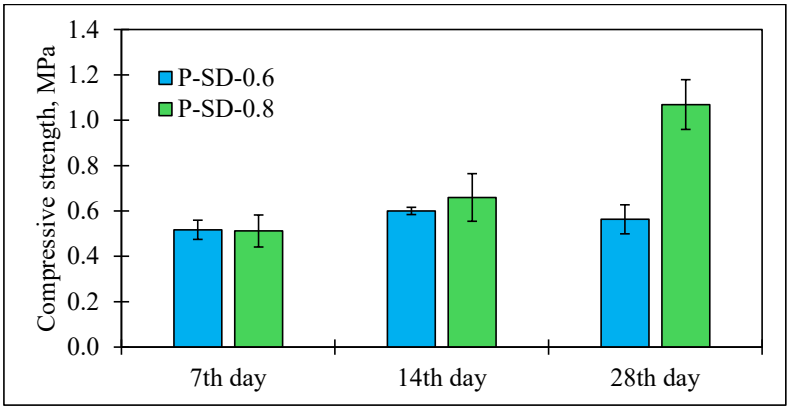

Figure 5.3. Effect of W/B ratio on compressive strength.

Effect of Milling Time

During the milling process, the SD particles are milled into a finer fraction, which can improve the cement's overall strength by breaking up hydrated conglomerates to free unhydrated cement particles or initiating fine-grained cement particles that will act as fine-grained crystallisation centres [169,170]. Using the same W/B ratio, it is possible to directly infer the effect on the material's workability as the milling time varies. A W/B ratio 0.7 was chosen based on the previous section's data. According to Argalis [168], the material has no mineralogical change when the milling time is changed (1-30 min). The change occurs at the physical level as the conglomerates break up and particle size decreases.

The flowability of the reference P-SD sample (unmilled) differs notably from that of the milled SD samples. The unmilled P-SD exhibited a flowability of 11.5 cm. However, milling the SD even briefly—just 1 minute—significantly improves workability, achieving a flow of 17 cm after 20 jolts on the impact table. Extending milling time to 10 minutes (P-10min) further enhances flowability to 19.5 cm, facilitating easier casting into moulds. While milling beyond 10 minutes slightly reduces flowability, the material remains workable, with the P-30min sample reaching 15 cm after 20 jolts.

In terms of setting time, extending milling up to 10 minutes has minimal impact on the initiation of setting. The P-10min sample began setting the earliest, 32 minutes post-mixing. Although the P-5min sample initiated setting later, it completed the process in the shortest total time—22 hours and 58 minutes. The P-SD had the slowest setting rate, reaching the final set after 24 hours and 15 minutes. Notably, SD milled for more than 10 minutes demonstrated a significantly faster setting, with the P-30min mix achieving a full set in just 4 hours.

The P-10min sample demonstrates the best overall balance, considering workability and setting performance. It offers excellent flowability (19.5 cm) for easy handling, casting and a fast setting initiation, making it the most suitable choice for practical applications.

The data reflects that increasing the milling time of the raw materials can lead to a more easily workable material and a faster setting start time, but does not significantly affect the total setting time. Figure 5.4 shows the visual appearance of the samples.

Figure 5.4. The visual appearance of the samples on day 28, a) P-SD; b) P-10min; c) P-15min; d) P-20min; e) P-30min.

Looking at the compressive strength results (Fig. 5.5), there is a trend of increasing compressive strength from day 7 to day 28, which means that the hydration of the cement was qualitative [171]. Comparing the mechanical data obtained for reference P-SD and the rest of the P-series samples, it can be observed that milling the SD in the planetary ball mill positively affected the compressive strength, improving it as the milling time increased.

The P-SD reached 0.85 MPa on day 7, while on day 28, the strength increased to 1.65 MPa. When the SD was processed for 1 min in a planetary mill (P-1min), the compressive strength reached 1.15 MPa on day 7 and increased to 1.96 MPa on day 28. The compressive strength reached 3 MPa on the 28th day after 2 minutes of milling (P-2min). The strength changes within the error range for 5 minutes of milling (P-5min) compared to P-2min. Increasing the milling time to 10 minutes (P-10min) resulted in compressive strength of 2.40 MPa on day 7 and 4.26 MPa on day 28. Milling the SD for 15 minutes (P-15min) increases the compressive strength to 3.44 MPa on day 7 and 6.50 MPa on day 28. There is no significant difference in compressive strength with increasing time to 20 and 30 minutes, and compressive strength changes within a marginal error. The P-30min showed a compressive strength of 3.68 MPa on day 7 and 6.98 MPa on day 28. The findings reveal that increasing the milling time above 15 minutes does not increase the compressive strength. Nevertheless, it is possible to increase the compressive strength by 4 times by processing SD in a planetary ball mill.

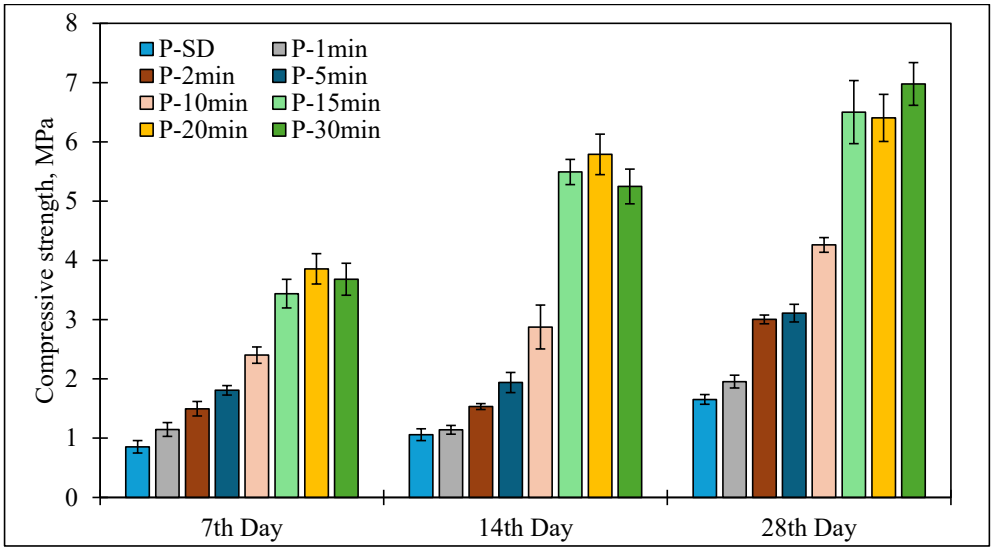

Figure 5.5. Summary of compressive strength results for the planetary ball milling method.

The processing of SD with planetary ball milling has been extensively characterised in [168], where Argalis et al. additionally characterised the effects of the addition of superplasticiser, the sifting and drying of the SD, and how the mortars of SD behave with different flowability.

5.2. Sanding Dust Reactivated by Collision Milling

Mix Design and Sample Preparation

25 Hz and 50 Hz frequencies, with 1, 3, and 5 milling cycles, were selected to investigate impact intensity and duration effects on sanding dust (SD) reactivation. Collision milling reduces particle size via high-speed impacts, where frequency (Hz) controls impact rate. Using 25 Hz and 50 Hz allows comparison of impact intensities. Milling cycles control the material's cumulative impact exposure, varying milling duration [93–95].

Sanding dust (SD) processed in the disintegrator was used as the binder. A total of 7 compositions were created that differed in the sanding dust processing frequency and cycles described in section 4.2. Three compositions were made with a 25 Hz processing frequency and three with 50 Hz, and the processing cycles varied between 1, 3 and 5 times. Sample D-SD was made as a reference sample for data comparison. The sample notation representing its milling process is depicted in Table 5.2.

Table 5.2

Sample denotation

Processing parameters	Sample denotation
Sieved sanding dust	D-SD
Sieved sanding dust milled 1 time at 25Hz	D-1x-25Hz
Sieved sanding dust milled 3 times at 25Hz	D-3x-25Hz
Sieved sanding dust milled 5 times at 25Hz	D-5x-25Hz
Sieved sanding dust milled 1 time at 50Hz	D-1x-50Hz
Sieved sanding dust milled 3 times at 50Hz	D-3x-50Hz
Sieved sanding dust milled 5 times at 50Hz	D-5x-50Hz

For all compositions, a W/B ratio of 0.7 was used. The required mass with the SD was added to the mixing bowl as the binder, and the appropriate amount of water was added. The mixture was mixed with a mixer for 2 minutes on the slowest setting. The mixed material was placed in moulds (20 × 20 × 20 mm) and left to cure in a high-humidity environment (20 ± 2 ℃, RH > 90 %) for 5 days; then, the samples were demoulded, labelled and left to cure at room temperature.

The samples were tested for compressive strength on days 7, 14, 28, 90 and 180. For each testing time, 4-5 replicate samples were created to obtain more reliable results.

Results

The compressive strength has been compiled in Figure 5.6. The compressive strength improves from 0.5 MPa to 4-5 MPa. On day 7, all samples exhibited relatively low compressive strength of approximately 0.5 MPa, with minimal variation between the milling times and frequency. This suggests that the initial processing method did not impact early-stage strength development.

As time progressed, there was a consistent increase in compressive strength across all samples. By day 14, compressive strength increased slightly to around 0.8-1.0 MPa; by day 28, it reached approximately 1.5 MPa. The strength development continued significantly, reaching about 2.5-3.0 MPa by day 90.

The most remarkable strength development occurred between days 90 and 180, where all samples showed substantial increases in compressive strength. Interestingly, on day 180, there was a notable differentiation between processing conditions. The D-3x-50Hz and D-5x-50Hz demonstrated higher compressive strengths at around 4.9-5.0 MPa compared to their 25 Hz counterparts (D-3x-25Hz and D-5x-25Hz), reaching 3.6-3.8 MPa. The D-SD sample reached 3.9 MPa on day 180, showing that milling at 25 Hz is insufficient to propose any enhancement to compressive strength.

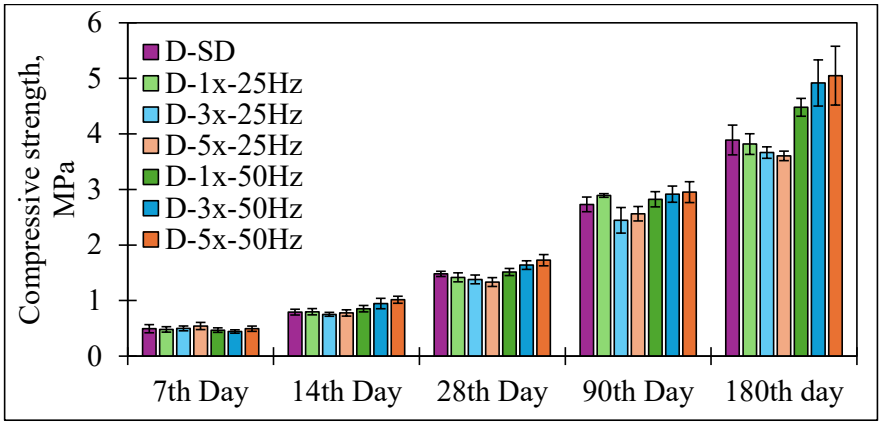

Figure 5.6. Compilation of the compressive strength.

The role of processing frequency (25 Hz vs 50 Hz) becomes more pronounced at later stages. By day 180, the 50 Hz processed samples show higher compressive strengths than the 25 Hz samples. This could indicate that SD processed at a higher frequency might lead to better particle distribution or more efficient reactivation of the partially hydrated cement in the SD. The multiple processing cycles (3 and 5 times) at 50 Hz enhance this effect.

From a materials science perspective, this behaviour might be explained by several mechanisms:

- The increasing strength suggests retarded but continued cement hydration processes and better bonding between wood particles and cement over time;
- The higher frequency processing (50 Hz) creates a more optimal particle size distribution or exposes more surface area [172,173] of the partially hydrated cement for new hydration reactions [174].

The D-SD shows moderate performance in compressive strength, suggesting that mechanical processing in low frequencies does not influence the material's properties. The compressive strength of the samples did not achieve the feasibility threshold, as the strength gain was not high enough for the spent energy.

5.3. Sanding Dust Reactivated by Vibration Mill

Mix Design and Sample Preparation

The proposed binder was sanding dust milled for 5, 10, 15 and 20 minutes in a vibration mill, and 4 compositions were created. Additionally, 1 more composition was made as a reference. The selection of 5, 10, 15, and 20 minutes for vibration milling was chosen to investigate the effect of milling duration on sanding dust (SD) reactivation. Vibration milling employs oscillatory motion to cause impact and rubbing between grinding media and particles, reducing the size [91,96]. Varying the milling time allows for examining how the duration of this impact and rubbing influences flowability, setting time, and compressive strength development.

A W/B ratio of 0.8 was used for all sample series to observe differences in flowability, which further affects the material's workability and other physical parameters. The required amount of mass with the processed SD was added to the mixing vessel, the appropriate mass of water was added, and the mortar

was mixed for 2 minutes with a hand mixer on the slowest setting. After mixing, the flowability of the mortar was determined.

In parallel with the flowability, the setting time was determined using a Vicat device. The mixed material was placed in moulds (20 × 20 × 20 mm), and the moulds were wrapped in plastic film to ensure the moisture in the samples did not evaporate. The moulds were left to cure at ambient conditions (20 ± 2 ℃) for 5 days; then, the samples were demoulded, labelled, and placed in a resealable plastic bag (22 ± 2 ℃, RH > 90 %) to ensure sufficient moisture for further curing for 23 days.

The compressive strength of the samples was calculated on days 7, 14, and 28. For each testing time, 6 samples were created to repeat the data to obtain more reliable results.

Results

A summary of the rheological properties can be found in Table 5.3. When the milling time is 5 minutes (V-5min), the flowability reaches 12 cm, which makes workability difficult. After milling SD for 10 minutes (V-10min), the flowability reaches 16 cm. By increasing the milling time to 15 minutes (V-15min), the flowability increases to 16.25 cm, and the material is easily workable. After 20 minutes of milling (V-20min), the flowability decreased to 13.25 cm, which, like 5-minute milling, makes workability difficult.

Table 5.3

Summary of W/B ratio, rheological properties and setting time with increasing milling time

Sample	Water/Binder ratio	Flowability after 20 jolts, cm	Setting start, hours
V-SD	0.8	14.5	04:00
V-5min		12	03:28
V-10min		16	02:28
V-15min		16.25	>04:00
V-20min		13.25	>03:00

Summarising the compressive strength results, there is an increase in compressive strength with increasing milling time. Figure 5.7 shows the compressive strength data. The lowest compressive strength was obtained for V-SD, achieving 0.8 MPa at day 28. Marginally close V-5min achieved 0.9 MPa. Sample V-15min achieved 1.4 MPa; the highest compressive strength was obtained for the V-20min, reaching 1.6 MPa on day 28. From these results, it can be concluded that increasing the milling time of SD can increase the compressive strength of the mortars.

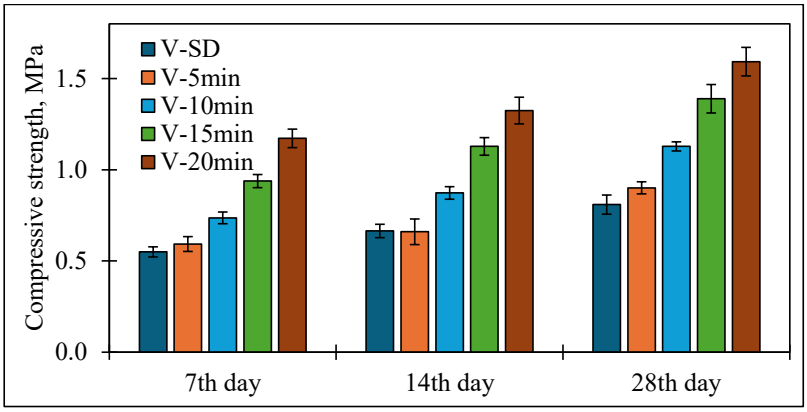

Figure 5.7. Summary of compressive strength results for V-series samples.

The compressive strength differences remain significant and even appear to widen slightly with time. This suggests that more prolonged milling influences strength development based on the rheological and compressive strength data.

5.4. Chapter Summary

The experimental investigation of sanding dust reactivation using a planetary ball mill yielded several findings. High-humidity (22 ± 2 °C, RH > 90 %) and water-curing (22 ± 2 °C, RH = 100 %) environments produced the most favourable compressive strength results, with samples reaching 1.9 MPa and 2.2 MPa, respectively, outperforming room-condition curing at 1.6 MPa. For practical applications, high-humidity curing was selected as the preferred method to avoid potential dissolution issues associated with water curing while maintaining optimal strength development. The water-to-binder ratio emerged as an important parameter, increasing from 0.6 to 0.8, resulting in a 90% improvement in 28-day compressive strength. This enhancement can be attributed to sufficient water availability for continued cement hydration. However, at the 0.8 ratio, material segregation was observed, establishing this as the upper workability threshold and confirming an optimal W/B range of 0.6-0.8 for future investigations.

Perhaps the most compelling results came from varying the milling duration. Just one minute of milling significantly improved workability, increasing flowability from 11.5 cm to 17 cm, with peak flowability of 19.5 cm achieved after 10 minutes. The milling process also accelerated the setting time, with the P-30min sample setting after just 4 hours compared to 24 hours for the reference P-SD sample. Compressive strength showed improvements with an increased milling duration of up to 15 minutes. P-SD achieved 1.65 MPa at 28 days, while P-15min reached 6.50 MPa—a nearly fourfold increase. Interestingly, extending milling beyond 15 minutes yielded no significant additional strength gains. These results conclusively demonstrate that mechanical processing via planetary ball milling can transform sanding dust, typically considered a waste material, into a viable cementitious material with improved workability and strength properties. The optimal processing method involves 15 minutes of milling with a W/B ratio between 0.6-0.8 and curing in high-humidity (22 ± 2 °C, RH > 90 %) conditions. Despite these improvements, the laboratory-scale process lacks industrial scalability.

Using the collision milling method, the compressive strength of the mortar samples improved, increasing from 0.4 MPa on day 7 to 1.3-1.7 MPa on day 28 to 5.0 MPa by day 180. Notably, SD

processed at 50 Hz achieved slightly higher compressive strength than those processed at 25 Hz or the D-SD sample on day 28. However, the strength gain is not proportionate to energy input, making this method unfeasible for industrial applications.

Vibration milling revealed optimal processing parameters, with 15-minute milling providing the best workability (16.25 cm flowability), while longer milling times delayed setting (from 2:28 hours at 10 minutes to >4 hours at 15 minutes). Compressive strength increased with milling duration, reaching 1.6 MPa at 28 days for sample V-20min. This method proved efficient and scalable, making V-20min suitable for further experimentation.

Comparing the three mechanical activation approaches reveals distinct performance-to-scalability relationships. While planetary ball milling achieved the highest absolute strength (7 MPa at 28 days), its laboratory-scale nature limits industrial application. Collision milling reached moderate long-term strength (5 MPa at 180 days) but with unfavourable energy efficiency. Though yielding the lowest compressive strength (1.6 MPa at 28 days), vibration milling offers the most favourable combination of performance, energy efficiency, and scalability.

This chapter has documented the experimental investigations into various milling methods for the effective mechanical activation and processing of wood-wool cement panel manufacturing waste, aiming to derive a suitable cementitious binder. The analysis of mechanical strength and initial reactivity has revealed the impact of milling parameters on binder properties, achieving advancements in the material's latent hydraulic activity. While mechanical activation through optimised milling has yielded promising results, further enhancement of the binder's reactivity and performance is hypothesised to be achievable through heat treatment. Therefore, the subsequent chapter will determine the properties associated with applying heat to the sanding dust, aiming to further promote its pozzolanic and hydraulic reactivity for improved binder performance.

6. HEAT TREATMENT EFFECT ON THE REACTIVATION OF THE SANDING DUST

All the samples using heat treatment followed a similar mix design, which is visualised in Figure 6.1. Their respective thesis chapters explain the differences in mix design and sample preparation.

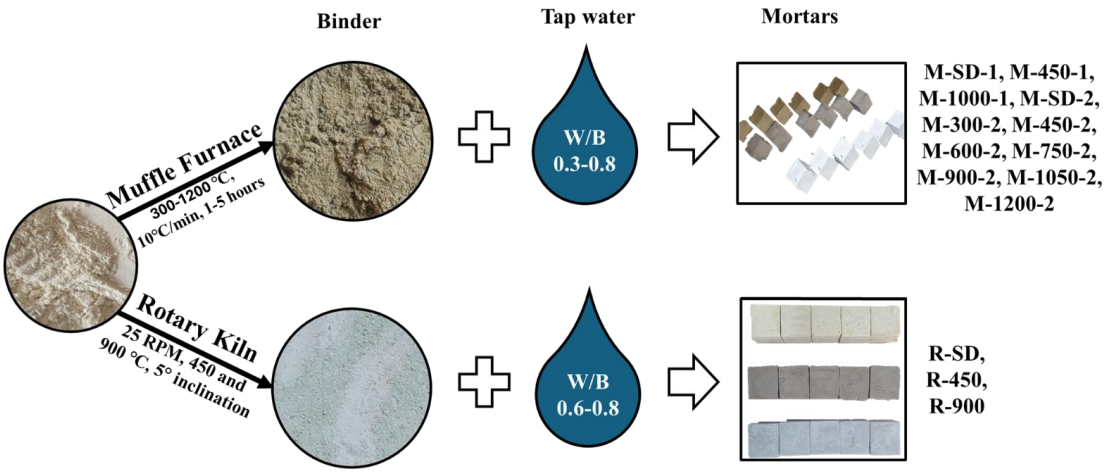

Figure 6.1. Visualisation of the mix designs of the heat treatment experiments.

6.1. Sanding Dust Reactivated by Heating in Muffle Furnace

Heat treatment was done in 2 phases. The first phase aimed to characterise the heat-treated SD properties in raw and hydrated states, preliminarily to understand if this processing method has potential. Based on the literature review [175,176], 450 and 1000 °C were found to be potential starting points in the heat treatment and were chosen as temperatures at which SD was heated. SD was heated for 3 hours at 450 °C and 1 hour at 1000 °C.

In the second phase of the heat treatment, the temperature range was broadened to see how it affected the SD. Temperature was chosen in increments of 150 °C, starting from 300 to 1200 °C, holding the selected temperature for 4 hours. 4 hours was considered sufficient time to heat the entire batch of material. The temperatures were chosen based on studies available in the literature [177,178] and the results of the previous phase.

Mix Design and Sample Preparation

Using sanding dust processed in a muffle furnace as the binder, 11 compositions were created for both phases. The compositions differed in the processing temperature and treatment duration.

Of the 1st phase

Mix designs of the 1st phase heating experiment are compiled in Table 6.1. Different W/B ratios were used to achieve the same workability.

Table 6.1

Mix design for the 1st phase muffle furnace samples

Sample	Sample denotation	Binder, mass parts	Water, mass parts
Sieved Sanding Dust	M-SD-1	1	0.75
450 ℃ Heated Sieved SD	M-450-1		0.60
1000 ℃ Heated Sieved SD	M-1000-1		0.80

Sample preparation for the 1st phase of heat treatment experiments was done using sanding dust (SD), and an appropriate amount of water (W/B ratio based on mix design) was added to the mixing vessel. The mixture was mixed for three minutes at 300 RPM with a hand mixer. After mixing, the mortar was poured into a ring of the Vicat machine for rheological properties, moulded (20 × 20 × 20 mm), covered with a plastic film, and set for three days at ambient conditions (23 ± 2 ℃). After the initial curing of 2 days, the samples were removed from the moulds, labelled, and placed in resealable plastic bags to retain moisture and ensure quality hydration. After being transferred to the bags, the samples continued to cure. The bags were unzipped 5 times when the samples required for testing were removed. In total, 5 parallel samples were tested on each testing day to reduce the error in the results.

Of the 2nd phase

The mix designs of the 2nd phase samples can be seen in Table 6.2. A total of 7 temperatures were selected. A series of reference samples were created and tested at each phase since differences in the reference results were observed. This means that the SD cannot be seen as a uniform waste but as a material that varies in composition depending on the material produced in the factory. The underscore and the number denote the sample of the phase concerned, as some samples have the same processing temperatures. Different W/B ratios were used to achieve the same workability.

Table 6.2

Mix design for 2nd phase muffle furnace samples

Sample	Sample denotation	Binder, mass parts	Water, according to EN 196-3, mass parts
Sieved Sanding Dust	M-SD-2	1	0.70
300 ℃ Heated Sieved SD	M-300-2		0.60
450 ℃ Heated Sieved SD	M-450-2		0.73
600 ℃ Heated Sieved SD	M-600-2		0.60
750 ℃ Heated Sieved SD	M-750-2		0.65
900 ℃ Heated Sieved SD	M-900-2		0.65
1050 ℃ Heated Sieved SD	M-1050-2		0.70
1200 ℃ Heated Sieved SD	M-1200-2		0.25

The samples were made similarly to 1st phase but using a Hubert automatic mixer on the slowest mode (140 RPM). The required amount of material for this stage, taken from the EN 196-3 standard, is 500 grams, which, mixed with the required amount of water (based on Schwenk's results and own experience), is mixed for 2 minutes, then stirred with a spoon to disperse all the material in the mixing bowl and continue mixing until homogeneous for 2-3 minutes. The mortar is moulded into a ring of

the Vicat apparatus, and 20 × 20 × 20 mm moulds are covered with plastic film. The samples were demoulded, labelled, and put in resealable plastic bags following the initial two-day curing period to maintain moisture and guarantee further curing. On each testing day, 3 parallel samples were tested to reduce the error of the results.

Results

The initial phase of this research yielded promising results in the processing of sanding dust (SD) using a thermal treatment method. Notably, the thermal processing of SD resulted in a range of materials, each exhibiting distinct colourations and properties, suggesting potential for diverse applications. Building on these findings, the subsequent phase of this research further confirmed the technical viability of thermally treating SD as a recycling strategy. The data acquired during this second phase provide valuable insights into the underlying physical, chemical, and mineralogical transformations within the SD during thermal processing. This understanding explains how the properties of this waste material are modified and evolve throughout the treatment, bringing them closer in character to those of virgin cement and thus highlighting its potential as a sustainable resource.

Of the 1st phase

In addition to analysing various parameters, it should also be mentioned that there are also visual differences between the raw materials and the mortars prepared from them. The visual appearance of raw materials can be seen in Figure 6.2. A change of colour from yellow to light grey can be observed. The M-SD-1 looks yellowish due to the wood. The M-450-1 looks dark grey; the colour is because, at 450 °C, the organics burn off; the organics contain carbon, which, after heating, colours the material dark grey. It should be noted that not all the organics have completely decomposed – ash particles are found in the mix. M-1000-1 additionally undergoes a calcium carbonate decomposition reaction. However, the colour is grey because it was held at a higher temperature, which caused the carbon in the organics to decompose completely, leaving the colour of M-1000-1 quite close to the colour of grey cement. The DTA graphs that further explain this fact are in Figures 4.6 and 6.11.

Figure 6.2. The visual appearance of raw materials heated at different temperatures.

A few observations can be made when comparing the cumulative particle distribution. A cement/limestone mix of 90 % Aalborg white cement and 10 % limestone is used for wood-wool cement panel production in the Cewood Ltd. manufacturing plant and was tested for its particle morphology. M-SD-1, M-450-1 and M-1000-1 were compared. Figure 6.3 shows the cumulative particle size distribution of cement/limestone. It can be observed that 90 % of the material is up to 28.89 µm in diameter, 50 % is up to 7.16 µm, and 10 % is up to 0.42 µm. The average particle size in this mixture is 11.06 µm.

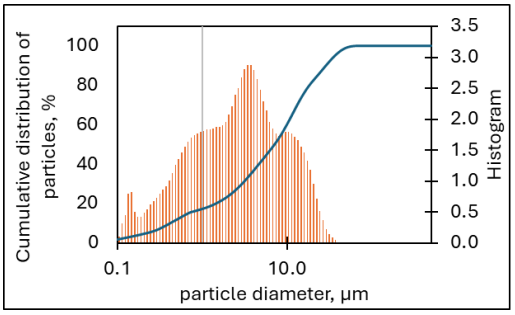

CEM I/$CaCO_3$ (90/10)	
D10, µm	0.42
D50, µm	7.16
D90, µm	28.89
Average particle size, µm	11.06

Figure 6.3. Cumulative particle distribution of CEM I/$CaCO_3$ mix.

The M-SD-1 (Fig. 6.4) sample exhibits larger particles throughout the distribution range, with particles approximately twice the size of the cement/limestone mix. 90 % of the M-SD-1 sample has an average particle size of 74.89 µm, 50 % of 16.61 µm, 10 % of 0.95 µm, and an average particle size of 29.21 µm. The size difference comes from the conglomerated hydration products and wood particles. The difference would affect the material's reactivity and performance in cement applications, as smaller particles generally provide greater surface area for hydration reactions [179].

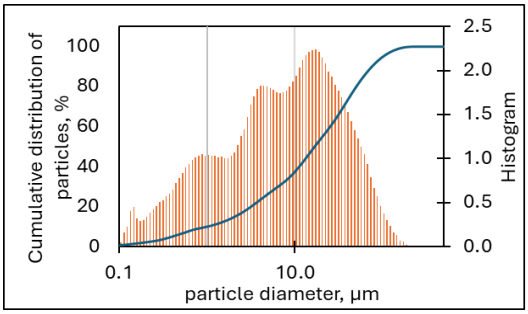

M-SD-1	
D_{10}, µm	0.95
D_{50}, µm	16.61
D_{90}, µm	74.89
Average particle size, µm	29.21

Figure 6.4. Cumulative particle distribution of M-SD-1.

Heat treatment of the M-450-1 (Fig. 6.5) reduces the overall particle size compared to M-SD-1. 90 % of the M-450-1 particles are up to 48.10 µm, 50 % are up to 12.46 µm, and 10 % are up to 0.47 µm. The average particle size was 19.11 µm, 35 % smaller than M-SD-1. As thermal treatment at this temperature causes partial decomposition or structural changes in the SD (TG/DTA graph Figure 6.11), particle morphology has also been affected.

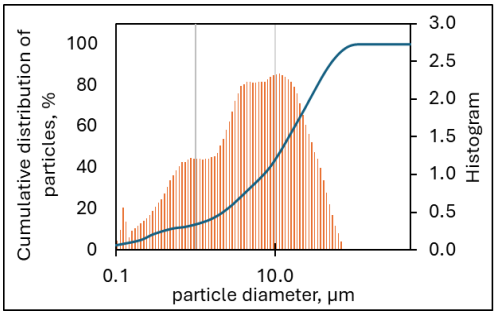

M-450-1	
D_{10}, µm	0.47
D_{50}, µm	12.46
D_{90}, µm	48.10
Average particle size, µm	19.11

Figure 6.5. Cumulative particle distribution of M-450-1.

Further increasing the heating temperature to 1000 °C continues this trend of particle size reduction (Fig. 6.6). The M-1000-1 showed that 90 % of the particles are up to 45.03 µm, 50 % are up to 13.00 µm, and 10 % are up to 0.27 µm, with an average particle size of 18.53 µm. Notably, the smallest particle in this sample reaches the smallest diameter among all tested materials, indicating that high-temperature treatment affects the particle size of the material.

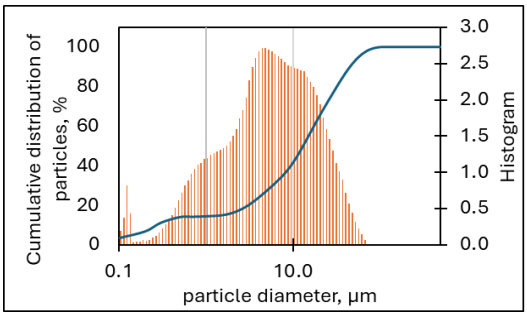

M-1000-1	
D_{10}, µm	0.27
D_{50}, µm	13.00
D_{90}, µm	45.03
Average particle size, µm	18.53

Figure 6.6. Cumulative particle distribution of M-1000-1.

Table 6.3 summarises the data obtained from the XRF apparatus. The table shows the most prevalent chemical compounds found in cement. The table compares data for cement (C), calcium carbonate ($CaCO_3$), and cement/limestone mixtures as reference data. Those are the same materials the manufacturing company uses. The analysis was also carried out for sieved sanding dust (M-SD-1) and sieved SD heat treated at 450 and 1000 °C (M-450-1 and M-1000-1). Comparing the data with the literature [180–186], the effect of heat treatment on M-SD-1 can be judged. The main oxides for comparison are CaO, SiO_2, Al_2O_3 and Fe_2O_3. Oxides of minor importance in this case are MgO, SO_3, K_2O and Na_2O, whose changes were not noticed and analysed. No significant effect on the properties was noticed, as the changes are marginal.

The CaO content, when compared with the literature values [180–186] for CEM I cement (ranging from 58.2 to 68.2 %), shows that samples are within the typical range. The SiO_2 content (literature range 19.7-21.6 %) in samples differs more significantly, with 14.6 – 19.7 % values showing notable variations from the expected range. Interestingly, the samples' Al_2O_3 content (literature range 3.8-5.4%) is consistently lower than typical values, with 2.0 – 2.7 % measurements. The Fe_2O_3 content can be contextualised within the literature range of 0.4-0.6 %. CaO differs by almost 20 % for M-SD-1 and M-1000-1, increasing from 47.4 to 67.0 %, with the M-450-1 sample achieving 53.1 %.

M-SD-1 treated at these temperatures shows a chemical composition similar to the literature-reported CEM I cement values. This suggests that the thermal treatment affects the M-SD-1 and aligns the M-1000-1 more closely with typical cement characteristics.

Table 6.3

XRF data summary for raw materials

Oxides of elements	CEM I	$CaCO_3$	CEM I/$CaCO_3$	M-SD-1	M-450-1	M-1000-1	CEM I from literature [180–186]
CaO	67.1	52.8	65.8	47.4	53.1	67.0	58.2-68.2
SiO_2	21.9	2.7	20.6	14.6	16.0	19.7	19.7-21.6
Al_2O_3	2.2	1.2	2.2	2.0	2.2	2.7	3.8-5.4
SO_3	0.9	0.1	1.0	0.8	0.8	1.0	2.8-3.5

MgO	0.5	1.1	0.5	0.6	0.7	1.0	1.4-3.8
Fe_2O_3	0.3	0.4	0.3	0.4	0.5	0.6	0.2-3.3
Na_2O	0.3	0.1	0.2	0.2	0.3	0.3	0.2-0.3
K_2O	0.1	0.3	0.1	0.2	0.2	0.3	0.1-1.0
P_2O_5	0.4	0.0	0.3	0.2	0.2	0.2	0.1-0.4
TiO_2	0.1	0.1	0.1	0.1	0.1	0.1	0.1-0.5

The XRD patterns in Figure 6.7 reveal significant changes in the crystalline phases of M-SD-1 treated at two different temperatures - 450 ℃ and 1000 ℃. The diffractograms are dominated by $Ca(OH)_2$, $CaCO_3$, alite and belite phases, with notable transformations occurring as temperature increases [187]. In M-SD-1, the dominant peak at 29-30 ° 2Θ is characteristic of calcite ($CaCO_3$) from raw materials and indicates carbonation of the cement mineral phases [188]. At 450 ℃, while the calcite peak remains prominent, some changes in the relative intensities of other peaks are noticeable, likely due to the dehydration of cement hydrates and the beginning of transformations in the clinker phases [189]. The most dramatic changes occur in the M-1000-1, where the calcite peak has diminished, indicating the near-complete decomposition of $CaCO_3$ into CaO, which occurs around 800 ℃ [190]. Intense peaks emerge, particularly in the 32-33 ° 2Θ region, likely attributed to the formation of belite (C_2S) polymorphs, like β-C_2S [191], and alite. The samples also contain small quantities of dolomite, corroborated by XRF analysis showing Mg compounds below 1 % [192].

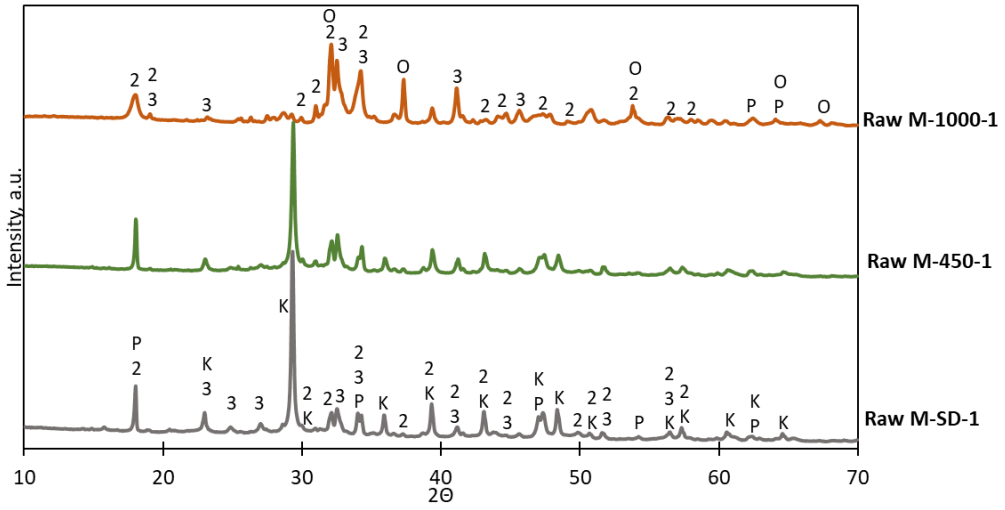

Figure 6.7. XRD data summary for raw M-SD-1, M-450-1, and M-1000-1, where 2 - Bellite, C_2S, 033-0302; 3 - Allite, C_3S, 031-0301; P - Portlandite, $Ca(OH)_2$, 044-1481; K – Calcium Carbonate, $CaCO_3$, 005-0586; O – Calcium Oxide, CaO, 037-1497.

Significant differences are observed at several 2Θ angles: At 18 °, a $Ca(OH)_2$ phase is observed, which dehydrates with increasing temperature. The 31-33 ° range, crucial for cement-containing materials, shows increasing intensity with temperature, suggesting changes in mineralogical composition, particularly in alite and belite phases [193]. At 37 ° and 41 °, intense peaks in the M-1000-1 sample are attributed to belite, a key mineral in fresh cement [194]. The 47-49 ° interval shows decreasing $Ca(OH)_2$ and $CaCO_3$ peaks for the M-1000-1 sample, confirming thermal decomposition. Finally, at 54 °, a pronounced CaO peak is seen for the M-1000-1 sample, correlating with the

decomposition of $CaCO_3$ to CaO [195]. These changes in crystalline phases demonstrate the significant impact of thermal treatment on the mineralogical composition of wood-wool cement panel manufacturing waste.

Different W/B ratios were used in the design of the samples to achieve a similar workability for all the samples. A W/B ratio of 0.75 was used for M-SD-1, 0.6 for M-450-1 and 0.8 for M-1000-1. The required W/B ratio is higher than virgin cement [179,196]. However, it should be noted that, for example, M-SD-1 has wood particles present, capable of absorbing additional water. Flowability tests showed that the mortars have an optimal flowability of 15-20 cm after 20 jolts of the impact table. The first heat treatment phase investigated the compressive strength of the samples, whose manufacturing used M-SD-1 heat-treated at different temperatures. The visual appearance of the samples can be seen in Figure 6.8.

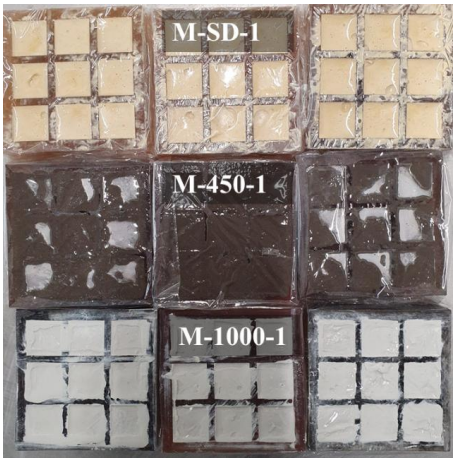

Figure 6.8. The visual appearance of the freshly formed mortars.

A summary of the compressive strength can be seen in Figure 6.9. The data reveal a clear trend of increasing compressive strength over time for all samples, which is typical for cement-based materials as hydration progresses. More notably, thermal treatment has a significant impact on strength development. The untreated sample (M-SD-1) shows the lowest strength at all ages, starting at just 0.55 MPa at 7 days and reaching 2.82 MPa by 28 days. This relatively low strength suggests that the untreated sanding dust does not have high-cementitious properties and even interferes with cement hydration. Samples treated at 450 °C (M-450-1) exhibit a marked improvement in strength, with values of 5.73 MPa at 7 days, increasing to 10.37 MPa at 28 days. This substantial enhancement could be attributed to removing organic matter from the wood fibres and the dehydration of portlandite and C-S-H mineral phases, potentially increasing the material's reactivity.

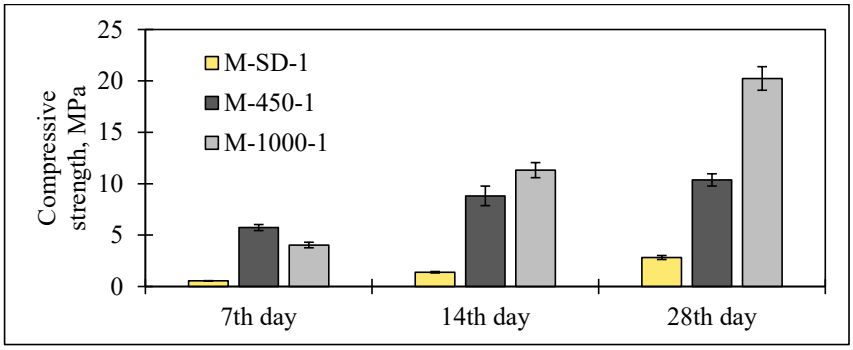

Figure 6.9. Summary of the compressive strength of the samples.

The greatest strength gain was observed in M-1000-1 samples, which achieved 4.04 MPa at 7 days and an impressive 20.24 MPa at 28 days. This significant strength is likely to result from high-temperature phase transformations in the cement components, particularly reactive belite (β-C_2S) formation as observed in the XRD analysis and the complete removal of organic matter. The results demonstrate that thermal treatment, especially at higher temperatures, can effectively activate the cementitious properties of the sanding dust, transforming it from a potentially inert or detrimental waste material into a valuable supplementary cementitious material. This finding has important implications for the sustainable management of wood-cement composite waste, suggesting that with appropriate thermal processing, this material could be successfully recycled into new cement-based products, contributing to circular economy principles in the construction industry.

After the compressive strength test, the samples were subjected to an XRD test to test the hydrated products and compare them with the raw state of the material. The XRD graph (Fig. 6.10) compares the M-SD-1, M-450-1 and M-1000-1 samples in raw material and hydrated mortar states. The analysis reveals significant phase transformations and hydration reactions occurring in the material.

For the M-SD-1, the dominant peak at around 29-30 2Θ, characteristic of calcite ($CaCO_3$), remains prominent in both the raw and hydrated states. This suggests that the carbonation products are stable and do not change significantly during hydration at room temperature.

M-450-1 shows similar patterns between raw and hydrated forms, indicating that this temperature can alter the material's reactivity. Portlandite phase peaks have decreased in intensity, and the calcite peaks remain strong, suggesting that decarbonisation has not occurred at this temperature.

Notable changes are observed in the M-1000-1. In the raw state, the calcite peak is greatly diminished, and new sharp peaks emerge, particularly in the 32-33 2Θ region, likely corresponding to belite (C_2S) polymorphs. Upon hydration, these peaks decrease in intensity, and new peaks appear, indicating the formation of hydration products. The broad peak around 29-30 ° 2Θ in the hydrated M-1000-1 sample likely represents calcium silicate hydrate (C-S-H), the primary binding phase in cement-based materials.

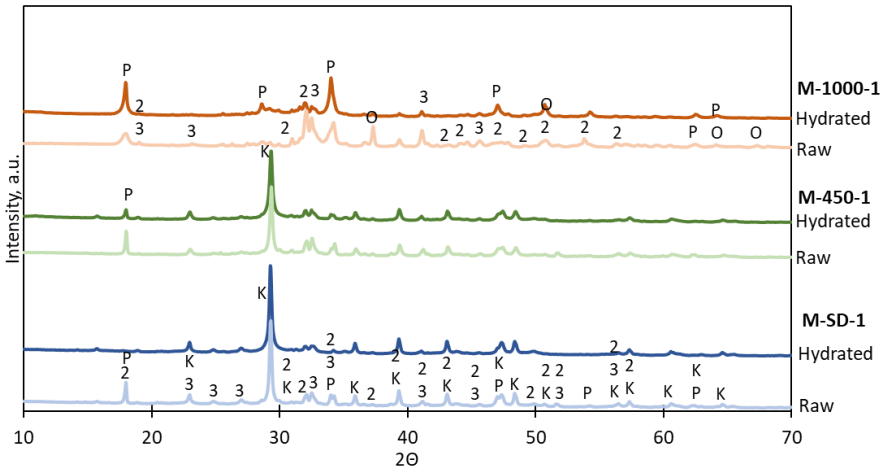

Figure 6.10. XRD data summary for raw and hydrated M-SD-1, M-450-1 and M-1000-1, where 2 - Bellite, C_2S, 033-0302; 3 - Allite, C_3S, 031-0301; P - Portlandite, $Ca(OH)_2$, 044-1481; K – Calcium Carbonate, $CaCO_3$, 005-0586; O – Calcium Oxide, CaO, 037-1497.

The hydrated M-1000-1 sample also shows a distinct peak at about 18 ° 2Θ, characteristic of portlandite ($Ca(OH)_2$), a common hydration product. This peak is absent or much less pronounced in the other samples, indicating that the high-temperature treatment has enhanced the material's hydraulic reactivity.

These XRD patterns demonstrate the evolution of the sanding dust from a primarily inert and hydrated cement paste to a reactive cementitious substance when treated at elevated temperatures. The hydration of the M-1000-1 sample produces phases typical of cement hydration, explaining the strength development observed in previous compressive strength tests. This analysis confirms the potential of high-temperature treatment in converting sanding dust into a valuable supplementary cementitious material.

Of the 2nd Phase

After the preliminary results of the tests, heat treatment was found to be a feasible potential method of reactivating the sanding dust (SD). The material needed to be characterised more extensively to prove the effectiveness of this method. In this heat treatment phase, the temperature range was broadened to see how the sieved SD is affected in a more extensive temperature range. Temperature was chosen in increments of 150 ℃, starting from 300 to 1200 ℃, holding the selected temperature for 4 hours.

The thermal behaviour of wood-wool cement panel sanding dust demonstrates complex decomposition patterns characteristic of both lignocellulosic and cementitious materials. The thermogravimetric (TG) analysis in the 300-900 ℃ temperature range reveals multiple mass loss stages. At the same time, the DTA curves show corresponding thermal events that can be attributed to specific chemical and physical transformations (Fig. 6.11).

The initial dehydration stage (50-150 ℃) shows approximately 10 % mass loss in the SD sample, primarily attributed to the evaporation of physically bound water from multiple sources[140,142]. This includes the release of adsorbed water from wood fibres [142,197], interlayer water from C-S-H gel structures [198], and zeolitic water from AFm phases in the cement matrix [199]. Dehydration of

ettringites (90-120 °C) [147] has also been noticed. The endothermic character of this region in the DTA curve confirms the dehydration nature of these processes.

The intermediate temperature region (150-400 °C) exhibits a gradual mass decline corresponding to the thermal degradation of wood components [143,146,149]. This begins with hemicellulose decomposition (220-315 °C) [143,145,148,149], followed by cellulose degradation initiation (315-400 °C) [143,145,200]. Lignin decomposition occurs gradually across a broad temperature range (200-500 °C) [142–144,147–149]. The cement phases also contribute to mass loss in this region through the dehydration of ettringite (AFt) around 120 °C and monosulfoaluminate (AFm) phases between 180-200 °C [201].

A distinctive endothermic event occurs around 450 °C, accompanied by a mass loss step, indicating the dihydroxylation of $Ca(OH)_2$ (Portlandite): $Ca(OH)_2 \rightarrow CaO + H_2O$. This reaction is fundamental in cement chemistry and affects the material's subsequent carbonation behaviour [140–152].

The most pronounced endothermic peak appears at approximately 750 °C, coinciding with a sharp 10-15 % mass loss, representing the decarbonisation of calcium carbonate: $CaCO_3 \rightarrow CaO + CO_2$. The presence of $CaCO_3$ suggests either carbonation of $Ca(OH)_2$ during material processing/storage or limestone in the original cement composition [202]. The carbonation process in cement-based materials follows the reaction: $Ca(OH)_2 + CO_2 \rightarrow CaCO_3 + H_2O$. This process is particularly relevant for fine particles like sanding dust due to their high surface area [140,142,144,146–152,154].

The heat-treated SD (300-900 °C) demonstrates progressively reduced mass loss at lower temperatures, confirming the irreversibility of thermal decomposition processes. However, the persistence of some thermal events in pre-heated samples suggests several possibilities:

1. Incomplete reactions during initial heating due to kinetic limitations [203];
2. Reformation of hydrates and carbonates during cooling/storage [204];
3. Protection of some phases within the composite matrix [205].

The final residual mass between 70-95 % provides quantitative information about the total volatile and decomposable content, reflecting the combined effects of the decomposition of organics and dehydration, dihydroxylation, and decarbonisation processes of minerals [206]. Heat treating SD above 750 °C resulted in a small fraction of portlandite phase reforming during the cooling or storage process [207,208].

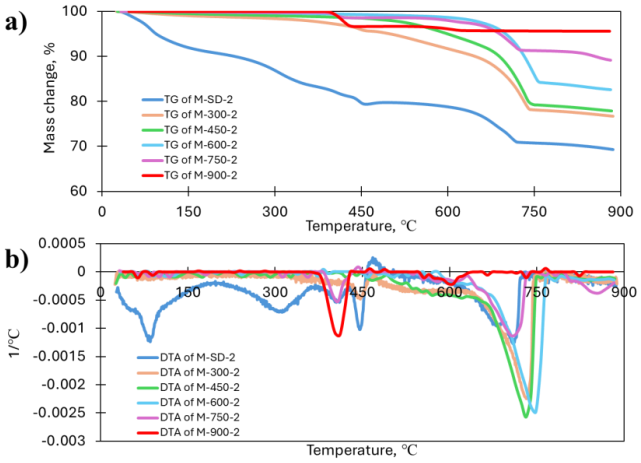

Figure 6.11. a) TG, b) DTA curves for 2nd phase samples.

The physical and mechanical properties of the materials were also re-investigated after the results of the first phase. The materials' elemental distribution and mineralogical composition were determined in cooperation with the cement manufacturer SCHWENK and their laboratory. The data on the elemental distribution are summarised in Table 6.7. As the temperature increases, the material undergoes phase changes and decomposition reactions, further explained by the TG/DTA graph shown in Figure 6.12.

The XRF data is provided in Table 6.4 reveals significant changes in the oxide composition of wood-wool cement panel manufacturing waste as it was heated from 0 ℃ to 1200 ℃. The most notable change is the substantial increase in CaO content from 51.11 % to a peak of 68.84 % at 1050 ℃, due to the decomposition of calcium-containing compounds such as calcium carbonates from hydrated cement, as can be seen from TG/DTA data in Figure 6.11. Simultaneously, there is a decrease in CO_2 content from 25.12 % to 2.26 % at 1050 ℃, further indicating the breakdown of carbonates. The similar amounts of CO_2 after 900 ℃ indicate that all carbonates have decomposed, and the remaining CO_2 is crystalline-bonded CO_2. SiO_2 gradually increases from 17.02 % to 22.05 %, possibly resulting from the decomposition of calcium silicate hydrates in cement and the oxidation of silicon-containing compounds in wood. Al_2O_3 content rises slightly from 2.49 % to 3.13 % due to the dehydration of aluminium-containing phases in the cement.

Table 6.4

Oxide distribution of minerals

Sample	SiO_2	Al_2O_3	Fe_2O_3	CaO	MgO	SO_3	Na_2O	K_2O	TiO_2	Mn_2O_3	P_2O_5	Cl	CO_2	Na_2O eq
M-SD-2	17.02	2.49	0.60	51.11	1.70	1.33	0.16	0.16	0.10	0.17	0.03	0.03	25.12	0.26
M-450-2	18.28	2.72	0.67	56.96	1.79	1.56	0.19	0.19	0.11	0.17	0.03	0.03	19.72	0.31
M-600-2	18.95	2.70	0.64	59.08	1.76	1.53	0.19	0.16	0.10	0.19	0.03	0.02	16.71	0.30
M-750-2	20.01	2.91	0.68	63.60	1.81	1.56	0.19	0.17	0.11	0.19	0.04	0.02	8.70	0.30
M-900-2	21.53	3.00	0.68	67.66	1.86	1.64	0.19	0.16	0.12	0.21	0.04	0.02	3.75	0.29
M-1050-2	21.97	3.04	0.70	68.84	1.87	1.33	0.14	0.09	0.12	0.22	0.04	0.02	2.26	0.19
M-1200-2	22.05	3.13	0.70	67.65	1.88	1.23	0.10	0.06	0.12	0.22	0.04	0.01	3.19	0.14

Other oxides like Fe_2O_3, MgO, and minor components show relatively small changes throughout the heating process. SO_3 phase intensity increases slightly up to 900 ℃ before decreasing at higher temperatures, suggesting the decomposition of sulphate-containing phases [209]. Alkali oxides (Na_2O and K_2O) show slight increases up to 750 ℃, due to the concentration effects as other components degrade and then decrease due to volatilisation at high temperatures in the cement matrix [210]. These changes indicate the dehydration and decomposition of hydrated cement phases, breakdown of carbonates, and formation of calcium, silicon, and aluminium oxides typical of cement clinker as the temperature increases.

This data is further explained by the XRD results, shown graphically in Figures 6.12 and 6.13. The XRD analysis of the wood-wool cement panel sanding dust provides a comprehensive picture of the complex mineralogical transformations occurring as the material is subjected to increasing temperatures. This analysis is crucial for understanding the material's behaviour and potential applications in recycling or reuse strategies.

At room temperature, the M-SD-2 composition reflects the carbonates contained and the carbonation process that occurs during the lifecycle of cement-based materials. Calcite ($CaCO_3$) is the predominant phase, indicating added calcite in the manufacturing process and carbonation of the

cement phases. This is a common phenomenon in cement-based materials exposed to atmospheric CO_2 over time [211]. Small amounts of portlandite ($Ca(OH)_2$) also represent the remaining hydration products. Heat treating SD above 750 °C resulted in a small fraction of portlandite phase reforming during the cooling or storage process [207,208].

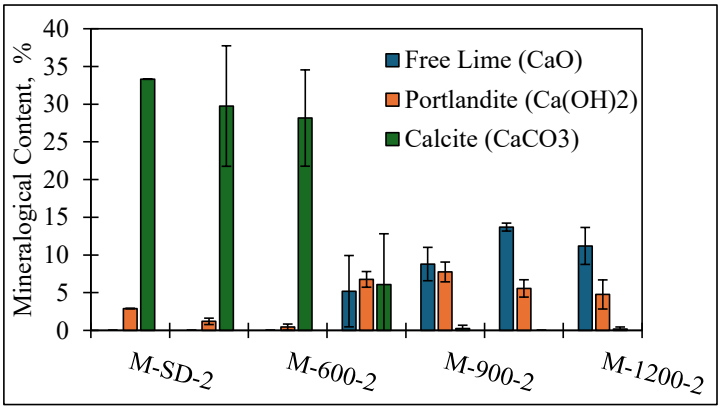

Figure 6.12. Summary of the mineralogical content of free lime, portlandite, and calcite.

We observe decomposition reactions and phase transformations as the temperature increases. The portlandite decomposes around 450-600 °C, converting to calcium oxide and water vapour. This aligns with the findings of Alarcon-Ruiz et al. [212], who noted this decomposition occurring typically between 400-500 °C in cement pastes.

The most dramatic change occurs with the thermal decomposition of calcite, which begins around 600-700 °C and is essentially complete by 750 °C. This process, represented by the reaction $CaCO_3 \rightarrow CaO + CO_2 \uparrow$, is responsible for the significant mass loss observed in this temperature range. This decomposition's kinetics and exact temperature can vary based on particle size, heating rate, and CO_2 partial pressure in the environment [213].

Concurrently with these decomposition processes, the cement clinker phases (C_3S and C_2S) undergo significant transformations. The behaviour of alite (C_3S) and the various polymorphs of belite (C_2S) are particularly noteworthy. Alite content decreases with increasing temperature, likely due to its thermal instability and potential reaction with decomposition products. While pure alite typically decomposes around 1250 °C, in complex systems like this, it can begin to transform at lower temperatures [187].

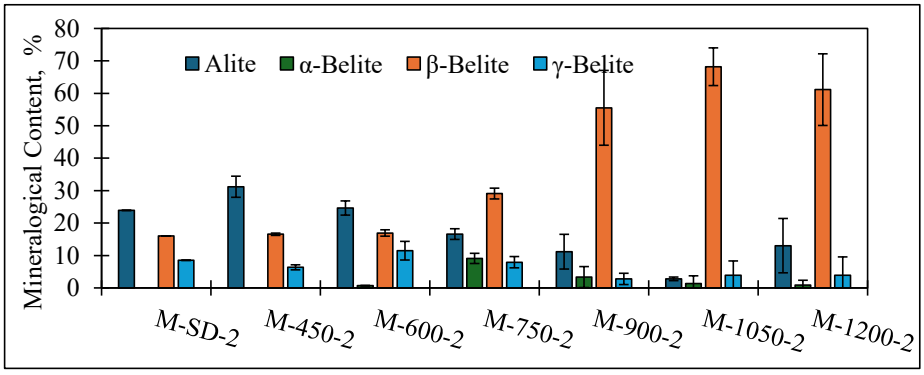

Figure 6.13. Summary of the mineralogical content of the alite and belite phases.

The belite phases exhibit a series of polymorphic transformations critical to understanding the material's evolving properties. The conversion of γ-C_2S to β-C_2S, becoming dominant above 725 °C, is a key transition. This transformation is significant because β-C_2S is more reactive than γ-C_2S, potentially enhancing the hydraulic activity of the thermally treated dust [214]. The appearance of small amounts of α-C_2S at higher temperatures (above 750 °C) is intriguing and may be due to the stabilisation of this high-temperature polymorph by impurities or specific cooling conditions [215]

These phase transformations have important implications for the potential reuse of the material. The increase in reactive phases like β-C_2S at higher temperatures suggests that thermal treatment could enhance the cementitious properties of the SD. This aligns with research by Shui et al. [202], who found that dehydrated cement pastes can regain hydraulic activity, potentially serving as a supplementary cementitious material.

Another critical aspect is the presence and evolution of free lime (CaO) with increasing temperature (> 900 °C). While some free lime benefits cement reactivity, excessive amounts can lead to expansion and durability issues in hardened cement-based materials (Fig. 6.14), similar to Rikoto analysed in [216]. Therefore, carefully considering the optimal treatment temperature is necessary to balance the formation of reactive phases with the potential risks associated with high free lime content [217].

Figure 6.14. Expansion of M-1200-2 sample (mould for 20 × 20 × 20 mm samples).

Understanding these complex phase transformations and their implications is essential for developing effective strategies for recycling or repurposing wood-wool cement panel waste material. Potential applications could range from a supplementary cementitious material in new concrete mixes to a raw material component in cement clinker production, depending on the specific composition and treatment conditions [218].

The materials' setting time and mechanical properties were determined. A summary of the setting times is shown in Table 6.5. The reference sample M-SD-2 showed the longest setting time, starting after about 10 h and finally setting after about 24 h. Increasing the processing temperature allows for the material to set faster. For the M-300-2 sample, the start of the setting was recorded at 5.5 hours, and the end of the setting was recorded at about 11 hours. Increasing the temperature to 450 °C (M-450-2) resulted in a significant decrease in setting time, with setting starting at just over 1 hour and ending at 3 hours. Further increasing the processing temperature to 600 °C (M-600-2), the setting time shifted by 40 minutes compared to the M-450-2 - the setting start was around 1 hour and 45 minutes and the end around 3 hours and 45 minutes. The setting start for M-750-2 and M-900-2 samples was around 5 hours, ending at 8 hours. The M-1050-2 showed high setting times as they barely held together after 24 hours. The M-1200-2 samples started to set after 1 h and were fully set after just over 2 h. This

is explained by the amount of free lime in the material, which, when added to water, causes the lime to undergo a slaking reaction and set.

Table 6.5

Summary of setting times for 2nd phase samples

Sample	M-SD-2	M-300-2	M-450-2	M-600-2	M-750-2	M-900-2	M-1050-2	M-1200-2
Setting start, min	593-1168	330	65	105	323	300	>460	60
Setting end, min	~1348	680	180	225	480	460	>1560	130

The samples' compressive strength shows that heating the raw materials has affected them. Treatment at different temperatures initiates different mineral and chemical changes in the material; in the case of wood additives, it is heating at 450 °C, where the wood particles burn to form charcoal, which can be considered a pozzolanic additive. For cement in M-SD-2, heating means dehydration of the hydrates formed, resulting in dehydration from the hydrate crystals and allowing the compounds to reset with water and form new hydration products. Figure 6.15 shows the compressive strength data obtained for the samples.

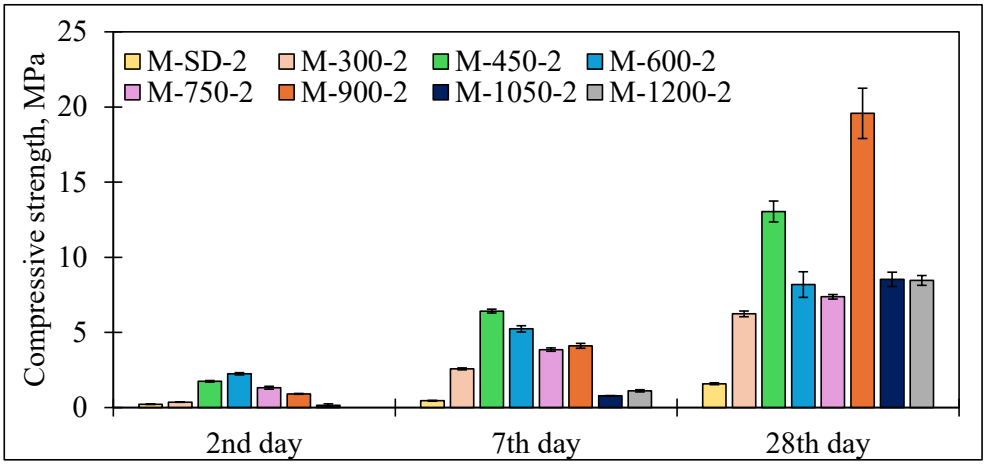

Figure 6.15. Summary of compressive strengths for the 2nd phase samples.

The compressive strength of the samples was also observed to increase with the increase in treatment temperature, but with a specific characteristic. The compressive strength of the samples also increased as they aged, which is consistent with the theory of cement hydration, meaning that hydration was successful for these samples. In the results of Day 2, it can be observed that the M-600-2 shows the highest compressive strength, reaching 2.2 MPa. As the samples aged, on Day 7, the M-450-2 showed the highest compressive strength, reaching 6.4 MPa, while the M-600-2 and M-900-2 also showed elevated results, reaching 5.2 and 4.1 MPa. As the samples aged to day 28, the compressive strength of all samples increased. For the M-1050-2 and M-1200-2 between day 7 and day 28, the compressive strength increased rapidly from 0.8 to 8.5 MPa and from 1.1 to 8.5 MPa, respectively. The M-450-2 and M-900-2 showed the highest compressive strengths, reaching 13.0 and 19.6 MPa on day 28, respectively.

6.2. Sanding Dust Reactivated by Heating in Rotary Kiln

Mix Design and Sample Preparation

Using sanding dust processed in a rotary kiln as the binder, 2 compositions were created. Additionally, 1 composition was made as a reference series for data comparison. The compositions differed in the processing temperature, and the aim was to see the effect of the treatment temperature on the SD mortar samples.

The SD heated in the rotary kiln mix designs are not different from the previous section's mixes. The mix design is summarised in Table 6.6. Demoulding of the samples and curing conditions were the same as for the muffle furnace experiment to compare data.

Table 6.6

Mix design for SD treated in the rotary kiln

Sample	Sample denotation	Binder, mass parts	Water, mass parts
Sieved sanding dust	R-SD	1	0.75
450 ℃ heated SD	R-450		0.60
900 ℃ heated SD	R-900		0.80

The samples from the SD thermally treated in a rotary kiln were made as follows. The mixing vessel was filled with the required amount of binder, to which the appropriate amount of water was added. The mixture was mixed for two minutes at 300 RPM with a hand mixer. After mixing, the mortar was poured into a ring of the Vicat machine for rheological properties. The rest of the mix was moulded (20 × 20 × 20 mm) and allowed to set for two days at ambient conditions (23 ± 2 ℃), the mould being covered with a plastic film. After the initial curing, the samples were removed from the moulds, labelled, and placed in resealable plastic bags to retain moisture and ensure hydration. After being transferred to the bags, the samples continued to cure. At least 5 parallel samples were tested on each testing day to reduce the marginal error in the results.

Results

The flowability data show that the R-SD and R-900 samples required more water to form a formable material. The water-to-binder ratio was 0.75 for the R-SD, 0.8 for the R-900, and 0.6 for the R-450, which was also the lowest water-to-binder ratio in this series of experiments. The largest flowability after 20 jolts of the impact table was for the R-SD sample, which means that theoretically, the water-to-binder ratio could be reduced, but in practice, it was challenging to mix with less water; regardless of this, segregation could be observed in the mix - the water slowly began to separate from the total mass. Such water segregation was not observed for R-450 and R-900 because of the lack of organics that decomposed until 400 ℃ that could absorb the water. For the R-900, the second largest flowability was obtained after 20 jolts of the impact table, reaching 22.75 cm. This parameter showed that, like the reference series, the water-to-binder ratio could be reduced but at the expense of workability. R-450 had the smallest flowability, but the samples were formidable. Increasing the water-

to-binder ratio would also increase the flowability, but that was not the objective. The aim was to achieve a workable mortar, which all compositions achieved.

Analysing the setting time data, the R-SD sets the longest, fully setting after more than 36 hours. The R-900 showed a faster setting than the R-SD, fully setting after 10 h. The R-450 showed the fastest setting, fully set after almost 6 h.

Figure 6.16 summarises the compressive strength data at different sample ages. The samples were tested at ages 7, 14, 28, 90, and 180 days (half a year). The compressive strength increased with the age of the specimens, which is consistent with the cement theory. The R-SD showed 0.43 MPa on day 7, 0.63 MPa on day 14, 1.09 MPa on day 28, and 2.52 MPa on day 180. The R-450 and R-900 samples achieved higher results. The R-450 samples reached 4.73 MPa on Day 7, 6.71 MPa on Day 14, almost 10 MPa on Day 28, and 13.83 MPa by Day 180. The R-900 samples had slightly higher results, reaching 6.43 MPa on day 7, 7.51 MPa on day 14, 10.62 MPa on day 28, and their highest strength of 18.62 MPa by day 180.

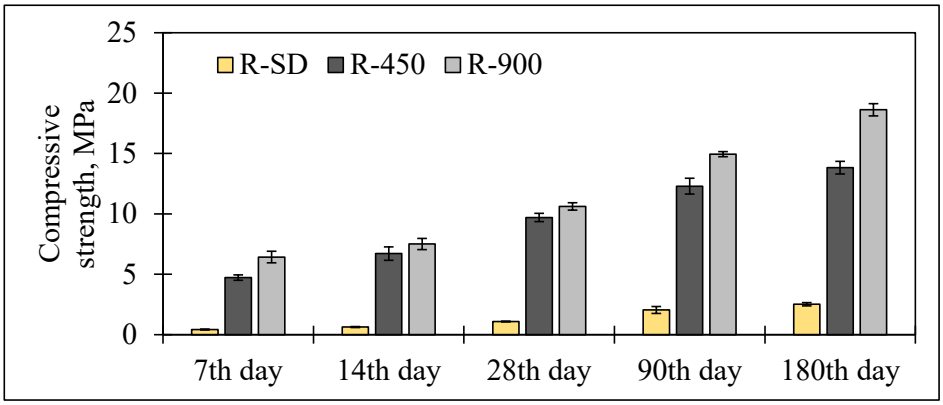

Figure 6.16. Compressive strength summary of rotary kiln experiment samples.

The results were promising for further developing the rotary kiln heat treatment method to reactivate SD and produce a cementitious binder. Comparing the compressive strengths of the previous section's M-SD-2, M-450-2, and M-900-2 shows similarities. The muffle furnace, as a processing method, at both treatment temperatures showed higher compressive strength than the rotary kiln. Remember that durations of heat treatment differed – SD in a muffle furnace was heated for 4 hours, while SD in a rotary kiln was treated for about 15 minutes. On the 28th day, M-450-2 achieved 13.0 MPa, while R-450 achieved 9.7 MPa. M-900-2 achieved 19.6 MPa, while R-900 achieved only 10.6 MPa. From those results, a conclusion can be drawn that SD can be reactivated using heat treatment methods. If the SD needs to be heated at higher temperatures (> 600 °C), it is better to heat it in a muffle furnace. If low-temperature heating is necessary, a rotary kiln is more efficient.

The heated material obtained can be used as a binder and added back into the production line to create new products to reduce the need for virgin cement. It should be noted that the material is grey after heating, which also affects the colour of subsequent products if this binder is used.

6.3. Chapter Summary

From section 6.1, many conclusions can be drawn about the characteristics of the SD and the effect of heat treatment. Heat treatment significantly affects the particle size distribution of wood-cement panel sanding dust, reducing D90 values from 74.89 μm (raw) to 45.03 μm (900 °C) and average particle size from 29.21 μm to 18.53 μm. The visual appearance changes from yellowish to dark grey (450 °C) and light grey (900 °C), reflecting organic matter decomposition.

XRD analysis shows the transformation of calcium-bearing phases, with calcite decomposing between 600-750 °C, portlandite around 450-600 °C, and the formation of reactive belite at higher temperatures. XRF data have further confirmed these processes, which reveal a CO_2 decrease from 25.1 % to 3.2 %, which is further explained by DTA results.

Thermal analysis identifies distinct stages: moisture evaporation (30-200 °C), organic components decomposition (200-430 °C), and dehydration of portlandite and decomposition of calcium carbonate (430-730 °C). Setting time varies significantly with treatment temperature, from 24 hours for M-SD-2 to 3 hours for M-450-2 and 2 hours for M-1200-2. As mentioned previously, the sudden shortening of setting time can be explained by portlandite phase dehydration at 450 °C and calcium carbonate decomposition in the temperature range of 600-750 °C.

The highest achieved compressive strengths were for samples M-450-2 and M-900-2, achieving 13.0 and 19.6 MPa on the 28^{th} day, respectively. The strength increase is explained by the dehydration and rehydration of the portlandite phase and the decomposition of calcium carbonates.

Using a muffle furnace as a processing method for sanding dust proved feasible. Although the method is scalable, the energy input would be much greater than the strength increase gained. Different methods of heat treatment have proven to be more energy efficient. Processing in a rotary kiln is a promising alternative for cement-containing waste reactivation, offering improved energy efficiency through continuous material stirring that ensures uniform thermal energy distribution for dehydration.

The study identified two optimal treatment temperatures: 450 °C, providing balanced setting time (3 hours full set), workability, and energy efficiency (lower energy consumption) and 900 °C, yielding maximum strength (19.6 MPa) and favourable physical properties. These findings demonstrate that heat-treated SD is viable as a supplementary cementitious material, with treatment temperature selection based on desired properties - 450 °C for faster setting or 900 °C for maximum strength. This process effectively supports construction waste recycling and circular economy principles.

Setting time performance demonstrates significant improvements: from over 24 hours for R-SD (reference) to approximately 6 hours for R-450 and 10 hours for R-900. Long-term strength development is particularly noteworthy, with R-SD reaching only 2.52 MPa after half a year. In comparison, R-450 and R-900 achieved 13.8 MPa and 18.6 MPa, respectively, confirming the substantial benefits of thermal activation. All of the made samples are within the proposed limits of the research.

Comparing both thermal treatment methods reveals complementary insights into cement-containing waste valorisation. Both methods identify 450 °C and 900 °C as optimal treatment temperatures, with the higher temperature consistently yielding higher compressive strength, as mentioned previously. The rotary kiln demonstrates comparable long-term performance (18.6 MPa at 900 °C) with potentially lower energy inputs due to its continuous operation and improved thermal transfer efficiency. The rotary kiln's "stirring" mechanism offers processing uniformity and energy distribution advantages, making it more suitable for industrial-scale implementation.

Building upon the investigations into milling methods detailed in Chapter 5 and the subsequent thermal treatment studies presented herein, this chapter concludes by developing and optimising the cementitious binders derived from wood-wool cement panel manufacturing waste. Through experimentation, including mechanical and thermal activation strategies, a range of binders with enhanced reactivity and desirable properties has been successfully developed and thoroughly characterised. This analysis has enabled the identification of optimal binder compositions and activation pathways. Consequently, the succeeding chapter will focus on the practical application of these most promising and optimised binders in producing innovative biocomposites, where their performance will be evaluated in composite form, transitioning from binder development to material characterisation.

7. CHARACTERISATION AND PERFORMANCE OF BIOCOMPOSITES WITH REACTIVATED BINDERS

Biocomposites were made according to Table 7.1, which represents the mix designs of all the biocomposites made. The mix designs were calculated in mass parts, and the mix designs were simple. The filler was wetted and mixed, then a binder was added, followed by continuous material mixing. Afterwards, water for the binder was added and mixing continued till the mixture was homogeneous.

Table 7.1

Mix design compilation in the mass parts of all biocomposite samples

Sample	Binder				Water	Filler		Water for wetting*
	V-20min	M-450-2	M-600-2	CEM II/A-LL 42.5 N		PLW	Hemp Shives	
P1	10				7	10		1
P2	5				3.5			
P3	3				2.1			
H12		1			0.6	2		0.6
H13		0.67			0.4			
H14		0.5			0.3			
PLW12			1		0.6	2		1
Hemp12							2	2.4
Mix12						1	1	1.8
PLW21			2		1.2	2		0.5
Hemp21							2	1.2
Mix21						1	1	0.85
I				1	0.4	2		0.7
II						3		1.3
III						4		1.6
H25						1.5	0.5	1.4
H50						1	1	1.6
H75						0.5	1.5	2

*The filler was moistened before mixing so that the filler did not absorb the water intended for the binder.

A visual representation of the mix design can be seen in Figure 7.1. From the figure, it can be acknowledged that for each biocomposite series, a constant W/B ratio was added to analyse the B/F ratio effect on the properties of the biocomposites.

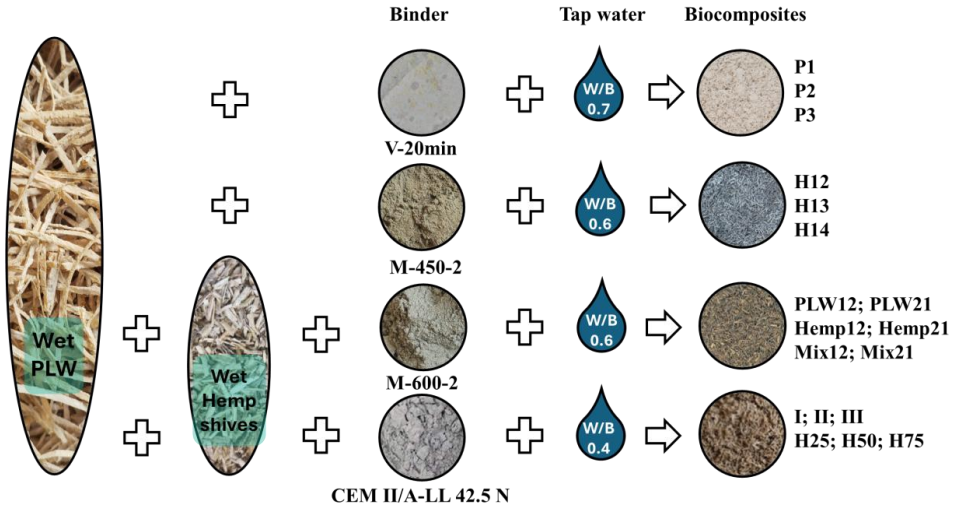

Figure 7.1. Visual representation of the biocomposites mix design.

7.1. Biocomposites with Mechanically Activated Binder

Mix Design and Sample Preparation

The binder used in this experiment is 20-minute vibration-milled, sieved sanding dust (V-20min), and the filler is Production Line Waste (PLW), described in section 4.1. Three compositions of bio-based building materials were made with varying binder content. The mixture design is compiled in Table 7.2.

Table 7.2

Mix design of the developed bio-based building materials, mass parts

Sample	Binder		PLW (Filler)	
	V-20min	Water	Dry	Water for wetting*
P1	10.0	7.0		
P2	5.0	3.5	10.0	1.0
P3	3.0	2.1		

*The filler was moistened before mixing so that the filler did not absorb the water intended for the binder.

A flow chart of the sample production process is shown in Figure 7.2. One mass part of the water was used to wet the filler material for easier incorporation of the binder, which was added after 3 minutes of filler and water mixing. Based on the mix design, 10, 5, and 3 mass parts of the binder were gradually added to the wet filler material and mixed, resulting in a homogeneous coating of the fibres. Afterwards, the water necessary for the binder was added to the mix. For each composition, a W/B ratio of 0.7 was used. Then, the mixture was remixed to form a homogenous composition and formed in oiled moulds of dimensions 35 × 35 × 10 cm.

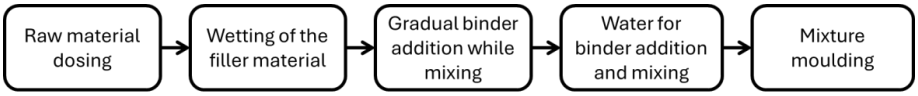

Figure 7.2. Flowchart for biocomposite production.

A plate was put on top after the mixture had been formed to ensure pressure and a smoother surface structure. An initial pressure of 571 Pa was added to the samples to ensure better bonding between the binder and the wood fibres. Initial pressure was applied for 60 seconds, after which an additional weight was added to ensure a pressure of 65 Pa to the samples as a secondary pressurisation as they cured. Samples were demoulded after seven days, wrapped with plastic film, and cured for 21 days to ensure a minimal humidity loss for the rest of the curing process. After the curing process of 28 days, the plastic film was removed, and the samples were dried in a curing chamber at 45 ℃ till constant mass.

Results and Discussion

Developed bio-based building materials were characterised by their visual appearance, macrostructure, material density, thermal conductivity and compressive strength. The visual appearance of the bio-based building materials is seen in Figure 7.3.

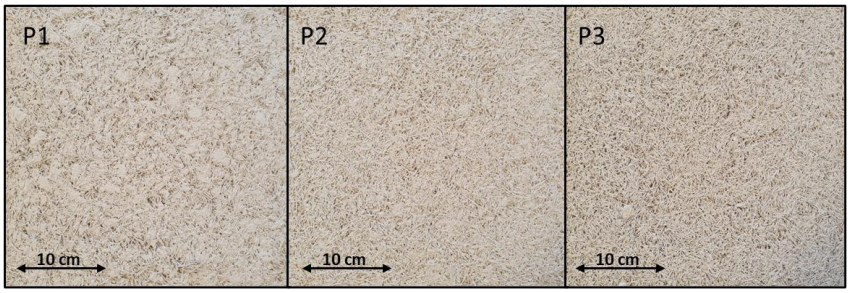

Figure 7.3. The visual appearance of the developed bio-based building materials.

From Figure 7.3, the P1 sample has a lot of larger patches of binder clumping together, making the visual look inhomogeneous. A more homogenous sample was obtained by lowering the binder amount (P2) to decrease the larger voids filled with binder. Decreasing the binder amount further allows more voids to be observed (P3), and the material's structure becomes brittle.

Looking at the macrostructure of all the samples (Fig. 7.4), note the considerable difference between the samples. P1 has the highest material density, which can be explained by the voids being filled with binder, and the binder covers most of the wood fibres in a thick coating. Separate voids can be seen, but the contact areas between the fibres are entirely covered with the binder. The P2 sample has some similarities with P1, with the binder covering almost all the fibres, but in P2, larger voids can be seen, and the contact zones are not entirely covered with the binder. In the P3 sample, the binder covers only individual fibres, and the contact area between them is thin, significantly affecting the sample's strength. However, the gaps between the fibres are not filled with a binder, which decreases thermal conductivity. During the inspection, individual wood fibres crumbled away from the sample because of the weak contact area between them.

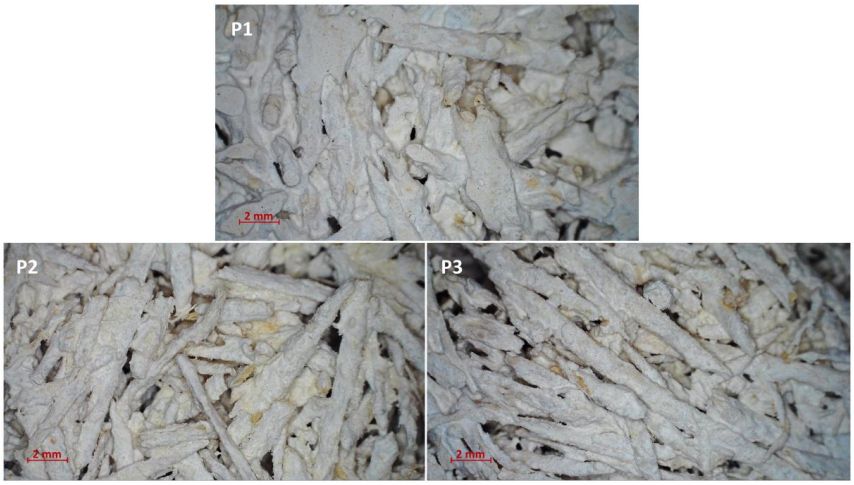

Figure 7.4. The macrostructure of the developed bio-based building materials.

Physical properties were evaluated as the primary properties of the feasibility of this material. The properties looked at were material density and thermal conductivity, compiled in Table 7.3.

Table 7.3

Physical properties of the developed bio-based building materials

Sample	Material density, kg/m^3	Thermal conductivity, W/(m·K)
P1	613	0.117
P2	494	0.093
P3	430	0.083

The material density of the samples ranges from 430 to 613 kg/m^3. Sample P3 exhibited the lowest density (430 kg/m³), while sample P1 had the highest (613 kg/m³). This variation stems from the different binder content used during sample preparation, as documented in Table 7.2. The density values provide crucial guidance for material selection in applications where weight is critical, such as in lightweight construction elements or thermal insulation systems.

The thermal conductivity of the samples ranges from 0.083 to 0.117 W/(m·K). This parameter determines the rate at which heat flows through the material, and it is an important consideration when designing thermal insulation materials. The dependence of thermal conductivity on material density is visualised in Figure 7.5. A correlation between material density and thermal conductivity can be seen in a study by Sahmenko [219], where hempcrete samples were tested, differentiating the material density and thermal conductivity. It was found that even with different binders used, comparing that study to this study's developed materials, a conclusion can be drawn that these materials have lower thermal conductivity with the same material density. However, compressive strength is lower, as the binder is not strong.

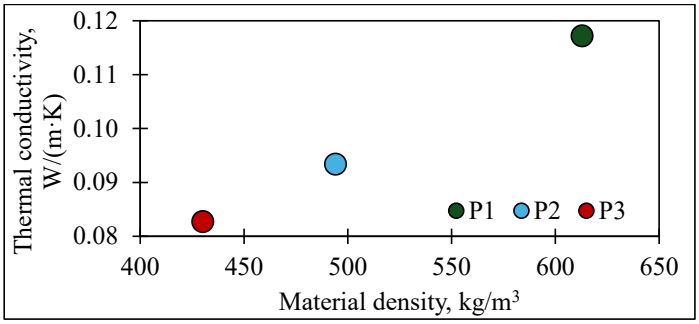

Figure 7.5. Thermal conductivity dependence on material density.

The compressive strength-deformation graph can be seen in Figure 7.6. For the perpendicular direction testing, a critical load (marked by the end of the elastic zone) was used to calculate compressive strength as the sample started to delaminate as the deformation increased. A 10 % deformation was used for the calculations for the parallel direction testing, as the material was easy to deform. A marker was put on each representative graph as the value point of calculation.

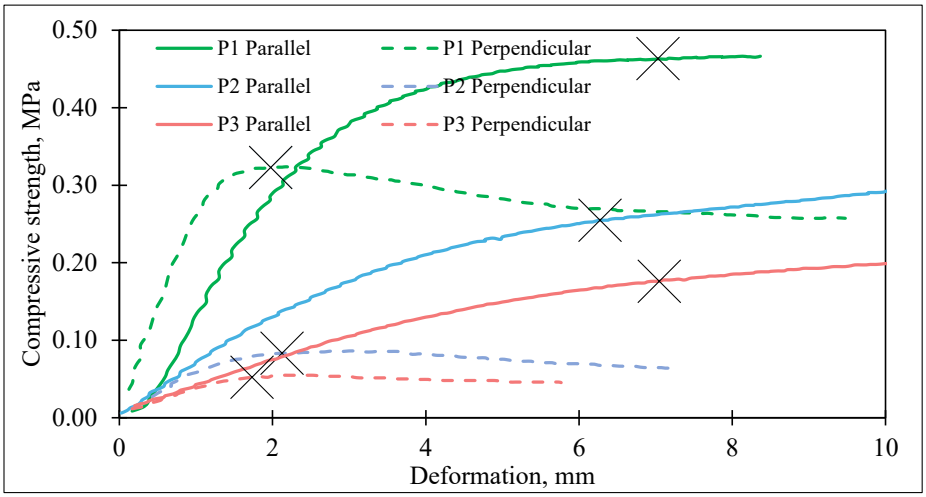

Figure 7.6. Compressive strength-deformation graph for the developed bio-based building materials.

Based on the flexural and compressive strength values provided in Table 7.4, it can be concluded that the bio-based building material exhibits moderate to low strength characteristics. The flexural strength values range from 0.06 to 0.24 MPa, indicating that the material is weak in resisting bending forces. The compressive strength values are also moderate, ranging from 0.06 to 0.47 MPa, depending on the forming direction.

Table 7.4

Mechanical properties of the developed bio-based building materials

Sample	Flexural strength, MPa	Compressive strength based on the forming direction, MPa	
		Parallel	Perpendicular
P1	0.24	0.47	0.33

P2	0.11	0.26	0.09
P3	0.06	0.18	0.06

Comparing the three developed bio-based building material prototypes, the highest values in both directions of compressive strength and flexural strength are for sample P1, reaching 0.24 kPa of flexural strength and 0.47 and 0.33 MPa in parallel and perpendicular compressive strength, respectively. The lowest values were found for sample P3, which confirms that the lowest amount of binder used would result in the lowest flexural and compressive strength. P3 showed 0.06 MPa of flexural strength, 0.18 MPa, and 0.06 MPa of compressive strength in parallel and perpendicular directions. The P2 sample reached a flexural strength of 0.11 MPa and a compressive strength of 0.26 MPa in parallel and 0.09 MPa in perpendicular forming direction. The developed biocomposites had good thermal properties compared to other bio-based building materials. Biocomposites showed promise for use in envelope systems as the middle layer, filling the role of thermal insulation materials.

Based on their physical and mechanical properties, the developed bio-building materials could be used in non-load-bearing applications such as interior wall partitions and insulation. The moderate compressive strength could make it a viable option for low-stress construction projects. Additionally, its eco-friendly nature could make it attractive for sustainable construction practices.

The material has potential applications in construction, especially in building envelopes where thermal insulation and mechanical strength are critical. It could be suitable for insulation for walls, roofs, and floors in buildings, where it can help reduce heat transfer and maintain thermal comfort while providing adequate mechanical support. The approximate envelope system application is visualised in Figure 2.10. The developed bio-based building material could be used as a middle layer made of reactivated binder and recovered wood fibres.

It is worth noting that further testing and evaluation would be necessary to determine the material's suitability for specific applications. The material's properties and behaviour under different environmental conditions should also be considered before deciding on its use in construction projects.

Similarities can be drawn by analysing different bio-based building materials as thermal insulation materials. In research about hempcrete, a material density of 150-500 kg/m^3 can be seen, with the compressive strength and thermal conductivity being in the ranges of 150 - 552 kPa [220] and 0.056 - 0.102 W/(m·K) [221,222]. Flexural strength changed in the 130-200 kPa range [223]. All the materials can be made with different compositions; thus, different properties can be gained.

A similar picture can be seen when comparing straw bale materials, with a material density ranging from around 150 kg/m^3 [224] and thermal conductivity ranging from 0.052-0.060 W/(m·K) [225].

Wood fibre insulation materials show increased flexural and compressive strength (910 -1130 kPa and 1000-1200 kPa, respectively) in developed insulation material studies, which the fibres' orientation can explain. Cross-oriented fibres can achieve higher strength values. Densities for wood fibre materials can vary between 250-500 kg/m^3 and achieve 0.069-0.093 W/(m·K) [226].

Cork materials, on the other hand, can range from 300-400 kg/m^3 with flexural and compressive strength reaching up to 1000 kPa. Thermal conductivity for these materials ranges from 0.068 to 0.100 W/(m·K) [227]. The comparison between the developed and previously mentioned materials can be seen in Figure 7.7. Based on the material density and thermal conductivity, the developed materials P2 and P3 are comparable and competitive with commercially available bio-based materials. P1 slightly increases material density and thermal conductivity, resulting in the material being at the worst part of the comparison.

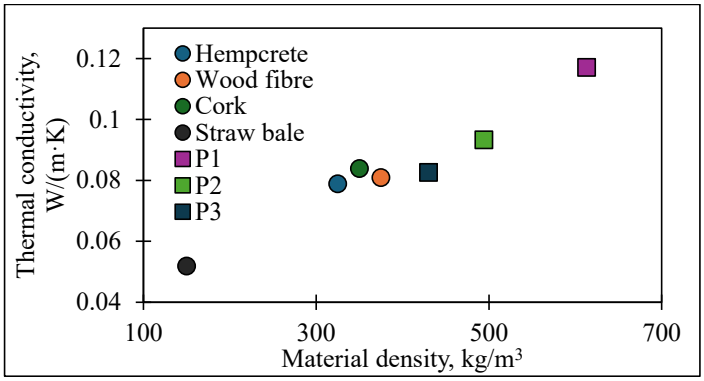

Figure 7.7. Comparison between the developed and commercially available bio-based thermal insulation materials.

The thermal properties of bio-based building materials can vary depending on moisture content, material density, and manufacturing processes. Therefore, these comparisons are only meant to provide a rough idea of how the samples compared to similar materials, and further studies may be necessary to make more specific comparisons.

The developed bio-based building material is sustainable and environmentally friendly due to its bio-based nature. It may be suitable for non-load-bearing walls or interior partitions where high strength is not critical. The material's performance could be enhanced through reinforcement or composite fabrication, depending on the specific application. Therefore, it could be an attractive alternative to traditional building materials for those prioritising sustainable and eco-friendly solutions.

7.2. Biocomposites with Thermally Treated Sanding Dust

7.2.1. Biocomposites with 450 ℃ Treated Sanding Dust

Mix Design and Sample Preparation

Sanding Dust (SD) heat-treated at 450 ℃ was used as a binder (M-450-2). Production Line Waste (PLW) is described in section 4.1. was used as filler. Three different bio-based building material compositions were created, each with a different amount of binder. PLW is described in section 4.1. It is used as filler material. In Table 7.5, the mixture design is compiled.

Table 7.5

Mix design of the biocomposites made with 450 ℃ heated SD, mass parts

Sample	Binder		PLW (Filler)	
	M-450-2	Water	Dry	Water for wetting*
H12	1.00	0.60	2.00	0.60
H13	0.67	0.40		
H14	0.50	0.30		

*The filler was moistened before mixing so that the filler did not absorb the water intended for the binder.

Sample preparation was done according to the flow chart in Figure 7.1. When the sample was created, a plate was placed on top to ensure pressure and a smoother surface structure. To improve the bonding between the binder and the wood fibres, an initial pressure of 571 Pa was applied to the samples. After applying initial pressure for 60 seconds, a weight was applied to the samples to maintain a secondary pressurisation of 65 Pa as they cured. After seven days, the samples were demoulded and covered in plastic film to ensure that there was as little loss of humidity as possible, and they were cured for a further 21 days.

Results

Samples were first evaluated visually (Fig. 7.8). From visual inspection, nothing stands out, and all the samples look the same. However, for each sample, the composition differs in the binder-to-filler ratio.

Fig. 7.8. Visual appearance of the samples.

Thermal conductivity and mechanical properties of the developed biocomposites were evaluated. Mechanical properties include flexural and compressive strength. The samples were dried before testing for thermal conductivity. The curing chamber was set to 45 ℃, and the drying process was continued until the mass did not change (around 1 week). Material density and thermal conductivity have been compiled in Table 7.6.

Table 7.6

Material density and thermal conductivity compilation

Sample	Material density, kg/m^3	Thermal conductivity, W/(m·K)
H12	415	0.075
H13	388	0.071
H14	369	0.068

However, the data has been compiled in Fig. 7.9 for a better visual understanding. This figure reveals a positive correlation between material density and thermal conductivity in biocomposite materials with varying binder-to-filler ratios. Both properties show a clear upward trend as the ratio changes from 1:4 (H14) to 1:2 (H12). The H14 sample, with the highest filler content, shows the lowest

values with approximately 370 kg/m³ material density and 0.068 W/(m·K) thermal conductivity. H13 (1:3 ratio), both properties increase to about 390 kg/m³ and 0.071 W/(m·K), respectively. The H12 sample, with the lowest filler content (1:2 ratio), exhibits the highest values at roughly 415 kg/m³ and 0.075 W/(m·K).

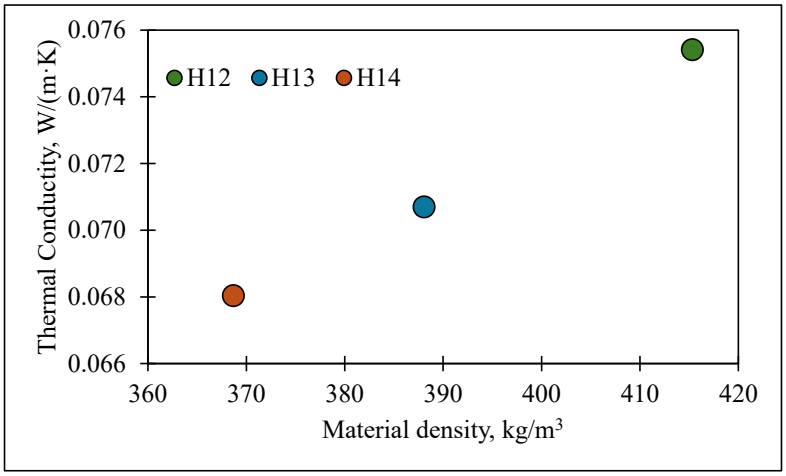

Figure 7.9. Thermal conductivity dependence of the material density of the biocomposite samples.

This trend suggests that decreasing the filler content (or increasing the relative binder content) leads to denser materials with higher thermal conductivity [228]. This relationship could be attributed to the binder potentially creating a more continuous matrix with fewer void spaces, resulting in better heat transfer pathways through the material [229]. However, it is worth noting that this is a relatively linear relationship, indicating a consistent impact of the binder-to-filler ratio on the biocomposites' physical and thermal properties [230]. This understanding could be valuable for tailoring the material properties for specific applications where either thermal insulation or conductivity is desired.

In Table 7.7, mechanical properties are compiled. From the table, it is evident that compressive strength has been tested at 10 and 20 % compression rates based on the sample's height, and the samples have been tested in two directions – forming direction and perpendicular to forming direction.

Table 7.7

Compressive and flexural strength compilation of the samples

Sample	Testing direction	Average compressive strength 10 % (perpendicular to forming direction - critical strength), kPa	Average compressive strength 20 %, kPa	Flexural strength, kPa
H12	Forming direction	175 ± 10	184 ± 14	100 ± 28
	Perpendicular to forming direction	97 ± 13		87 ± 42
H13	Forming direction	75 ± 10	119 ± 15	31 ± 1
	Perpendicular to forming direction	27 ± 2		64 ± 21
H14	Forming direction	26 ± 8	62 ± 5	38 ± 8
	Perpendicular to forming direction	61 ± 7		38 ± 19

The analysis of the compressive and flexural strengths of samples H12, H13, and H14 reveals distinct variations in their mechanical properties. Sample H12 demonstrates a compressive strength in the forming direction, with 175 ± 10 kPa at 10 % deformation and 184 ± 14 kPa at 20 % deformation, alongside a notable flexural strength of 100 ± 28 kPa. In contrast, the perpendicular direction shows a lower compressive strength of 97 ± 13 kPa at 10 % deformation and a lower flexural strength of 87 ± 42 kPa. Sample H13 exhibits significantly lower strengths, with compressive strengths of 75 ± 10 kPa and 119 ± 15 kPa in the forming direction (10 and 20 % compression, respectively) and 27 ± 2 kPa in the perpendicular direction at 10 % deformation. Flexural strength for sample H13 in the forming direction was 31 ± 1 kPa, and in the perpendicular direction to the forming direction, 64 ± 21 kPa. Sample H14 presents higher compressive strength perpendicular to the forming direction at 10 % deformation (61 ± 7 kPa) compared to the forming direction (26 ± 8 kPa). However, this trend reverses at 20 % deformation, with the forming direction showing 62 ± 5 kPa. The flexural strength for H14 is moderate at 38 ± 8 kPa. These findings highlight the influence of testing direction on the mechanical properties of the samples, with significant implications for their potential applications. For better data visualisation, see Figure 7.10, which has been compiled with all the mechanical properties.

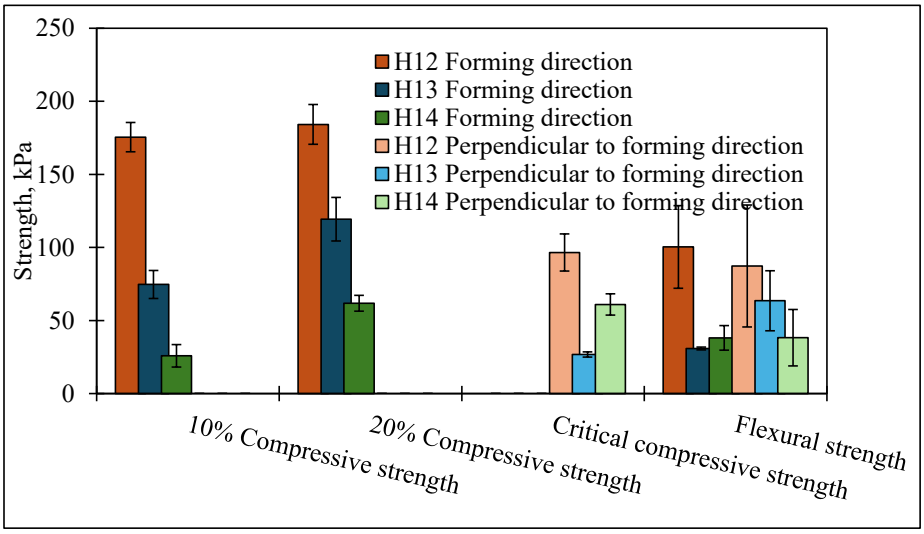

Figure 7.10. Mechanical property compilation.

7.2.2. Biocomposites with 600 °C Treated Sanding Dust

Mix Design and Sample Preparation

Sanding Dust (SD) heat-treated at 600 °C was used as a binder (M-600-2). The properties of the binder have been characterised in Section 6.1. Production Line Waste (PLW) and hemp shives were bio-based aggregates. Additionally, to PLW, hemp shives were used to see how low the thermal conductivity coefficient can get, although hypothesising the result in low compressive strength. Mix designs of the biocomposites made with 600 °C heated SD are compiled in Table 7.8.

Table 7.8

Mix designs of the biocomposites made with 600 °C heated SD, mass parts

Sample	Binder		Filler		
	M-600-2	Water	Dry		Water for wetting*
			PLW	Hemp Shives	
PLW12	1.00	0.60	2.00		1.00
Hemp12				2.00	2.40
Mix12			1.00	1.00	1.80
PLW21	2.00	1.20	2.00		0.50
Hemp21				2.00	1.20
Mix21			1.00	1.00	0.85

*The filler was moistened before mixing so that the filler did not absorb the water intended for the binder.

More water was used to wet hemp shives because they absorb more than PLW. The amount of water added to the binder was the same for all samples at 0.6 mass parts of the binder. This ratio was chosen based on the results of section 6. A flow chart of the sample production process is shown in Figure 7.2. After the mixture was moulded in the forms, the surface was smoothed with a plate to obtain better surface characteristics, as seen in Figure 7.11. The samples with the plate and the load were left to cure for the first 7 days, till the samples were demoulded and wrapped in plastic film to ensure humidity in the samples. The biocomposites were cured for a further 14 days. The samples were dried at 45 °C until a constant sample mass was obtained. For the characterisation of the material, only dry samples were used.

Figure 7.11. Fresh Hemp12 sample in the mould.

Results

Six different sample compositions were produced: three samples had a binder-to-filler weight ratio of 1:2, while the other three samples had a binder-to-filler weight ratio of 2:1. The main physical and

mechanical properties of the material, including structure, material density, thermal conductivity, and compressive and flexural strength, were determined in experimental studies.

Figures 7.12 to 7.17 show the macrostructure of the produced biocomposites at 8 times magnification. The PLW12 macrostructure (Fig. 7.12) shows that the binder uniformly covers the PLW, indicating an optimum filler-to-binder ratio.

Figure 7.12. The macrostructure of the PLW12 sample.

The Hemp12 macrostructure of the sample (Fig. 7.13) shows that the amount of binder adhered to the hemp shives is lower than that adhered to the PLW (Fig. 7.12), which reduces the material's mechanical strength. On the structure of the hemp sample, black dots were noticed that could be *Rhizopus sp.* or *Aspergillus niger,* as those are the most popular moulds in hemp-related products [231].

Figure 7.13. The macrostructure of the Hemp12 sample.

The macrostructure of the Mix12 sample (Fig. 7.14) shows that the binder adheres better to PLW than to hemp shives, similar to previous samples. The figure shows a long hemp fibre that could provide additional strength to the biocomposite if it were intertwined more in the structure of other shives.

Figure 7.14. The macrostructure of the Mix12 sample.

In the PLW21 macrostructure of the sample (Fig. 7.15), the binder covers the surface of the filler more evenly due to the higher binder content in the biocomposite. However, during the manufacturing process, it has been observed that the higher binder content makes it more challenging to work with the material. As the binder coats the filler more evenly and forms a more extensive contact zone, the mechanical strength is expected to be higher than in samples with a lower binder content.

Figure 7.15. The macrostructure of the PLW21 sample.

The macrostructure of Hemp21 (Fig. 7.16) shows a similar trend to Hemp12. Hemp21 contains more filler and is not coated with the binder compared to PLW21.

Figure 7.16. The macrostructure of the Hemp21 sample.

The macrostructure of the Mix21 sample (Fig. 7.17) shows that the binder covers the PLW surface more evenly so that a homogeneous distribution of contact zones is not formed in the bulk of the material. The presence of hemp shives interferes with the hydration reaction as the hemp shives absorb the moisture required for the binder reaction, thus preventing complete hydration of the binder. Hemp also releases biologically active substances which interfere with the curing of mineral binders. All of the hemp and mix samples showed possible contamination of black mould.

Figure 7.17. The macrostructure of the Mix21 sample.

Figure 7.18 shows the macrostructures of the samples without magnification. The PLW12 sample has the most uniformly binder-coated filler and the best-formed contact zone among the six compositions. The biocomposites with PLW filler are grey in shade compared to the other compositions, indicating the presence of a uniform binder. Biocomposites with a binder-to-filler ratio of 2:1 show an uneven structure, implying lower workability, which should be improved by modifying composition and manufacturing technology. PLW21 is characterised by binder-filler heterogeneity and a relatively rough surface, indicating that the material is not uniform in workability. A similar trend is also observed for the Mix21 composition.

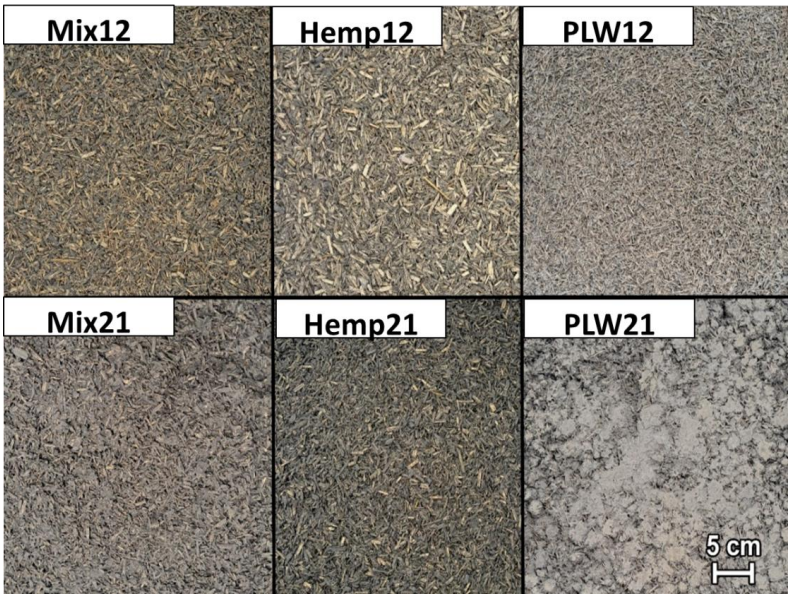

Figure 7.18. The visual appearance of the biocomposites produced.

This study produced biocomposites with material densities ranging from 171 to 782 kg/m³, depending on the material composition (Table 7.8). Figure 7.19 shows the material density values of the produced samples.

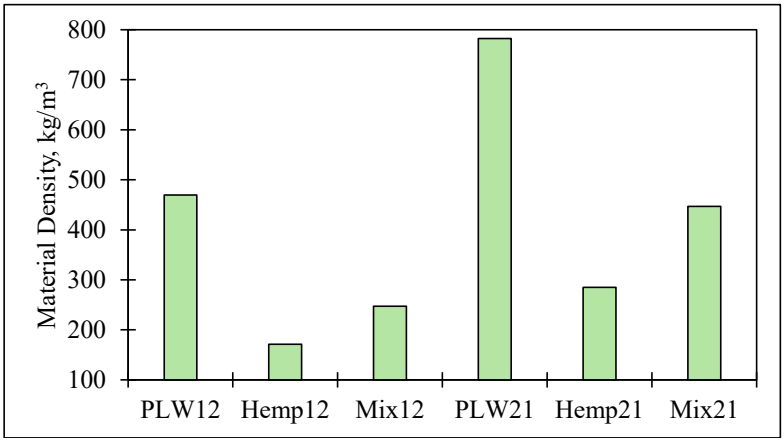

Figure 7.19. Material density for each sample.

Comparing bio-composites with binder-to-filler ratios of 1:2 and 2:1, it was observed that the material density increases by 65-80 % with increasing binder content. Cewood Ltd. wood-wool cement panels have a material density between 420 and 560 kg/m^3.

A clear positive correlation exists between material density and thermal conductivity across all samples (Fig. 7.20). The PLW21 sample stands out with notably higher values in both properties (782 kg/m³ material density and 0.139 W/(m·K) thermal conductivity), suggesting that production line waste at a 2:1 ratio creates a denser, more thermally conductive material. In contrast, Hemp12 shows

the lowest values (171 kg/m³ and 0.052 W/(m·K)), indicating that hemp shives at a 1:2 ratio produce a lighter, more insulating material.

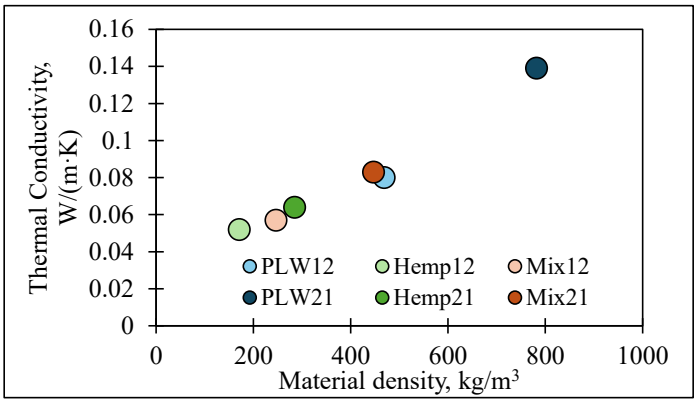

Figure 7.20. Thermal conductivity dependence on the material density of the samples.

Foreseeably, the mix samples (Mix12 and Mix21) cluster together in the middle range (around 247-447 kg/m³ and 0.057-0.083 W/(m·K)), suggesting that combining both fillers or using PLW at a lower ratio leads to intermediate properties. Hemp21 shows slightly higher values than Hemp12 but remains relatively lightweight compared to PLW samples, demonstrating how hemp shives consistently contribute to lighter composites regardless of ratio. This variation in properties based on filler type and ratio provides flexibility in tailoring the biocomposites for different applications, from insulation (hemp-rich compositions) to structural applications (PLW-rich compositions).

Figure 7.21 shows the flexural strength results of the biocomposites produced. The biocomposites exhibit flexural strengths up to 288 kPa depending on the composition.

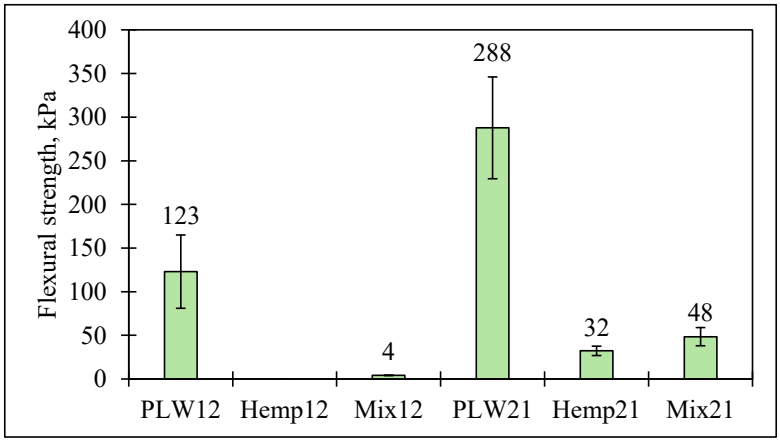

Figure 7.21. Flexural strength of the samples.

The results show that the presence of hemp shives in the material significantly reduces the flexural strength of the sample. This is due to the relatively lower contact zone and high water uptake in hemp shive biocomposites, which release bioactive substances, reducing the strength.

Compressive strength was tested at 10 % strain for all samples and at the failure load for the PLW21 sample, as this was the only sample where the load/deformation curves showed a pronounced failure

of the material. Figure 7.22 shows the compressive strength results of the biocomposites produced. The compressive strength of the biocomposites produced parallel to the forming direction varies from 0.02 to 1.65 MPa, depending on the filler used and the binder/filler ratio. For the Mix12 samples, performing a compressive strength test was impossible due to the material being brittle.

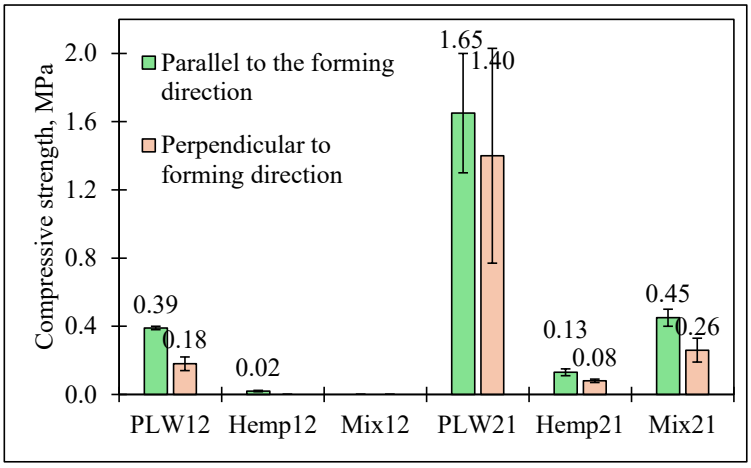

Figure 7.22. Compressive strength of the bio-composites at 10 % strain.

Compared to commercially available wood-wool cement panels, the PLW12 sample produced is similar in properties to commercial wood-wool cement panels with a compressive strength parallel to the direction of forming of 0.3 MPa. It should be noted that commercial wood-wool cement panels are produced more homogeneously, so the experimental results could be improved by modifying the fabrication technology. The PLW21 sample shows more than twice the compressive strength of PLW12, although the material density of these biocomposites differs by less than a factor of two.

The compressive strength of the samples is perpendicular to the direction of forming, and in all cases, it is approximately twice as low as parallel to the direction of forming. This indicates that all the biocomposites produced are anisotropic and that their mechanical properties vary significantly depending on the orientation of the filler in the material and the operating direction.

Given the study's objective to investigate the use of wood-wool cement panel production wastes, the two biocomposites produced (PLW 1:2 and PLW 2:1) were compared with commercially available acoustic wood-wool cement panel sheets produced by Cewood Ltd. The comparison is shown in Table 7.9.

Table 7.9

Property comparison of the manufactured biocomposites and Cewood Ltd. wood-wool cement panels

Property	Cewood acoustic panel	PLW12	PLW21
Width of the fibre, mm	1.5	1.5	1.5
Thickness, mm	25	40	31
Material density of material, kg/m^3	420	470	780
Thermal conductivity (λD), W/(m·K)	0.066	0.080	0.139
Flexural strength (EN 12089), kPa	≥ 1300	≥ 75	≥ 220
Compressive strength (EN 826), kPa	≥ 300	≥ 380	≥ 1500

As shown in the table, the biocomposites produced in the study have lower flexural strength (≥ 220 kPa PLW 2:1 and ≥ 75 kPa PLW 1:2) and higher compressive strength (≥ 1500 kPa PLW21 and ≥ 380 kPa PLW12) than commercially available materials. Although commercial wood-wool cement panel products are made with fresh cement and longer wood shavings, the results of this study can be considered satisfactory. PLW21 is unsuitable for visual aspects, while PLW12 is comparable to Cewood.

7.3. Biocomposites with CEM II/A-LL 42.5 N

Mix Design and Sample Preparation

CEM II/A-LL 42.5 N was used as the binder to compare the biocomposites' properties with the properties of biocomposites made with the developed binders. By using a commercially available binder, a comparison of the effectiveness of the developed binders can be evaluated.

Production Line Waste (PLW) was examined as a filler to produce biocomposites. The effect of the binder-to-filler ratio was examined and evaluated. The biocomposites were prepared with different CEM II/A-LL 42.5 N to PLW ratios (Table 7.10). The CEM II/A-LL 42.5 N to PLW ratio was 1:2, 1:3, and 1:4. The water-to-filler (W/F) ratio was increased with the increase of PLW content in the mixture composition. The 1:2 mixture had a W/F ratio of 0.7. In mixture 1:3, it increased to 1.3; for 1:4, the W/F increased to 1.6. In previous research, water could reach and be above a 1:1 ratio to filler content [232–234].

A partial PLW substitution with the hemp shives (HS) was evaluated to reduce the material density of biocomposites. Previous research showed that adding HS allows the obtaining of biocomposites with a material density of 200 to 400 kg/m^3 [235]. The replacement of 25 %, 50 % and 75 % by the weight of PLW with HS was assumed (Table 7.10). The CEM II/A-LL 42.5 N to filler ratio remained 1:2 by weight. The bulk material density of HS is significantly lower than that of PLW (100 kg/m^3 for HS compared to 300 kg/m^3 for PLW).

Table 7.10

Mix designs of the biocomposites made with CEM II/A-LL 42.5 N, mass parts

Sample	Binder		Filler		
			Dry		Water for wetting*
	CEM II/A-LL 42.5 N	Water	PLW	Hemp Shives	
I	1.0	0.4	2.0		0.7
II			3.0		1.3
III			4.0		1.6
H25			1.5	0.5	1.4
H50			1.0	1.0	1.6
H75			0.5	1.5	2.0

*The filler was moistened before mixing so that the filler did not absorb the water intended for the binder.

All dry components were weighed, but before mixing (Fig. 7.23a), fillers were mixed with water to wet the surface for 2 min (Fig. 7.23b). A single-shaft electrical mixer, RubiMix, was used for mixing. Then, CEM II/A-LL 42.5 N was added, and the mixture was homogenised for 2 min (Fig. 7.23c). Then, the mixture was cast in prepared moulds (Fig. 7.23d). The samples with 35 × 35 × 5 to 35 × 35 × 10cm were prepared for further testing.

Figure 7.23. Mixing procedure of biocomposites: a) PLW filler; b) filler wetting; c) binder incorporation in the mixture; d) casting of the biocomposite.

Results and Discussion

The macrostructure of the biocomposites is given in Figure 7.24. PLW fillers are entirely covered with cement particles, and only for sample H25 can the large-sized hemp shives be identified separately. Hemp shives have a larger particle size distribution than PLW; therefore, it is much easier to identify individual hemp shives. Mixture compositions containing only PLW and CEM II/A-LL 42.5 N have similar microstructures. The change of CEM II/A-LL 42.5 N content in the mixture composition had a minor effect on the macrostructure observed by the microscope.

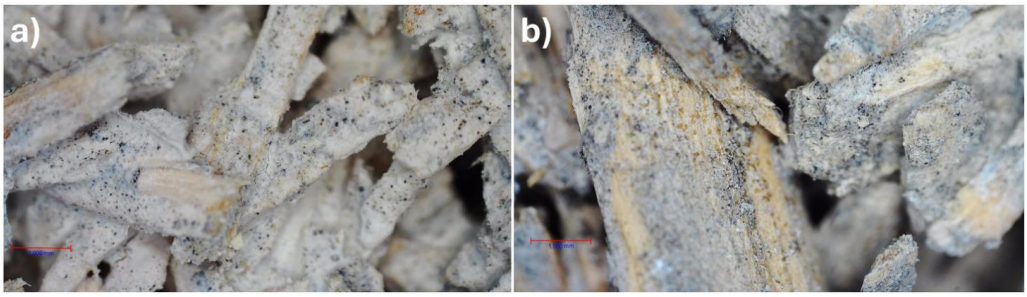

Figure 7.24. Macrostructure of the biocomposites, a) composition I; b) composition H25.

The physical properties of the obtained biocomposites are given in Table 7.11. The material density of the biocomposites decreased as the cement-to-filler ratio increased. CEM II/A-LL 42.5 N to PLW ratio increase from 1:2 to 1:4 decreased the material density of the biocomposites from 474 to 391 kg/m^3. The decrease in material density reduced thermal conductivity from 0.082 W/(m·K) to 0.070 W/(m·K). The gradual decrease is associated with dense cement particle reduction in the

composition. Thermal conductivity for the hemp filler samples was 0.064 to 0.054 W/(m·K) based on the hemp shive percentage. The addition of hemp shives reduced material density significantly. Even 25 % incorporation of HS reduced material density to 329 kg/m^3, and material density reduced to 197 kg/m^3 with 75 % PLW substitution with HS (H75). A compelling 0.054 W/(m·K) can be reached; however, little reduction was observed between mixtures H50 and H75.

Table 7.11

Physical properties of the biocomposites

Sample	I	II	III	H25	H50	H75
Material density, kg/m^3	474	415	391	329	240	197
Thermal Conductivity, W/(m·K)	0.082	0.077	0.070	0.064	0.055	0.054

Looking at Figure 7.25, there is a clear transition in material behaviour. Samples I, II, and III (with PLW filler) show higher material densities (391-474 kg/m³) and thermal conductivity values (0.070-0.082 W/(m·K)). As hemp shive percentage increases from 0 % to 75 %, material density and thermal conductivity decrease systematically, with H75 showing the lowest values of 197 kg/m³ and 0.054 W/(m·K). This trend can be attributed to hemp's inherent lightweight nature and cellular structure, as documented by Arnaud and Gourlay [236].

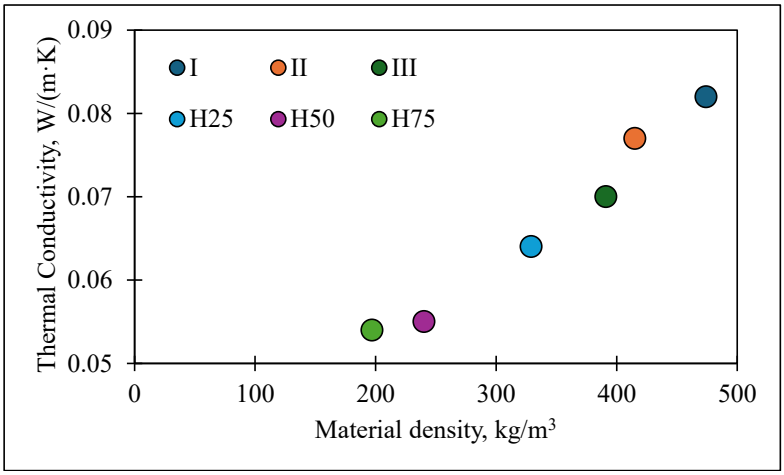

Figure 7.25. Thermal conductivity dependence on material density.

The inverse relationship between hemp content and material density/thermal conductivity aligns with findings from Benfratello et al. [237], who demonstrated that increasing hemp shive percentages creates more void spaces in the matrix, enhancing insulating properties. The increasing water for wetting requirements (1.4-2.0 parts) with higher hemp percentages reflects hemp's high water absorption capacity. This characteristic significantly influences the final composite structure, as detailed by Diquélou et al. [238].

The compilation of mechanical strength is given in Figure 7.26. H50 and H75 were too brittle to test, and thus, we concluded that those samples were not feasible for the objectives of this thesis. The highest amount of CEM II/A-LL 42.5 N in the biocomposite (I) shows a flexural strength of 0.31 MPa and compressive strength of 0.56 MPa at 20 % deformation. The reduction of the CEM II/A-LL 42.5

N (II) led to a decrease in flexural strength of 0.12 MPa and compressive strength of 0.31 MPa at 20 % deformation. Sample III flexural strength achieved 0.06 MPa and a compressive strength of 0.21 MPa at 20 % deformation. However, the lowest strength was for a mixture with HS. Only H25 was possible to test, and the flexural strength was 0.02 MPa, and the compressive strength achieved 0.20 MPa at 20 % deformation.

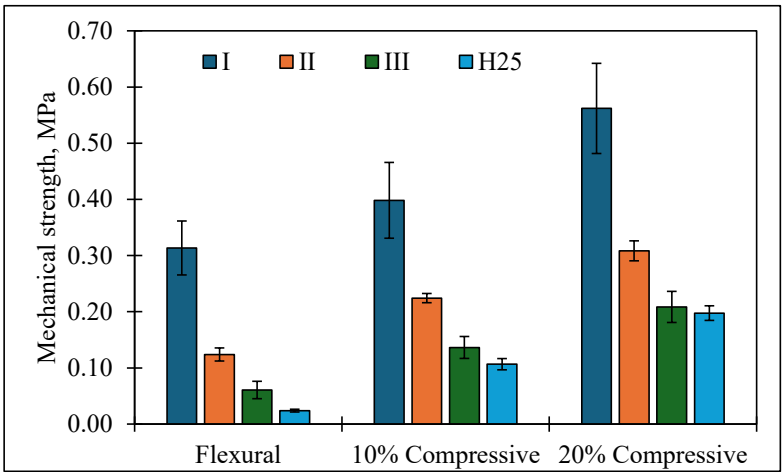

Figure 7.26. Mechanical strength compilation of biocomposites.

7.4. Demonstration of biocomposites

The workability and feasibility of the biocomposite made with a mechanically activated binder were practically approbated in a semi-industrial setting. An experimental stand (Fig. 7.27) was built using 2 compositions of the developed biocomposites. The binder used was vibration-milled SD that was milled for 20 minutes. A vibration mill was used because of its capacity to mill larger amounts of material than a planetary mill. The filler was PLW (Fig. 4.8), collected from the WWCP manufacturing plant a few days before building. The construction of the experimental stand took two days.

Figure 7.27. Timber frame of the experimental stand.

A total of two walls were filled with the designed material. Both walls had slight variations in composition for the variety of results. On the first day, measurements of the materials were taken to increase work effectiveness later. The density of the dry wool was determined using a bucket of a specific volume (Fig. 7.28) into which the wool was placed and weighed, and the density was calculated. The bulk density is about 70 kg/m^3, while when the material is compressed (simulating a fill in a partition), the density is about 200 kg/m^3, which varies when the wool is wet or dry. In the case of wet wool, the density can reach 270 kg/m^3. Both the binder and filler were weighed before each mixing.

Figure 7.28. Manual collection of the wood wool in the bucket.

The inner and outer layers of the timber frame consisted of defective WWCP, which were then filled in the middle with the developed biocomposite (Fig. 7.29a).

Figure 7.29. a) The inner and outer layers are attached, and b) the middle layer is added.

The filler was poured into a drum mixer, and water was added to moisten the wood-wool in the ratio of 0.15 of the mass of the filler. Then, the binder is added in the ratio of 0.25-0.30 of the filler mass and mixed. When the binder has been dispersed, more water is added in a ratio of 0.60 of the

amount of the binder's mass. Everything is mixed for 2 minutes and, with slight packing, is filled into the wall (Fig. 7.29b).

While the material was added to the wall, temperature and relative humidity sensors were placed on one of the walls to get real-life data about the material's performance (Fig. 7.30).

Figure 7.30. Sensor addition in the filling process.

Other wall sensors were drilled according to Figure 7.31. Angles were chosen to keep the linearity of the material as intact as possible.

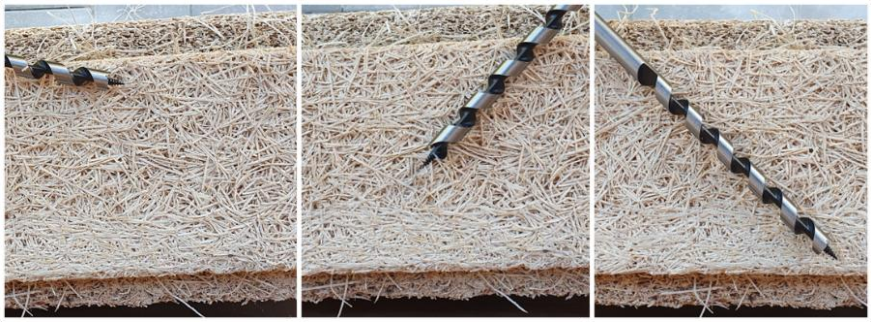

Figure 7.31. Drilling paths for sensor placement.

With the construction of this experimental stand, smaller laboratory-scale samples with dimensions 600 × 600 × 180 mm were made (Fig. 7.32). The laboratory samples were made from two defective WWCPS fastened to each side of a wooden frame, with the top part also being a WWCP. The middle layer of the panel consists of the developed material. The panels were tested for their density and thermal conductivity. The composition of laboratory samples was the same as the experimental stand and was close to the P3 sample from section 7.1. The density for the whole panel was 323 kg/m^3 with a thermal conductivity of 0.0709 W/(m·K). The middle layer was then taken out of the form and tested separately. It achieved a 245 kg/m^3 density with a thermal conductivity of 0.0796 W/(m·K).

Figure 7.32. Laboratory sample of the experimental stand.

After the walls have been filled and sensors placed, the experimental stand looks like Figure 7.33. Afterwards, construction of the experimental stand continued, with a roof, doors, façade, and heating system added. As of now, the house still stands and is in use.

Figure 7.33. Multilayer panel completion of the experimental stand.

7.5. Chapter Summary

This research investigated various biocomposites with different binders, analysing their physical and mechanical properties to evaluate their potential in sustainable construction applications.

The mechanically activated SD demonstrated a clear relationship between binder content and material properties across samples P1, P2, and P3 (densities 613-430 kg/m³). Higher binder content resulted in extensive fibre coverage and good mechanical properties, with P1 achieving a flexural strength of 236 kPa and compressive strengths of 469 kPa parallel and 330 kPa perpendicular to the forming direction. Conversely, lower binder content improved thermal insulation, with P3 achieving a

thermal conductivity of 0.083 W/(m·K). This inverse relationship between mechanical strength and thermal performance was consistent across all binders studied.

The biocomposites with 450 °C treated sanding dust (samples H12, H13, H14) exhibited similar trends within a lower density range (369-415 kg/m³). The direct correlation between density and thermal conductivity persisted, with values between 0.068 and 0.075 W/(m·K). H12, being the densest sample, demonstrated the highest mechanical properties, achieving compressive strengths of 175 kPa parallel and 97 kPa perpendicular to the forming direction, along with a flexural strength of 100 kPa. All samples using this binder exhibited anisotropic behaviour, though less pronounced than in the mechanically activated SD biocomposites.

Wood-wool cement panel production line waste with 600 °C treated sanding dust showed that while these materials cannot fully match the properties of original Cewood products, they remain viable for specific applications. A particularly notable finding was the difference in binder adhesion – the binder adhered well to PLW but less effectively to hemp shives due to water absorption and release of biologically active substances. The incorporation of hemp shives significantly improved thermal performance, with conductivity reaching as low as 0.052 W/(m·K), though at the expense of mechanical properties. This trade-off between thermal and mechanical properties remained consistent across all tested formulations.

The Portland cement (CEM II/A-LL 42.5 N) biocomposites using crushed wood-wool cement panels as fillers demonstrated promising results. These composites achieved 391-511 kg/m³ material densities with varying cement-to-filler ratios. The recycling approach proved technically feasible, though the thermal conductivity remained relatively high (0.070 W/(m·K)) due to the cement content in the crushed waste materials. However, incorporating hemp shives substantially reduced density (down to 197 kg/m³) and improved thermal performance (λ=0.054 W/(m·K)), creating a viable self-bearing insulation material.

Several significant patterns emerge across the research when comparing all four binders. Thermal properties consistently improve as material density decreases, regardless of the binder type, with hemp-incorporated compositions achieving the lowest thermal conductivity values (0.052-0.054 W/(m·K)). Mechanical properties correlate positively with material density in all biocomposites, with the mechanically activated SD achieving the highest absolute strength values. All systems exhibit anisotropic behaviour to varying degrees, with consistently higher strength values in the parallel forming direction, highlighting the importance of orientation in structural applications.

Based on the analysis, each binder offers advantages for specific applications. The mechanically activated SD compositions balance thermal insulation and mechanical strength, making them suitable for applications requiring both properties. Hemp-incorporated compositions with either M-600-2 or CEM II/A-LL 42.5 N cement achieve optimal thermal insulation, ideal for non-load-bearing insulation applications. CEM II cement and thermally treated SD provide mechanical performance for structural applications with secondary thermal requirements. From a sustainability perspective, Portland cement using crushed wood-wool cement panels as filler demonstrates the most promising approach for circular economy applications.

The thermal properties of all developed materials are comparable to those of commercial wood fibre products, while their mechanical properties align closely with hempcrete. These biocomposites are viable alternatives in specific building applications where a balance of mechanical strength and thermal insulation is required. The most promising applications include:

- Non-load-bearing wall elements;

- Void filling between structural elements;
- Thermal insulation in building envelopes;
- Acoustic panels for interior applications.

The practical applicability of the biocomposite with mechanically activated binder was successfully demonstrated through the construction of an experimental stand. Using vibration-milled sanding dust as binder and production line waste as filler, a multi-layer wall system was created with defective wood-wool cement panels as inner and outer layers filled with the developed biocomposite. Laboratory samples of this system achieved a density of 323 kg/m³ with a thermal conductivity of 0.0709 W/(m·K), while the biocomposite middle layer alone registered at 245 kg/m³ with 0.0796 W/(m·K) thermal conductivity. This real-world application validated the material's workability and feasibility in semi-industrial settings, confirming its potential for practical implementation in sustainable construction.

Results of all biocomposites have been compiled in Table 7.12. For visual representation, the relation between 10 % compressive strength and thermal conductivity has been visualised in Figure 7.34.

Table 7.12

Property compilation of the created biocomposites

Sample	Material density, kg/m^3	Thermal conductivity, W/(m·K)	Flexural Strength, kPa		Compressive strength, kPa		
			Forming direction	Perpendicular to the forming direction	10 %*	20 %*	Critical
P1	613	0.117	-	236 ± 21	469 ± 81	-	267 ± 39
P2	494	0.093	-	108 ± 6	256 ± 21	-	65 ± 7
P3	430	0.083	-	60 ± 12	177 ± 32	-	44 ± 6
H12	415	0.075	100 ± 28	87 ± 42	175 ± 10	184 ± 14	97 ± 13
H13	388	0.071	31 ± 1	64 ± 21	75 ± 10	119 ± 15	27 ± 2
H14	369	0.068	38 ± 8	38 ± 19	26 ± 8	62 ± 5	61 ± 7
PLW12	469	0.080	-	123 ± 42	392 ± 9	-	176 ± 45
Hemp12	171	0.052	-	-	24 ± 4	-	-
Mix12	247	0.057	-	4 ± 0	-	-	-
PLW21	782	0.139	-	288 ± 58	1652 ± 351	-	1402 ± 633
Hemp21	285	0.064	-	32 ± 5	128 ± 22	-	77 ± 9
Mix21	447	0.083	-	49 ± 10	449 ± 52	-	257 ± 71
I	474	0.082	-	313 ± 48	398 ± 67	562 ± 80	-
II	415	0.077	-	124 ± 12	224 ± 8	308 ± 18	-
III	391	0.07	-	61 ± 15	136 ± 20	209 ± 28	-
H25	329	0.064	-	24 ± 2	107 ± 10	198 ± 13	-
H50	240	0.055	-	-	-	-	-
H75	197	0.054	-	-	-	-	-

*Tested in forming direction, compression 10, 20 % of sample height.

From the figure, the most promising biocomposites would be PLW12, I, Mix21, Hemp21 and H25, showing the lowest thermal conductivity with compressive strength above the trendline. Sample

PLW21 was excluded from this list, although it was above the trendline because the thermal conductivity was more than twice that of the Hemp21 and H25 samples (0.139 W/(m·K)).

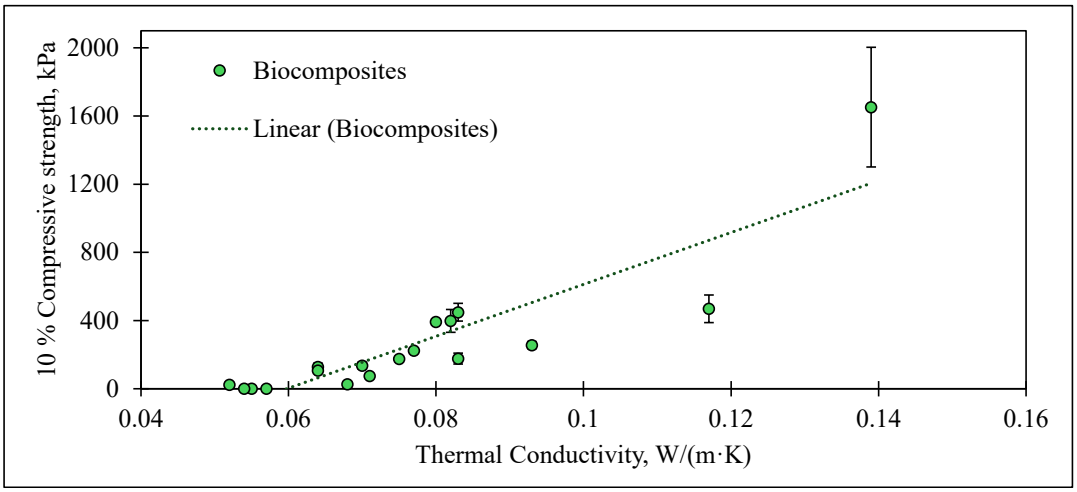

Figure 7.34. Biocomposite thermal conductivity and 10% compressive strength relation visual representation.

This research demonstrates that biocomposites using various recovered binders offer viable alternatives to conventional building materials, with promise for sustainable construction applications aligned with circular economy principles.

Future research will optimise binder-to-filler ratios to create materials with an improved balance between thermal and mechanical performance. The experimental stand will continue to provide valuable data on real-world performance, particularly regarding temperature and humidity regulation in varying environmental conditions. Additionally, investigating hybrid binder systems combining elements of the studied approaches may yield enhanced overall performance. Long-term durability testing for moisture sensitivity, fire resistance, and dimensional stability will be essential to establish these materials' viability in practical construction applications. Environmental impact assessment through life cycle analysis will further validate the sustainability advantages of these biocomposites, particularly those using recycled content. Finally, pilot-scale production of panels and real-world applications are necessary to address potential scaling challenges and optimise manufacturing processes.

The proposed wood-wool cement panel waste-based biocomposites' physical and mechanical characteristics have been examined in the previous chapters, indicating their potential for innovative building materials. While these findings affirm an application potential, a complete understanding of their sustainability profile necessitates a thorough assessment of their environmental implications across their entire life cycle. Consequently, the forthcoming chapter will analyse these materials' Life Cycle Assessment (LCA). It will provide a comprehensive assessment of their environmental impact from raw material acquisition to end-of-life scenarios, thus completing their sustainability characterisation.

8. LIFE CYCLE ASSESSMENT OF DEVELOPED BUILDING MATERIALS

8.1. Of the Developed Binders

The Life Cycle Assessment (LCA) revealed significant variations in global warming potential among different binder processing methods. The impact on global warming was calculated per 1 m^3 of the binder. The vibration-milled binder demonstrated the lowest environmental impact of 148 kg CO_2 eq., followed by thermal treatments at 450 ℃ and 600 ℃ (387 and 570 kg CO_2 eq., respectively). Conventional CEM II/A-LL 42.5 N cement showed the highest impact of 1040 kg CO_2 eq. (Fig. 8.1) However, a more comprehensive understanding of environmental efficiency emerges when analysing these emissions in relation to the binders' mechanical performance.

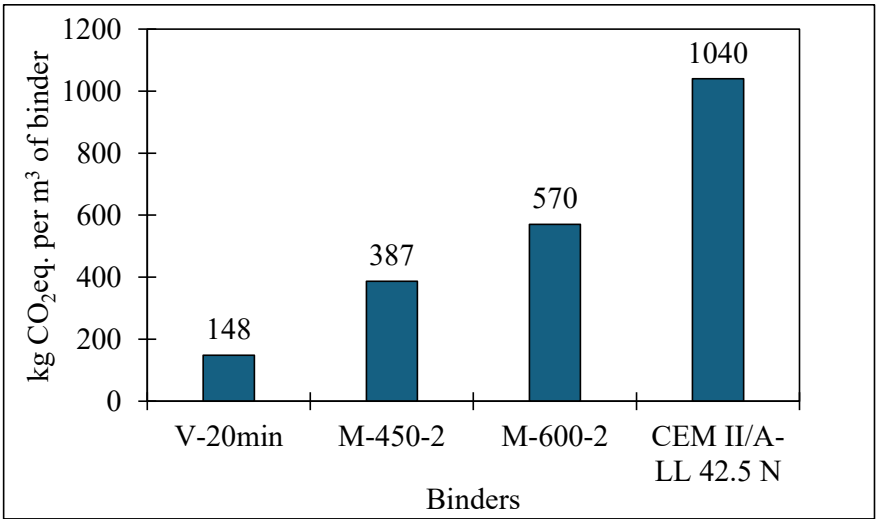

Figure 8.1. Global warming potential of the developed binders compared to commercial cement.

Despite having the lowest total emissions, the vibration-milled binder exhibited the highest emissions per MPa at 92.5 kg CO_2 eq./MPa due to its relatively low compressive strength of 1.6 MPa. In contrast, the sanding dust heated at 450 ℃, while producing higher total emissions (387 kg CO_2 eq.), achieved a better environmental efficiency with 37.3 kg CO_2 eq./MPa, supported by its improved compressive strength of 10.4 MPa. The 600 ℃ thermal treatment resulted in intermediate performance with 69.5 kg CO_2 eq./MPa, reflecting its compressive strength of 8.2 MPa.

Conventional CEM II/A-LL 42.5 N cement, despite having the highest total emissions at 1040 kg CO_2 eq., demonstrated the best environmental efficiency in strength-normalised emissions at 15.2 kg CO_2 eq./MPa. This superior performance is attributed to its significantly higher compressive strength of 68.3 MPa, highlighting the importance of considering both environmental impact and mechanical performance in material assessment.

Comparing the emissions of the developed binders with other researchers' results, like Tefa et al. [239], who developed and analysed a geopolymeric binder. The Tefa sample's lowest emissions were 357 and 358 kg CO_2 eq./m^3 for alkali-activated geopolymeric binders, comparable to the M-450-2 binder. The difference is that the M-450-2 is 100% waste without adding virgin material.

These findings underscore a crucial trade-off between total environmental impact and performance efficiency. While alternative binder production methods, particularly vibration milling, show promise in reducing total CO_2 emissions, their lower strength properties currently result in higher emissions per unit of performance. This suggests that future research should optimise these alternative methods to enhance mechanical properties while maintaining their lower environmental impact.

8.2. Of the Biocomposites

Following the environmental impact assessment of different binders, evaluating the life cycle performance of the resulting biocomposites is crucial, as their practical applications ultimately determine their environmental value. The environmental impact of the biocomposites was compared using interpolation and extrapolation methods to compare the data based on compressive strength of 0.05, 0.15 and 0.5 MPa. A compressive strength value of 0.05 MPa was chosen as a non-load-bearing middle layer material of a sandwich-type panel (Fig. 2.10). The 0.15 MPa compressive strength was chosen according to EN 996, representing other biobased building materials. 0.5 MPa compressive strength was chosen as a non-load-bearing construction block compressive strength.

To establish a comprehensive foundation for the life cycle assessment, interpolated data sets were developed based on experimental results, providing mix designs and resulting properties for each binder type and target strength level (Table 8.1). The data sets include the required quantities of binder, water, and filler per cubic meter and the resulting composite properties such as compressive strength, density and thermal conductivity. These interpolated values enable a systematic comparison across different binder types while maintaining consistent performance criteria. The thickness required to achieve a U-value of 0.18 W/(m²K) is particularly interesting, representing a practical metric for thermal insulation applications in construction.

The resulting physical properties demonstrate a clear correlation between binder content, density, and thermal conductivity. As the compressive strength increases, density is notable across all binder types, ranging from approximately 360-380 kg/m³ for 0.05 MPa samples to 500-634 kg/m³ for 0.5 MPa samples. This increase in density corresponds with higher thermal conductivity values, ranging from 0.068-0.074 W/(m·K) for lower strength composites to 0.087-0.121 W/(m·K) for higher strength variants. Consequently, the required thickness to achieve a U-value of 0.18 W/(m²K) varies significantly, with higher-strength composites generally requiring greater thickness due to their increased thermal conductivity.

Table 8.1

Properties of the functional unit based on the binder used

Binder type	Name	Binder, kg/m^3	Water for binder, kg/m^3	Filler, kg/m^3	Compressive strength 10%, MPa	Thermal conductivity, W/(m·K)	Density, kg/m^3	Thickness at U=0.18 W/(m^{2}K), m
Vibration milled	Vibro(0.05)	24	17	326	0.05	0.068	359	0.38
	Vibro(0.15)	81	57	311	0.15	0.080	420	0.45
	Vibro(0.5)	280	196	257	0.50	0.121	634	0.67
Heated at 450 °C	450(0.05)	80	48	274	0.05	0.069	378	0.38
	450(0.15)	117	70	256	0.15	0.074	408	0.41
	450(0.5)	247	148	193	0.50	0.091	514	0.51
	600(0.05)	111	67	291	0.05	0.074	436	0.41

Heated at 600 °C	600(0.15)	135	81	286	0.15	0.079	461	0.44
	600(0.5)	219	131	267	0.50	0.095	551	0.53
CEM II cement	CEM(0.05)	51	20	301	0.05	0.068	361	0.38
	CEM(0.15)	79	31	299	0.15	0.072	394	0.40
	CEM(0.5)	176	70	294	0.50	0.087	506	0.48

Overall emissions have been compiled in Figure 8.2. The total emissions per cubic meter of biocomposite range from 4.1 kg CO_2 eq. for Vibro(0.05) to 111.0 kg CO_2 eq. for CEM(0.5), demonstrating a clear correlation between compressive strength and environmental impact.

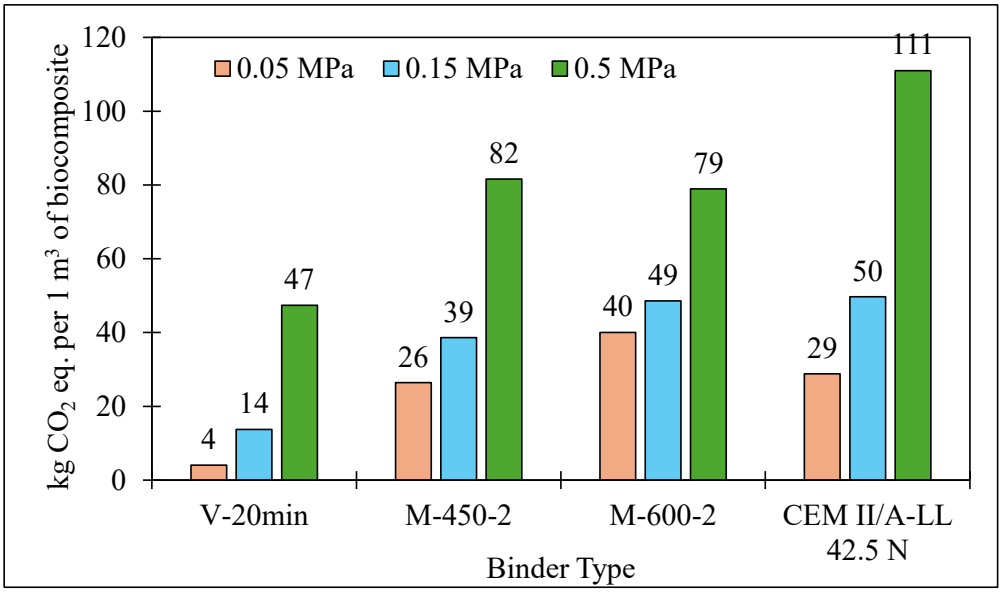

Figure 8.2. Overall emissions per 1 m^3 of biocomposites.

As mentioned before, most biocomposites use waste from wood-wool cement panel manufacturing, either as filler or as binder, thus resulting in zero emissions from the material itself, only from processing it, if needed. Overall, emissions sources are the processing of the binder, water, electricity, heating, and transportation, compiled in Figure 8.3.

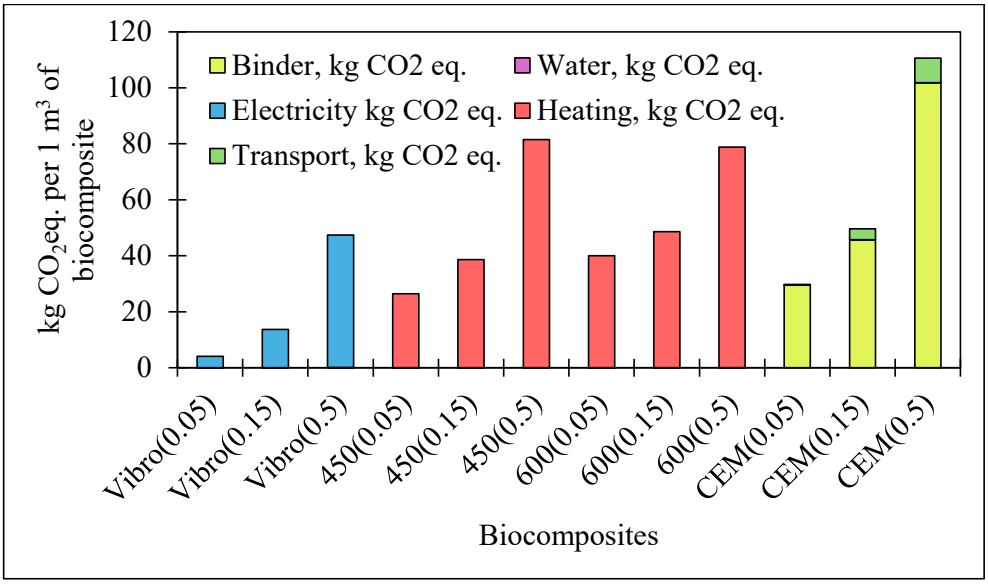

Figure 8.3. Emissions per 1 m^3 of biocomposites by sources.

For vibration-milled biocomposites, the emissions increase from 4.06 to 47.4 kg CO_2 eq./m^3 as strength increases from 0.05 to 0.5 MPa. The primary contributor to these emissions is electricity consumption for the milling process. Biocomposites with thermally treated binders at 450 °C show a similar trend, with emissions ranging from 26.4 to 81.6 kg CO_2 eq./m^3. However, their environmental impact is primarily attributed to heating energy requirements.

The 600 °C thermal treatment samples demonstrate higher emissions across all strength classes (40.0 to 78.9 kg CO_2 eq./m^3), with heating energy again being the dominant factor. CEM II cement-based biocomposites exhibit the highest environmental impact, ranging from 28.8 to 111 kg CO_2 eq./m^3, with binder production contributing the largest share of emissions, followed by transport-related emissions.

These results indicate that higher strength requirements generally lead to increased environmental impact across all binder types. However, the vibration-milled biocomposites maintain the lowest emissions profile, particularly for lower-strength applications. The choice of optimal binder type should consider both the required mechanical properties and the environmental impact for specific applications.

Analysis of emissions normalised by thermal performance (U-value 0.18 W/(m^2K)) reveals distinct environmental efficiency patterns across the biocomposites (Fig. 8.4). Vibration-milled samples demonstrate the lowest environmental impact, ranging from 2 to 32 kg CO_2 eq. per U-value unit, showing clear advantages for lower-strength applications.

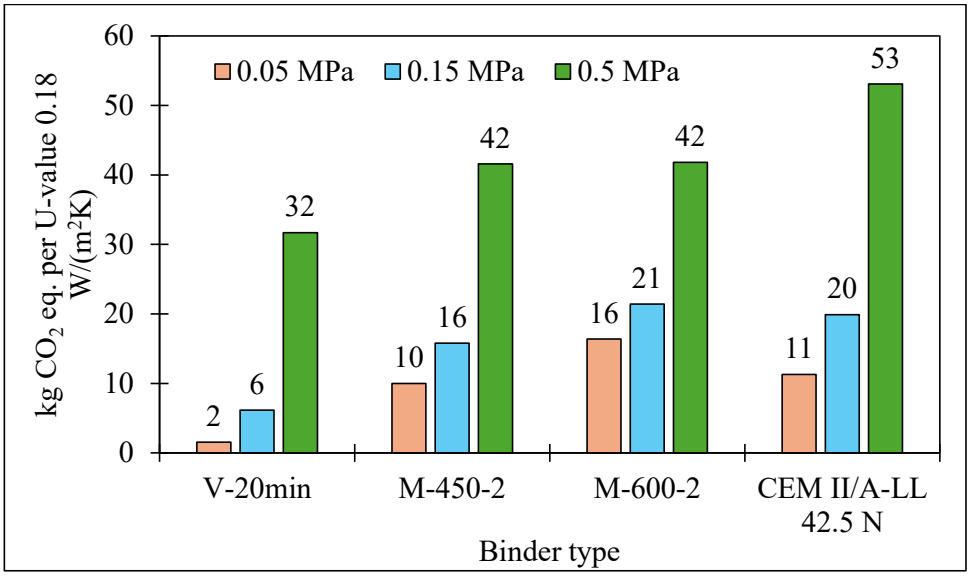

Figure 8.4. Overall emissions of biocomposites per U-value of 0.18 W/(m^{2}K).

Thermally treated binders at 450 °C and 600 °C show intermediate performance (10-42 kg CO_2 eq.), while CEM II cement-based composites exhibit the highest impact (11-53 kg CO_2 eq.). Across all binder types, achieving higher compressive strengths results in significantly increased environmental impact per unit of thermal performance, suggesting that optimal material selection should carefully balance strength requirements with thermal insulation needs.

A notable advancement in sustainable building materials can be demonstrated through hemp-shive-based biocomposites, which achieve negative carbon emissions while maintaining the required functional properties. Using thermally treated SD at 600 °C as binder combined with hemp shives results in total emissions of -246 kg CO_2 eq./m³ for 0.05 MPa strength class and -57 kg CO_2 eq./m³ for 0.15 MPa strength class. Biocomposites with a compressive strength of 0.5 MPa cannot be made. This carbon-negative performance is achieved through the substantial carbon sequestration capacity of hemp shives (-284 and -159 kg CO_2 eq., respectively), which more than compensates for the positive emissions from heating energy (38 and 102 kg CO_2 eq.). The negative emission aspect of hemp shives was also analysed by Sinka and Arrigoni et al. [240,241], who came to a similar conclusion when working with hemp-based biocomposites. When analysed from a thermal performance perspective (U-value 0.18 W/(m²K)), the biocomposites maintain their negative emissions at -79 and -25 kg CO_2 eq., while providing better thermal insulation properties (λ=0.058-0.078 W/(m·K)) than previous compositions. These results demonstrate that strategically combining thermally treated SD with bio-based aggregates like hemp shives makes it possible to create building materials that reduce environmental impact and actively contribute to carbon sequestration.

The life cycle assessment across different binder types and resulting biocomposites reveals a complex relationship between environmental impact, mechanical properties, and thermal performance. For binders alone, emissions ranged from 148 kg CO_2 eq. (V-20min) to 1040 kg CO_2 eq. (CEM II/A-LL 42.5 N), with thermal treatments showing intermediate values. When incorporated into biocomposites, the total emissions per cubic meter showed similar trends but greater variations based on strength requirements. The introduction of hemp shives as a bio-based aggregate marked a

significant breakthrough, enabling negative carbon emissions (-246 to -57 kg CO_2 eq./m³) while decreasing mechanical properties but improving thermal performance.

Developed biocomposites with the proposed compressive strength of 0.05 MPa embedded in an envelope system, according to Figure 7.28, were compared with commercially used envelope systems. Commercial systems included Autoclaved Aerated Concrete (AAC), Expanded Clay Cement Block (ECCB) and Ceramic Building Block (CBB) as load-bearing materials and expanded polystyrene (EPS), Stone Wool (SW) 15 and 80 as thermal insulation materials. All compared envelope systems provide a U-value of 0.18 W/m^{2}K. The system used with the developed biocomposites has much thermal inertia, so a comparison was made with similar materials.

Puzule et al. [242] analysed that starch and geopolymer biocomposites achieved GHG emissions of 83 and 68 kg CO_2 eq./m^3, while the developed biocomposites achieved emissions of 7-17 kg CO_2 eq./m^3. However, there are slight differences between the analysed U-values, with Puzule's research analysing a lower U-value, which proportionally would affect the data of the assessment, lowering it closer to the ones of the developed biocomposites. BG biocomposites in Sinkas' research [243] showed GHG emissions of 29 kg CO_2 eq./m^3, like the developed biocomposites in this study, particularly those with binder M-600-2, as it has the closest emission value (17 kg CO_2 eq./m^3).

The LCA data in Figure 8.5 demonstrates the significant environmental advantage of the newly developed biocomposites compared to conventional building envelope systems. The four biocomposite variants (Vibro(0.05), 450(0.05), 600(0.05), and CEM(0.05)) exhibit remarkably lower carbon footprints, ranging from 6.9 to 17.0 kg CO_2 eq., with Vibro(0.05) showing the lowest environmental impact at just 6.9 kg CO_2 eq.

In contrast, conventional building systems display higher carbon emissions. The AAC-EPS system produces 67.8 kg CO_2 eq., while AAC-SW 80 and ECCB-EPS generate 72.1 and 70.8 kg CO_2 eq., respectively. The highest emissions are associated with ECCB-SW 15 at 86.3 kg CO_2 eq., followed by CBB-SW 80 (83.0 kg CO_2 eq.) and CBB-EPS (79.7 kg CO_2 eq.).

Hafner and Özdemir [244] also compared how much CO_2 is produced when manufacturing buildings. The portrayed constructions of either brick or concrete as external walls show that emissions reach over 80 kg CO_2 eq./m^2. In timber construction, the emissions reach 35 kg CO_2 eq./m^2. The portrayed system in this research achieves a lower environmental impact than Hefner and Özdemir's reviewed systems. When comparing internal wall emissions, the values get more similar, with 20-25 kg CO_2 eq./m^2 for the systems in literature and 7-17 kg CO_2 eq./m^2 for the systems used in this study, showing that the systems presented are more environmentally friendly.

For 0.15 and 0.5 MPa biocomposites, the wall assembly system was done differently. Block material was encapsulated within 2 defective boards and plastered over with regular Stucco plaster. The calculated emissions are still lower than conventional systems with the same achievable U-value of 0.18 W/(m²K). Perspective emissions showed 0.15 MPa biocomposite systems achieving close to 0.05 MPa biocomposite systems. For lower strength (0.05 MPa and 0.15 MPa) biocomposites, the CEM II binder is more environmentally friendlier than the M-600-2 binder but not friendlier than the M-450-2 and V-20min binders. For 0.5 MPa biocomposite systems, the cement binder showed the highest emissions, suggesting that the developed biocomposites are more environmentally friendly.

This comparison reveals that the biocomposites developed from wood-wool cement panel manufacturing and production line waste achieve carbon emissions reductions of approximately 75-90 % compared to conventional systems. Even the highest-emitting biocomposite system (600(0.05)

at 17.0 kg CO_2 eq.) still produces only about 25 % of the carbon emissions of the most environmentally friendly conventional system (ACC-EPS at 67.8 kg CO_2 eq.).

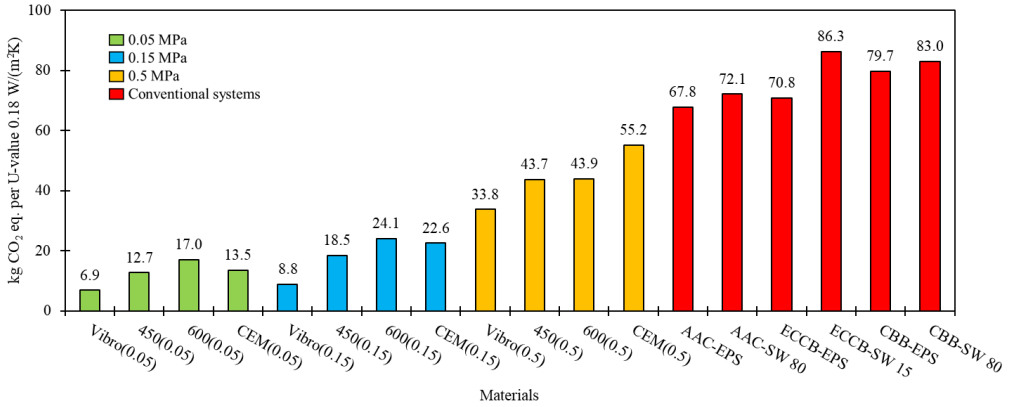

Figure 8.5. Emission comparison with conventional wall assembly systems.

These biocomposites represent a promising advancement for sustainable construction materials. Their ability to achieve the required thermal performance (U-value of 0.18 W/m²K) while dramatically reducing embodied carbon makes them particularly valuable for low-carbon building initiatives. The circular economy approach—repurposing manufacturing waste streams as binder and filler—aligns perfectly with growing industry demands for waste reduction and resource efficiency.

The materials could be especially relevant for regions with wood processing industries or wood-wool cement panel production facilities, where the waste streams are readily available. Their potential for end-of-life recycling further enhances their sustainability profile, potentially allowing multiple lifecycle uses. As building regulations increasingly focus on embodied carbon alongside operational energy efficiency, these biocomposites could gain significant market traction, particularly in green building certification programs and carbon-neutral construction projects.

The main challenge likely involves scaling production, standardising quality, and additional research into long-term durability, moisture behaviour, and fire resistance, which would benefit wider market adoption. Nevertheless, the carbon savings demonstrated in the LCA data suggest that these materials could play an important role in decarbonising the building sector.

Compared to traditional materials, this chapter has presented a thorough LCA of the created biocomposites, assessing their environmental performance and identifying areas of noticeable impact reduction. The LCA findings demonstrate the environmental advantages of using waste from manufacturing wood-wool cement panels and highlight the impact these materials have on a more circular economy in the building sector. Following the presentation of this assessment, the final chapter summarises the key findings from each experimental stage, explains the overall conclusions drawn from this study and suggests important directions for future research to further the advancement of sustainable building material development and practical application.

CONCLUSIONS

The research presented here explores innovative approaches to recycling wood-wool cement panel wastes through advanced material reactivation and biocomposite development. By systematically investigating mechanical, thermal, and chemical treatment methods, this study demonstrates a comprehensive strategy for transforming industrial waste into potential construction materials. The following concludes the key findings, highlighting the potential of material reengineering in pursuing sustainable and circular economy principles.

Three different milling techniques were investigated, yielding diverse results:

- Using a collision mill, a binder of up to 5 MPa in compressive strength on day 180 (up to 1.7 MPa on the 28th day) can be developed.
- Planetary ball milling of sanding dust improved its cementitious properties. High humidity and water curing yielded the best compressive strengths (1.9 MPa and 2.2 MPa), with high humidity chosen for practicality. Increasing the water-to-binder ratio from 0.6 to 0.8 improved 28-day strength by 90 %, but segregation limited the optimal range to 0.6-0.8. Milling for just one minute increased flowability (11.5 cm to 17 cm), with 10 minutes reaching 19.5 cm and accelerated setting time. 15-minute milling quadrupled compressive strength to 6.50 MPa, demonstrating sanding dust's potential as a viable cementitious material.
- Based on workability, the optimal processing time of 15 minutes in a vibration mill yields the best overall performance. However, extending to 20 minutes achieves the highest compressive strength of 1.6 MPa at 28 days. Setting time varies from 2:28 hours (10-minute milling) to over 4 hours (15-minute milling), with around 3 hours for 20-minute milling.

Two heat treatment methods were analysed in the context of binder recovery:

- Heat treatment in a muffle furnace shows two optimal temperatures: 450 °C and 900 °C, achieving compressive strengths of 13.0 and 19.6 MPa, respectively, with improved material density from 1384 kg/m³ (raw) to 1645-1713 kg/m³ (750-1200 °C). Treatment reduces particle size (D90 from 74.9 to 45.0 µm), increases CaO content (up to 68.8 % at 1050 °C), and accelerates setting time from 24 h (raw) to 2-3 hours (450-1200 °C) while transforming calcium-bearing phases through distinct thermal decomposition stages (30-730 °C).
- Rotary kiln treatment at 450 °C and 900 °C achieves significant strength improvements (13.8 and 18.6 MPa at 180 days) compared to raw material (2.5 MPa). Setting time reduces from >24 hours (R-SD) to 6 hours (R-450) and 10 hours (R-900), using W/B ratios of 0.75 (R-SD), 0.6 (R-450), and 0.8 (R-900).

The various treatment methods - collision mill, planetary mill, vibration mill, muffle furnace, and rotary kiln - each demonstrated distinct advantages in reactivating cement-containing wastes. While mechanical activation through collision and planetary milling achieved moderate strengths (5-15 MPa), thermal treatments proved the most effective, with muffle furnace treatment at 900 °C yielding the highest compressive strength (19.6 MPa on the 28th day). The rotary kiln showed comparable results (18.6 MPa) with potentially lower energy consumption. All treatments improved setting times compared to raw material, with thermal treatments generally providing faster setting.

Biocomposites with varying binder content demonstrate an inverse relationship between thermal and mechanical properties: the highest binder content (P1) achieves the best mechanical properties (236 kPa flexural, 469/330 kPa parallel/perpendicular compression) at 613 kg/m³. In contrast, the lowest content (P3) provides the best thermal insulation (0.083 W/(m·K)) at 430 kg/m³. Performance

compares favourably with wood fibre (thermal properties) and hempcrete (mechanical properties), suggesting potential applications in building envelopes and insulation.

Biocomposites with 450 °C treated binder show correlation between material density and performance: highest material density (H12, 415 kg/m³) achieves best mechanical properties (175/97 kPa parallel/perpendicular compression, 100 kPa flexural) but highest thermal conductivity (0.075 W/(m·K)), while lowest density (H14, 369 kg/m³) provides best insulation (0.068 W/(m·K)) with reduced strength (62/61 kPa parallel/perpendicular compression).

Biocomposites with 600 °C treated binder show distinct performance based on filler type: Production Line Waste (PLW) achieves highest performance (PLW21: 1.65/1.4 MPa parallel/perpendicular compression, 288 kPa flexural, 782 kg/m³) with higher thermal conductivity (0.139 W/(m·K)), while hemp-based composites provide superior insulation (Hemp12: 0.052 W/(m·K), 171 kg/m³) with lower strength (up to 0.45 MPa). Mixed compositions offer intermediate properties (247-447 kg/m³, 0.057-0.083 W/(m·K)), demonstrating flexibility in tailoring properties for different applications.

Biocomposites with CEM II cement show significant thermal performance improvement through hemp shives substitution: base composition (1:2-1:4 cement ratio) achieves 391-511 kg/m³ with 0.070 W/(m·K) thermal conductivity, while 25-75 % hemp shives reduce weight to 197 kg/m³ and thermal conductivity to 0.054 W/(m·K), positioning the material as a self-bearing insulation material with recycled wood-wool cement panel wastes.

The life cycle assessment demonstrated varying environmental impacts across biocomposites, with vibration-milled samples showing the lowest emissions (4.06-47.4 kg CO_2 eq./m³) followed by thermal treatments at 450 °C (26.4-81.6 kg CO_2 eq./m³) and 600 °C (40.0-78.9 kg CO_2 eq./m³), while cement-based compositions had the highest impact (28.8-111 kg CO_2 eq./m³). When hemp shives were incorporated, biocomposites achieved negative emissions (-246 to -57 kg CO_2 eq./m³) while maintaining the required mechanical properties. This demonstrates that the strategic selection of bio-based fillers can transform construction materials from carbon emitters to carbon sinks. The comprehensive investigation of biocomposites using mechanically and thermally activated binders reveals a nuanced approach to material design. By manipulating binder activation methods, filler types, and composition ratios, researchers demonstrated the potential to transform wood-wool cement panel wastes into adaptive materials. The findings highlight a performance trade-off: enhanced thermal insulation typically comes at the cost of reduced mechanical strength. However, this variability offers strategic opportunities for targeted applications, from lightweight insulation to semi-structural components. The research underscores the viability of circular economy principles in construction materials, showcasing how industrial waste can be reengineered into value-added, sustainable products.

This research demonstrates the feasibility of transforming wood-wool cement panel waste into valuable construction materials through advanced material reactivation and biocomposite development. Mechanical and thermal treatment methods effectively re-engineered the waste, yielding materials with diverse properties. While mechanical activation achieved moderate strength, thermal treatments, particularly muffle furnace processing at 900 °C, significantly enhanced compressive strength (up to 19.6 MPa). Biocomposites exhibited a tunable balance between thermal insulation and mechanical strength, with hemp shive incorporation achieving negative carbon emissions. These findings underscore the potential of circular economy principles to guide the development of sustainable building materials from industrial waste, paving the way for future applications in both insulation and semi-structural components.

ANNEX I

Environmental impact of construction building materials [245].

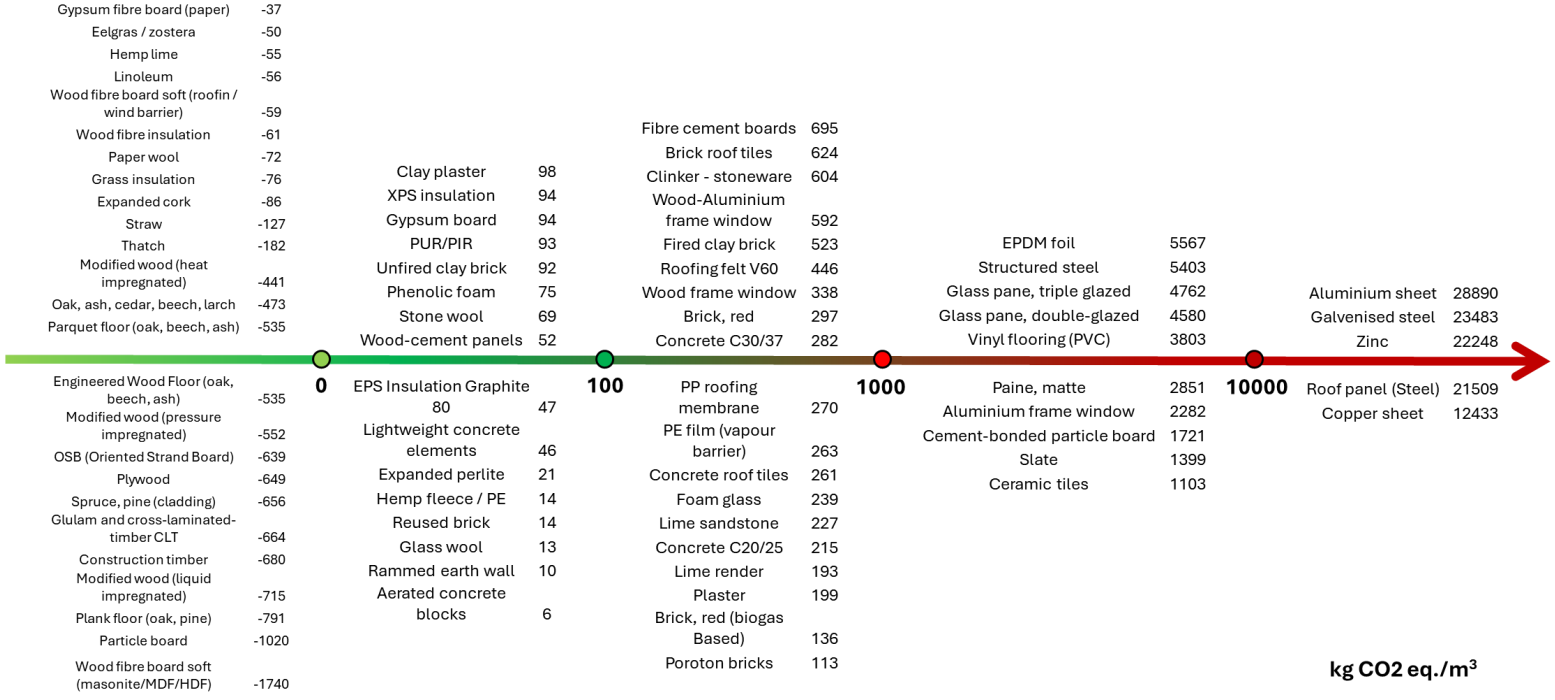

ANNEX II

List of challenges for more circular CDW management in Latvia [3].

Barriers	Examples according to interviews
1. New incineration capacity reduces the incentive for reusing or recycling.	The development of the capacity for non-recyclable waste incineration with energy recovery is a source of disagreement at the national level. The Ashes generated from incineration are not safe for the environment. They pose environmental and health risks. At the same time, having a new incineration facility reduces the motivation to reuse or recycle waste.
2. Waste generated in Latvia is insufficient to sustain large-scale circular practices in big plants.	• Latvia cannot produce the amount of waste that Schwenk (cement factory) needs for creating energy by burning waste; thus, the latter has to buy waste in Italy; • There is not enough 'gypsum' waste to supply to a company (Knauf), while some materials are already in the buildings built around 2000. Therefore, this waste stream must be sourced in other countries; • Company Kronospan is buying old furniture and wooden frames to produce furniture boards. However, Latvian sources are not enough; they also buy from another countrie/s.
3. Continuing the current practices of waste management (e.g., lack of waste separation) could lead to high landfill capacity.	Space is becoming a problem. If current practices in the landfill continue, the landfill will become full within a maximum of 6 years. Incineration is seen as a solution. In relation to the first discussed barrier, incineration reduces incentives for CE practices.
4. Production problem due to specific requirements of manufacturers (Unviable business model)	Some manufacturers deal with complex window frames that require specific design and composition (e.g., glass, plastics, and metals). Treating plastics could be time-consuming for companies, and they refuse to do it themselves.
5. Workers in the construction sector sometimes do not speak the Latvian language, making it challenging to follow instructions.	Some workers come from Kazakhstan, and most do not speak the region's major languages, such as Latvian, English, or Russian. Consequently, they lack ideas on waste separation or do not follow instructions on proper waste management.
6. Illegal dumping	Some CDWs, including hazardous ones such as asbestos (expensive to dispose of), are being dumped by individuals or companies into the forest.
7. Lack of awareness and/or education on (CD) waste management.	Many people deal with construction waste improperly, like throwing it in a household waste container if they are doing a minor renovation or not ordering the specific container for construction-based waste.
8. A single place available for waste disposal on multi-apartment buildings	A problem arises in areas with many apartments in one block. They have one space for waste disposal where everyone must go and throw their bulky waste. As a result, it is hard to control the waste flow.

in one block makes waste dumping challenging to control.	
9. The costs of upcycling materials are expensive.	When using recycled materials, there is a need to improve and check for quality and strength. However, this will be an expensive process.
10. Costs of logistics or transport are high.	Materials such as concrete are cheap and heavy, so logistics costs are high.
11. Resource constraints	Most small and medium businesses lack the capacity and time to engage (e.g., for circular activities). If they cannot find a specific niche market, they will do the minimum of what the government demands.
12. Lack of regulation on material passport	The regulation regarding the [material] passports is not very enforced. Unlike in other countries, when demolition happens, an audit is conducted to understand which secondhand materials could still be reused, e.g. window frames.
13. Low investment in research and innovation	The regulation can help push support for research and innovation. Currently, Latvia has very low investment in research and innovation, one of the lowest in Europe.
14. Asbestos dumping requires a high fee	Like Estonia, cleared out after the interviews, asbestos disposal requires a fee. In the case of Latvia, it requires [a lot] of payment.
15. National government's Lack of (financial) motivation to support municipalities to implement EU (circular) goals and strategies.	There is always an ongoing discussion between the (national) government and the municipalities regarding waste sorting and the environment. From the municipalities' point of view, the (Latvian) government agreed to EU goals and strategies while pushing the responsibility to implement and achieve these goals to them. Nevertheless, there is a need for financial resources and support to implement these. Therefore, municipalities have less motivation to take on many responsibilities even though they work closer to the people and have contracts with waste management companies.

ANNEX III

List of potential solutions for more circular CDW management [3].

Potential Solutions	Examples according to interviews
1. Government subsidies for second-hand material or recycling	There are two types of wood – packaging wood and construction wood- that a waste management and recycling company sells. This company sells wood for 30 euros/ton. However, the government pays more for second-use/recycled wood. The firm received a 16 euros per ton subsidy for packaging wood.
2. Presence of separation technology companies	Companies such as Clean R, EcoBaltia Vide, and PS Lautus Vide operate in Riga. They have CDW sorting facilities and a plastic factory that facilitates the management of CDW.
3. Possible niche markets (or economy)	• Banks in Latvia initiated a taxonomy for "brown" and "green" businesses. Non-green businesses get half per cent (0.5%) more expensive loans; • Many cafeterias, creative spaces, and tourist establishments proudly use old, used windows.
4. Sustainable financing of the banks	Banks in Latvia initiated a taxonomy for "brown" and "green" businesses. Non-green businesses get half per cent (0.5%) more expensive loans.
5. Green procurement	Green procurement guidelines focus on resource efficiency, yet there has been less focus on elements of circularity
6. Strong social media/ marketplace community	• People use Facebook, AndeleMandele platform, or www.ss.com if they want to sell, give away for free, or exchange CDW with reuse potential; • There is a WhatsApp group among 160 Viskali comune for those who want to exchange building materials
7. Educational centres and raising public awareness campaigns	• The landfill has an educational centre to teach people how to recycle and repurpose household materials to raise awareness; • Some public awareness campaigns were done by a landfill operator related to waste sorting, incineration, biowaste, etc. Other campaigns are related to reducing and sorting waste, including household (e.g., kitchen-, biowastes) and general wastes.
8. Community's willingness to pay for an idea of URC	According to a survey by Free Riga, customers are willing to pay for a community that facilitates material exchange, design consultations, and education on repairing things. The organization checked the willingness to pay with a survey, and the options are: 1) Monthly payments for members; 2) similar to what is done in Brussels, if you participate in the community or bring something, you earn value points, which is some alternative currency; and 3) you pay an entrance fee like 3 euros for coming in.
9. Mandatory waste sorting with a penalty for incorrect sorting	There is an existing agreement between waste management companies and citizens regarding sorting waste. Sorted waste such as plastics, metals, and glasses are free. If the pollution in sorted waste (incorrectly sorted) is more than 20%, residents must pay for contaminated containers like unsorted waste. This encourages citizens to observe proper waste sorting.
10. Increase in landfilling gate fee	The landfilling gate fee has increased from 80 euros to 165 euros, and companies are under more pressure to reuse or sell their materials, especially construction and bulky waste, instead of bringing them directly to landfills.
11. Local nationalism	There is strong local nationalism among citizens. This means using local products has a higher meaning than buying products from other countries, such as China. For example, according to a public survey, green and local products are popular among people.
12. Knowledge from technical university	Researchers from the Riga Technical University work on different construction materials, both new and second-hand. Work on CDWs includes incorporating them into new materials.

REFERENCES

1. Moschen-Schimek, J.; Kasper, T.; Huber-Humer, M. Critical Review of the Recovery Rates of Construction and Demolition Waste in the European Union – An Analysis of Influencing Factors in Selected EU Countries. *Waste Management* **2023**, *167*, 150–164, doi:10.1016/J.WASMAN.2023.05.020.
2. APlanet European Green Deal: Objectives and Initiatives for a Sustainable Future Available online: https://aplanet.org/resources/european-green-deal-objectives-and-initiatives-for-a-sustainable-future/ (accessed on 7 January 2025).
3. Rueda Raya, S.; Tolentino-Zondervan, F.; van Winden, W.; van Hemert, P. *CURE+ Baseline Study: City of Riga, Latvia*;
4. Klimata un enerģētikas ministrija *Latvijas Nacionālais Enerģētikas un Klimata Plāns 2021.-2030. gadam*; Riga, 2024;
5. European Commision A New Circular Economy Action Plan Available online: https://eur-lex.europa.eu/legal-content/EN/TXT/?qid=1583933814386&uri=COM:2020:98:FIN#footnote33 (accessed on 2 January 2025).
6. Schneider, M.; Romer, M.; Tschudin, M.; Bolio, H. Sustainable Cement Production—Present and Future. *Cem Concr Res* **2011**, *41*, 642–650, doi:10.1016/J.CEMCONRES.2011.03.019.
7. Wu, M.; Zhang, Y.; Ji, Y.; Liu, G.; Liu, C.; She, W.; Sun, W. Reducing Environmental Impacts and Carbon Emissions: Study of Effects of Superfine Cement Particles on Blended Cement Containing High Volume Mineral Admixtures. *J Clean Prod* **2018**, *196*, 358–369, doi:10.1016/J.JCLEPRO.2018.06.079.
8. Argalis, P.P.; Sinka, M.; Bajare, D. A Preliminary Study of Mechanical Treatments' Effect on the Reactivation of Hydrated Cement Paste. *J Phys Conf Ser* **2023**, *2423*, 012008, doi:10.1088/1742-6596/2423/1/012008.
9. Gholizadeh-Vayghan, A.; Meza Hernandez, G.; Kingne, F.K.; Gu, J.; Dilissen, N.; El Kadi, M.; Tysmans, T.; Vleugels, J.; Rahier, H.; Snellings, R. Thermal Reactivation of Hydrated Cement Paste: Properties and Impact on Cement Hydration. *Materials 2024, Vol. 17, Page 2659* **2024**, *17*, 2659, doi:10.3390/MA17112659.
10. Yang, H.; Che, Y.; Leng, F. Calcium Leaching Behavior of Cementitious Materials in Hydrochloric Acid Solution. *Scientific Reports 2018 8:1* **2018**, *8*, 1–9, doi:10.1038/s41598-018-27255-x.
11. Cordoba, G.; Paulo, C.I.; Irassar, E.F. Towards an Eco-Efficient Ready Mix-Concrete Industry: Advances and Opportunities. A Study of the Metropolitan Region of Buenos Aires. *Journal of Building Engineering* **2023**, *63*, 105449, doi:10.1016/J.JOBE.2022.105449.
12. Joseph, H.S.; Pachiappan, T.; Avudaiappan, S.; Maureira-Carsalade, N.; Roco-Videla, Á.; Guindos, P.; Parra, P.F. A Comprehensive Review on Recycling of

Construction Demolition Waste in Concrete. *Sustainability 2023, Vol. 15, Page 4932* **2023**, *15*, 4932, doi:10.3390/SU15064932.
13. Puskás, A.; Corbu, O.; Szilágyi, H.; Moga, L.M. Construction Waste Disposal Practices: The Recycling and Recovery of Waste. *WIT Transactions on Ecology and the Environment* **2014**, *191*, 1313–1321, doi:10.2495/SC141102.
14. Ahmad, Z.; Wee, L. siong; Fauzi, M.A. Mechanical Properties of Wood-Wool Cement Composite Board Manufactured Using Selected Malaysian Fast Grown Timber Species. *ASM Science Journal* **2011**, *5*, 27–35.
15. Mordor Intelligence *Cement Board Market - Share & Size*; 2024;
16. IEA *Breakthrough Agenda Report 2023*; Paris, 2023;
17. GlobalABC *Global Status Report*; 2023;
18. Gibbs, M.J.; Soyka, P.; Connely, D. CO 2 Emissions from Cement Production. In *Good Practice Guidance and Uncertainty Management in National Greenhouse Gas Inventories*; 2021; pp. 175–182.
19. Argalis, P.P.; Sinka, M.; Bajare, D. Recycling of Cement–Wood Board Production Waste into a Low-Strength Cementitious Binder. *Recycling* **2022**, *7*, 76, doi:10.3390/recycling7050076.
20. Ramsden, K. *Cement and Concrete: The Environmental Impact*; 2020;
21. Wang, P.; Ryberg, M.; Yang, Y.; Feng, K.; Kara, S.; Hauschild, M.; Chen, W.-Q. Efficiency Stagnation in Global Steel Production Urges Joint Supply- and Demand-Side Mitigation Efforts. *Nat Commun* **2021**, *12*, 2066, doi:10.1038/s41467-021-22245-6.
22. Statista *Global Cement CO_2 Emissions by Country*; 2023;
23. Andrew, R.M. Global CO≪Sub≫2≪/Sub≫ Emissions from Cement Production 2018.
24. Cheng, D.; Reiner, D.M.; Yang, F.; Cui, C.; Meng, J.; Shan, Y.; Liu, Y.; Tao, S.; Guan, D. Projecting Future Carbon Emissions from Cement Production in Developing Countries. *Nature Communications 2023 14:1* **2023**, *14*, 1–12, doi:10.1038/s41467-023-43660-x.
25. Central Statistical Bureau of Latvia Latvia GDP From Construction Available online: https://tradingeconomics.com/latvia/gdp-from-construction (accessed on 2 January 2025).
26. Eurostat Employment by A*10 Industry Breakdowns Available online: https://ec.europa.eu/eurostat/databrowser/view/nama_10_a10_e__custom_5685302/bookmark/table?lang=en&bookmarkId=cb2322c2-810c-4ae0-84e3-dacb1c60ca75 (accessed on 2 January 2025).
27. Official statistics of Latvia *Forests of Latvia*; Riga, 2024;
28. CSP *MEŽSAIMNIECĪBA 2023. GADĀ*;
29. Central Statistical Bureau Extraction of Raw Materials for Building Materials 2023.
30. Zhang, F.; Wang, S.; Jiang, J.; Chen, D.; Zhou, H.; Zhang, F.; Wang, S.; Jiang, J.; Chen, D.; Zhou, H. Effects of Growth Ring Width, Height from Tree Base, and Loading Direction on Transverse Compression of Plantation Japanese Larch Wood. *Forests 2023, Vol. 14, Page 1451* **2023**, *14*, 1451, doi:10.3390/F14071451.

31. Hull, B. Old vs. New Growth Trees and the Wood Products They Make Available online: https://brenthull.com/article/old-growth-wood (accessed on 7 January 2025).
32. Latvijas Vides, Ģ. un M.C. Zemes Dzīļu Informācijas Sistēma Available online: https://videscentrs.lvgmc.lv/iebuvets/zemes-dzilu-informacijas-sistema (accessed on 2 January 2025).
33. The State Audit Ofice of the Repupblic of Latvia Mineral Resources Are Latvia's Treasure, but We Do Not Manage Them Sustainably | Valsts Kontrole Available online: https://lrvk.gov.lv/en/news/mineral-resources-are-latvias-treasure-but-we-do-not-manage-them-sustainably (accessed on 2 January 2025).
34. European Investment Bank Riga Water Company Modernises the Water Infrastructure in the Capital Available online: https://www.eib.org/en/stories/riga-water-infrastructure-sustainable (accessed on 2 January 2025).
35. Houser, D.L.; Pruess, H. The Effects of Construction on Water Quality: A Case Study of the Culverting of Abram Creek. *Environ Monit Assess* **2009**, *155*, 431–442, doi:10.1007/S10661-008-0445-9.
36. Venskus, K. Environmental Problems in Latvia Available online: https://prezi.com/xhsvb_txqeuj/environmental-problems-in-latvia/ (accessed on 7 January 2025).
37. Tamma, P.; Schaart, E.; Gurzu, A. Europe's Green Deal Plan Unveiled Available online: https://www.politico.eu/article/the-commissions-green-deal-plan-unveiled/ (accessed on 2 January 2025).
38. European Commission Renovation Wave Available online: https://energy.ec.europa.eu/topics/energy-efficiency/energy-efficient-buildings/renovation-wave_en (accessed on 2 January 2025).
39. GRESB Establishing an Embodied Carbon Strategy in the EU Market Available online: https://www.gresb.com/nl-en/establishing-an-embodied-carbon-strategy-in-the-eu-market/ (accessed on 2 January 2025).
40. Zacharia, M. Guide to Construction Products Regulation (CPR) Available online: https://oneclicklca.com/en/resources/articles/revised-construction-products-regulation-to-include-epd-data (accessed on 2 January 2025).
41. Climate Earth Key Takeaways from the EU's Updated Construction Products Regulation (CPR) Available online: https://climateearth.com/news/key-takeaways-from-the-eus-updated-construction-products-regulation-cpr-conference/ (accessed on 2 January 2025).
42. Liselotte, J. *Latvia's Climate Action Strategy*; 2024;
43. Ministru Kabinets *Aktualizētais Nacionālais Enerģētikas Un Klimata Plāns 2021.–2030. Gadam*; Latvijas Vēstnesis, 2024;
44. Enterprise Agency, N. *The Circularity in Construction Sector in Latvia Opportunities and Obstacles for Dutch Entrepreneurs Commissioned by the Netherlands Enterprise Agency*;
45. - International Energy Agency, I. *Energy Policy Review Latvia 2024*; 2024;
46. Klavs, G.; Kudrenickis, I. *Energy Efficiency Trends and Policies in LATVIA*; 2021;
47. Latvian Saeima *Būvniecības Likums*; Saeima, 2014;

48. Interreg Baltic Sea Region Riga Pilot - NONHAZCITY 3 Available online: https://interreg-baltic.eu/project-pilots/nonhazcity-3/riga-pilot/ (accessed on 3 January 2025).
49. Impolevičiene, V.; Sprude, A.; Lumiste, E. *ESG Initiatives in Estonia, Latvia and Lithuania*; 2024;
50. Pelša, I. *Green Public Procurement | Viedās Administrācijas Un Reģionālās Attīstības Ministrija*; Riga, 2020;
51. CleanR grupa Uptake of Green Public Procurement Higher at Local Governments than Institutions of Direct Public Administration Available online: https://cleanrgrupa.lv/en/uptake-of-green-public-procurements-higher-at-local-governments-than-institutions-of-direct-public-administration/ (accessed on 3 January 2025).
52. Myclimate What Are the 17 Sustainable Development Goals Available online: https://www.myclimate.org/en/information/faq/faq-detail/what-are-the-sustainable-development-goals-sdgs/ (accessed on 7 January 2025).
53. State Chancellery *LATVIA'S OPEN GOVERNMENT NATIONAL ACTION PLAN 2022-2025 MID-TERM ASSESSMENT*;
54. Truhanova, K.; Kalnkambers, E. *Implementing the Energy Performance of Buildings Directive*; Riga, 2020;
55. European Environment Agency *Circular Economy Country Profile-Latvia*;
56. Wolff, G. *Resource Efficient Use of Mixed Wastes Improving Management of Construction and Demolition Waste - Final Report*; 2017;
57. LSM+ English; Vides fakti Riga April 3 2023,.
58. Mavlutova, I.; Atstaja, D.; Gusta, S.; Hermanis, J. Management of Household-Generated Construction and Demolition Waste: Circularity Principles and the Attitude of Latvian Residents. *Energies 2024, Vol. 17, Page 205* **2023**, *17*, 205, doi:10.3390/EN17010205.
59. Ķirule-Vīksne, B. *Atkritumi Kā Resursi Latvijā – Reģionālās Ilgtspējas Un Aprites Veicināšana, Ieviešot Atkritumu Kā Resursu Izmantošanas Koncepciju*;
60. Latvijas Valsts Ģeoloģijas un Meteroloģijas centrs Atkritumu Atskaite Ražotņu Griezumā 2023.
61. Faraca, G.; Boldrin, A.; Astrup, T. Resource Quality of Wood Waste: The Importance of Physical and Chemical Impurities in Wood Waste for Recycling. *Waste Management* **2019**, *87*, 135–147, doi:10.1016/J.WASMAN.2019.02.005.
62. Kiesnere, G.; Atstaja, D.; Cudecka-Purina, N.; Susniene, R. The Potential of Wood Construction Waste Circularity. *Environments* **2024**, *11*, 231, doi:10.3390/environments11110231.
63. Āboltiņš, R. *Circular Construction Challenge in Latvia: Guidelines for Construction and Demolition Waste Sorting at Construction Site*; 2024;
64. ISM waste & recycling What Is the Waste Hierarchy? Available online: https://ismwaste.co.uk/help/what-is-the-waste-hierarchy (accessed on 3 January 2025).
65. European Environment Agency *Waste Prevention Country Profile*;

66. Latvijas Būvuzņēmēju apvienība *BŪVNIECĪBAS ATKRITUMU ŠĶIROŠANA BŪVLAUKUMĀ*; Riga, 2024;
67. Irish Green Building Council Level(s) - EU Sustainable Buildings Framework Available online: https://www.igbc.ie/certification/levels-eu-sustainable-buildings-framework (accessed on 7 January 2025).
68. Casey, C. BREEAM vs LEED: Understand the Differences and How to Choose Available online: https://www.cim.io/blog/breeam-vs-leed-understanding-key-differences-in-green-building-certifications (accessed on 7 January 2025).
69. Archiroots Top 5 Reasons Why LEED In UK Is Better Than BREEAM Available online: https://archiroots.com/why-leed-in-uk-is-better-than-breeam/ (accessed on 7 January 2025).
70. Sustainable Governance Indicators Economic Sustainability Available online: https://www.sgi-network.org/2024/Latvia/Economic_Sustainability (accessed on 7 January 2025).
71. Leichter, M.; Piccardo, C. Assessing Life Cycle Sustainability of Building Renovation and Reconstruction: A Comprehensive Review of Case Studies and Methods. *Build Environ* **2024**, *262*, 111817, doi:10.1016/J.BUILDENV.2024.111817.
72. Vanclay, F. International Principles for Social Impact Assessment: Their Evolution. *Impact Assessment and Project Appraisal* **2012**, *21*, doi:10.3152/147154603781766464.
73. Tilt, B.; Braun, Y.; He, D. Social Impacts of Large Dam Projects: A Comparison of International Case Studies and Implications for Best Practice. *J Environ Manage* **2009**, *90*, S249–S257, doi:10.1016/J.JENVMAN.2008.07.030.
74. Vamza, I.; Diaz, F.; Resnais, P.; Radziņa, A.; Blumberga, D. Life Cycle Assessment of Reprocessed Cross Laminated Timber in Latvia. *Environmental and Climate Technologies* **2021**, *25*, 58–70, doi:10.2478/rtuect-2021-0005.
75. Olanrewaju, O.I.; Enegbuma, W.I.; Donn, M. Challenges in Life Cycle Assessment Implementation for Construction Environmental Product Declaration Development: A Mixed Approach and Global Perspective. *Sustain Prod Consum* **2024**, *49*, 502–528, doi:10.1016/J.SPC.2024.06.021.
76. Myronycheva, O.; Karlsson, O.; Sehlstedt-Persson, M.; Öhman, M.; Sandberg, D. Distribution of Low-Molecular Lipophilic Extractives beneath the Surface of Air- and Kiln-Dried Scots Pine Sapwood Boards. *PLoS One* **2018**, *13*, e0204212, doi:10.1371/JOURNAL.PONE.0204212.
77. Bumanis, G.; Argalis, P.P.; Sinka, M.; Korjakins, A.; Bajare, D. The Use of Recycled Cement-Bonded Particle Board Waste in the Development of Lightweight Biocomposites. *Materials* **2024**, *17*, 5890, doi:10.3390/ma17235890.
78. Cewood CEWOOD — Wood Wool Panels Available online: https://www.cewood.com/downloads-eng (accessed on 15 January 2025).
79. Bumanis, G.; Argalis, P.P.; Sinka, M.; Korjakins, A.; Bajare, D. The Use of Recycled Cement-Bonded Particle Board Waste in the Development of Lightweight Biocomposites. *Materials* **2024**, *17*, 5890, doi:10.3390/ma17235890.

80. Suarez-Riera, D.; Restuccia, L.; Falliano, D.; Ferro, G.A.; Tuliani, J.M.; Pavese, M.; Lavagna, L. An Overview of Methods to Enhance the Environmental Performance of Cement-Based Materials. *Infrastructures 2024, Vol. 9, Page 94* **2024**, *9*, 94, doi:10.3390/INFRASTRUCTURES9060094.
81. Kaptan, K.; Cunha, S.; Aguiar, J. A Review of the Utilization of Recycled Powder from Concrete Waste as a Cement Partial Replacement in Cement-Based Materials: Fundamental Properties and Activation Methods. *Applied Sciences 2024, Vol. 14, Page 9775* **2024**, *14*, 9775, doi:10.3390/APP14219775.
82. Tam, V.W.Y.; Tam, C.M. A Review on the Viable Technology for Construction Waste Recycling. *Resour Conserv Recycl* **2006**, *47*, 209–221, doi:10.1016/J.RESCONREC.2005.12.002.
83. Barbhuiya, S.; Kanavaris, F.; Das, B.B.; Idrees, M. Decarbonising Cement and Concrete Production: Strategies, Challenges and Pathways for Sustainable Development. *Journal of Building Engineering* **2024**, *86*, doi:10.1016/J.JOBE.2024.108861.
84. Seghir, N.T.; Benaimeche, O.; Krzywínski, K.; Sadowski, L. Ultrasonic Evaluation of Cement-Based Building Materials Modified Using Marble Powder Sourced from Industrial Wastes. *Buildings 2020, Vol. 10, Page 38* **2020**, *10*, 38, doi:10.3390/BUILDINGS10030038.
85. Lam, L.; Wong, Y.L.; Poon, C.S. Effect of Fly Ash and Silica Fume on Compression and Fracture Behaviors of Concrete. *Cem Concr Res* **1998**, *28*, 271–283, doi:10.1016/S0008-8846(97)00269-X.
86. Fernández-Jiménez, A.; Palomo, A. Composition and Microstructure of Alkali Activated Fly Ash Binder: Effect of the Activator. *Cem Concr Res* **2005**, *35*, 1984–1992, doi:10.1016/J.CEMCONRES.2005.03.003.
87. Lisowski, P.; Jóźwiak-Niedźwiedzka, D.; Osial, M.; Bochenek, K.; Denis, P.; Glinicki, M.A. Power Ultrasound-Assisted Enhancement of Granulated Blast Furnace Slag Reactivity in Cement Paste. *Cem Concr Compos* **2024**, *154*, 105781, doi:10.1016/J.CEMCONCOMP.2024.105781.
88. Burmeister, C.F.; Kwade, A. Process Engineering with Planetary Ball Millss. *Chem Soc Rev* **2013**, *42*, 7660–7667, doi:10.1039/c3cs35455e.
89. Sivasankaran, S.; Alaboodi, A.S. Structural Characterization and Mechanical Behavior of Al 6061 Nanostructured Matrix Reinforced with TiO2 Nanoparticles for Automotive Applications. *Functionalized Nanomaterials* **2016**, doi:10.5772/65947.
90. Hanke, T. Ultrafine Grinding with Laboratory Ball Mills 2015.
91. Guzzo, P.L.; Marinho de Barros, F.B.; Soares, B.R.; Santos, J.B. Evaluation of Particle Size Reduction and Agglomeration in Dry Grinding of Natural Quartz in a Planetary Ball Mill. *Powder Technol* **2020**, *368*, 149–159, doi:10.1016/J.POWTEC.2020.04.052.
92. Union process Planetary Ball Mills 101 Available online: https://www.unionprocess.com/resources/before-purchasing-tips/planetary-ball-mills-101/.
93. Tiwari, P. *SIZE REDUCTION*; 2023;

94. Albarki, M. Does Milling Reduce Particle Size? 4 Key Techniques Explained 2023, 1–37.
95. Veinthal, R.; Sergejev, F.; Zikin, A.; Tarbe, R.; Hornung, J. Abrasive Impact Wear and Surface Fatigue Wear Behaviour of Fe–Cr–C PTA Overlays. *Wear* **2013**, *301*, 102–108, doi:10.1016/J.WEAR.2013.01.077.
96. Alpha Grinding Media What Is a Ball Mill Machine? Its Types and Uses Available online: https://alphagrindingmedia.com/what-are-ball-mill-machines-and-why-do-i-use-them/ (accessed on 13 December 2024).
97. Dharmadhikari, S. Review of Treatment Methods for Enhancing Recycled Concrete Aggregates Properties. *Int J Res Appl Sci Eng Technol* **2024**, *12*, 2812–2820, doi:10.22214/IJRASET.2024.59486.
98. Pawluczuk, E.; Kalinowska-Wichrowska, K.; Bołtryk, M.; Jiménez, J.R.; Fernández, J.M. The Influence of Heat and Mechanical Treatment of Concrete Rubble on the Properties of Recycled Aggregate Concrete. *Materials 2019, Vol. 12, Page 367* **2019**, *12*, 367, doi:10.3390/MA12030367.
99. Sui, Y.; Ou, C.; Liu, S.; Zhang, J.; Tian, Q. Study on Properties of Waste Concrete Powder by Thermal Treatment and Application in Mortar. *Applied Sciences 2020, Vol. 10, Page 998* **2020**, *10*, 998, doi:10.3390/APP10030998.
100. Vengadesh Marshall Raman, J.; Ramasamy, V. Various Treatment Techniques Involved to Enhance the Recycled Coarse Aggregate in Concrete: A Review. *Mater Today Proc* **2020**, *45*, 6356–6363, doi:10.1016/J.MATPR.2020.10.935.
101. Pawluczuk, E.; Kalinowska-Wichrowska, K.; Bołtryk, M.; Jiménez, J.R.; Fernández, J.M. The Influence of Heat and Mechanical Treatment of Concrete Rubble on the Properties of Recycled Aggregate Concrete. *Materials* **2019**, *12*, doi:10.3390/MA12030367.
102. Shima, H.; Tateyashiki, H.; Matsuhashi, R.; Yoshida, Y. *An Advanced Concrete Recycling Technology and Its Applicability Assessment through Input-Output Analysis*; 2005; Vol. 3;.
103. Semugaza, G.; Mielke, T.; Castillo, M.E.; Gierth, A.Z.; Tam, J.X.; Nawrath, S.; Lupascu, D.C. Reactivation of Hydrated Cement Powder by Thermal Treatment for Partial Replacement of Ordinary Portland Cement. *Materials and Structures/Materiaux et Constructions* **2023**, *56*, doi:10.1617/s11527-023-02133-9.
104. Semugaza, G. Reactivation of Hydrated Cement and Recycled Concrete Powders by Thermal Treatment for Partial Replacement of Virgin Cement, Von der Fakultät für IngenieurwissenschaftenAbteilung Bauwissenschaften: Essen, 2024.
105. Carriço, A.; Bogas, J.A.; Guedes, M. Thermoactivated Cementitious Materials – A Review. *Constr Build Mater* **2020**, *250*, 118873, doi:10.1016/J.CONBUILDMAT.2020.118873.
106. Moreno-Juez, J.; Vegas, I.J.; Frías Rojas, M.; Vigil de la Villa, R.; Guede-Vázquez, E. Laboratory-Scale Study and Semi-Industrial Validation of Viability of Inorganic CDW Fine Fractions as SCMs in Blended Cements. *Constr Build Mater* **2021**, *271*, 121823, doi:10.1016/J.CONBUILDMAT.2020.121823.

107. Choi, H.; Lim, M.; Choi, H.; Kitagaki, R.; Noguchi, T.; Choi, H.; Lim, M.; Choi, H.; Kitagaki, R.; Noguchi, T. Using Microwave Heating to Completely Recycle Concrete. *J Environ Prot (Irvine, Calif)* **2014**, *5*, 583–596, doi:10.4236/JEP.2014.57060.
108. Laboratory Instruments Factors To Consider For A Muffle Furnace 2024.
109. Heatmasters Temperature Control Systems 2024.
110. Tantawy, M.A. Effect of High Temperatures on the Microstructure of Cement Paste. *Journal of Materials Science and Chemical Engineering* **2017**, *05*, 33–48, doi:10.4236/MSCE.2017.511004.
111. BAROT, R.S.; Ayar, M.; Beravala, D.H.S. Energy Efficient and Sustainable Design and Development of Muffle Furnace for Melting Alloys. *SSRN Electronic Journal* **2019**, doi:10.2139/SSRN.3462641.
112. Mungyeko Bisulandu, B.J.R.; Huchet, F. Rotary Kiln Process: An Overview of Physical Mechanisms, Models and Applications. *Appl Therm Eng* **2023**, *221*, doi:10.1016/j.applthermaleng.2022.119637.
113. Robert, J.; Bisulandu, M.; Huchet, F. Rotary Kiln Process: An Overview of Physical Mechanisms, Models and Applications., doi:10.1016/j.applthermaleng.2022.119637ï.
114. Ebben, A.; Carlson, C. Top Applications for Rotary Kilns Available online: https://feeco.com/top-applications-rotary-kilns/ (accessed on 13 December 2024).
115. AGICO Cement Rotary Kiln For Activated Carbon Production Available online: https://cementplantequipment.com/activated-carbon-plant/activated-carbon-rotary-kiln/chrome-extension://dagcmkpagjlhakfdhnbomgmjdpkdklff/results/0 (accessed on 13 December 2024).
116. Skocek, J.; Ouzia, A.; Vargas Serrano, E.; Pato, N. Recycled Sand and Aggregates for Structural Concrete: Toward the Industrial Production of High-Quality Recycled Materials with Low Water Absorption. *Sustainability (Switzerland)* **2024**, *16*, 814, doi:10.3390/SU16020814/S1.
117. Zheng, L.; Wang, J.; Li, K.; Wang, M.; Li, S.; Yuan, L. Advances in the Experiments of Leaching in Cement-Based Materials and Dissolution in Rocks. *Materials* **2023**, *16*, 7697, doi:10.3390/MA16247697.
118. Sakai, E.; Hisada, M.; Sugiyama, T. Leaching of Trace Elements and Hydrated Products from Cement and Concrete. *Concrete Journal* **2003**, *41*, 18–22, doi:10.3151/COJ1975.41.12_18.
119. Popov, K.; Glazkova, I.; Yachmenev, V.; Nikolayev, A. Electrokinetic Remediation of Concrete: Effect of Chelating Agents. *Environ Pollut* **2008**, *153*, 22–28, doi:10.1016/J.ENVPOL.2008.01.014.
120. Lu, R.; Guan, X. Transport Properties of Moisture and Ionic Chelators in Concrete. *Front Mater* **2023**, *10*, 1176873, doi:10.3389/FMATS.2023.1176873/BIBTEX.
121. Lizarazo-Marriaga, J.; García, F.; Higuera, C. Preliminary Electrochemical Cementation of High Volume Fly Ash Mortars. *Constr Build Mater* **2016**, *122*, 54–62, doi:10.1016/J.CONBUILDMAT.2016.06.070.

122. Rosewitz, J.A.; Wang, S.; Scarlata, S.F.; Rahbar, N. An Enzymatic Self-Healing Cementitious Material. *Appl Mater Today* **2021**, *23*, doi:10.1016/j.apmt.2021.101035.
123. Dickinson, G.H.; Vega, I.E.; Wahl, K.J.; Orihuela, B.; Beyley, V.; Rodriguez, E.N.; Everett, R.K.; Bonaventura, J.; Rittschof, D. Barnacle Cement: A Polymerization Model Based on Evolutionary Concepts. *J Exp Biol* **2009**, *212*, 3499, doi:10.1242/JEB.029884.
124. Wong, P.Y.; Mal, J.; Sandak, A.; Luo, L.; Jian, J.; Pradhan, N. Advances in Microbial Self-Healing Concrete: A Critical Review of Mechanisms, Developments, and Future Directions. *Science of The Total Environment* **2024**, *947*, 174553, doi:10.1016/J.SCITOTENV.2024.174553.
125. Abrão, P.C.R.A.; Cardoso, F.A.; John, V.M. Efficiency of Portland-Pozzolana Cements: Water Demand, Chemical Reactivity and Environmental Impact. *Constr Build Mater* **2020**, *247*, doi:10.1016/J.CONBUILDMAT.2020.118546.
126. Chen, L.; Yang, M.; Chen, Z.; Xie, Z.; Huang, L.; Osman, A.I.; Farghali, M.; Sandanayake, M.; Liu, E.; Ahn, Y.H.; et al. Conversion of Waste into Sustainable Construction Materials: A Review of Recent Developments and Prospects. *Materials Today Sustainability* **2024**, *27*, 100930, doi:10.1016/J.MTSUST.2024.100930.
127. Hou, J.; Liu, Z.; Ni, X. Unlocking the Potential: Transforming Hazardous Waste into Solid Cementitious Materials. *J Clean Prod* **2024**, *472*, 143483, doi:10.1016/J.JCLEPRO.2024.143483.
128. Akintayo, B.D.; Babatunde, O.M.; Olanrewaju, O.A. Comparative Analysis of Cement Production Methods Using a Life Cycle Assessment and a Multicriteria Decision-Making Approach. *Sustainability (Switzerland)* **2024**, *16*, 484, doi:10.3390/SU16020484/S1.
129. Hamada, H.M.; Abed, F.; Al-Sadoon, Z.A.; Alashkar, A. Enhancing Pozzolanic Activity of Fly Ash via Dry and Wet Milling: A Comparative Study for Sustainable Construction Material Enhancement. *Journal of CO2 Utilization* **2024**, *83*, 102811, doi:10.1016/J.JCOU.2024.102811.
130. Dunant, C.F.; Joseph, S.; Prajapati, R.; Allwood, J.M. Electric Recycling of Portland Cement at Scale. *Nature 2024 629:8014* **2024**, *629*, 1055–1061, doi:10.1038/s41586-024-07338-8.
131. ZKG Cement Thermal Recycling in India Is Increasing – with Certain Difficulties Available online: https://www.zkg.de/en/artikel/zkg_Thermal_recycling_in_India_is_increasing_with_certain_difficulties-3551980.html (accessed on 13 December 2024).
132. Dunant, C.F.; Joseph, S.; Prajapati, R.; Allwood, J.M. Electric Recycling of Portland Cement at Scale. *Nature 2024 629:8014* **2024**, *629*, 1055–1061, doi:10.1038/s41586-024-07338-8.
133. Ho, H.J.; Iizuka, A.; Shibata, E. Chemical Recycling and Use of Various Types of Concrete Waste: A Review. *J Clean Prod* **2021**, *284*, 124785, doi:10.1016/J.JCLEPRO.2020.124785.
134. Marmier, A. Decarbonisation Options for the Cement Industry.; 2000.

135. Klee, H. *World Business Council for Sustainable Development The Cement Sustainability Initiative Recycling Concrete*;
136. Ning, Z. *Thermal Treatment of Recycled Concrete Fines*;
137. ÇELEKLİ, A.; ZARİÇ, Ö.E. From Emissions to Environmental Impact: Understanding the Carbon Footprint. *International Journal of Environment and Geoinformatics* **2023**, *10*, 146–156, doi:10.30897/IJEGEO.1383311.
138. Chinedu Alex Ezeigweneme; Chibuike Daraojimba; Olawe Alaba Tula; Abimbola Oluwatoyin Adegbite; Joachim Osheyor Gidiagba A Review of Technological Innovations and Environmental Impact Mitigation. *World Journal of Advanced Research and Reviews* **2024**, *21*, 075–082, doi:10.30574/WJARR.2024.21.1.2687.
139. Statements, B.; Size, T. Standard Test Method for Sieve Analysis of Fine and Coarse Aggregates. *Annual Book of ASTM Standards* **2011**, 5–9.
140. Ermilova, E.; Kamalova, Z. The Influence of Complex Additives Based on Calcined Clays and Carbonate Fillers on Hydration Products Composition of Blended Cement Stone. *E3S Web of Conferences* **2021**, *274*, 04004, doi:10.1051/e3sconf/202127404004.
141. Kucharczyk, S.; Zajac, M.; Deja, J. The Influence of Limestone and Al2O3 Content in the Slag on the Performance of the Composite Cements. *Procedia Eng* **2015**, *108*, 402–409, doi:10.1016/j.proeng.2015.06.164.
142. Ye, G.; Liu, X.; De Schutter, G.; Poppe, A.M.; Taerwe, L. Influence of Limestone Powder Used as Filler in SCC on Hydration and Microstructure of Cement Pastes. *Cem Concr Compos* **2007**, *29*, 94–102, doi:10.1016/j.cemconcomp.2006.09.003.
143. Fraga, L.G.; Silva, J.; Teixeira, S.; Soares, D.; Ferreira, M.; Teixeira, J. Influence of Operating Conditions on the Thermal Behavior and Kinetics of Pine Wood Particles Using Thermogravimetric Analysis. *Energies (Basel)* **2020**, *13*, 2756, doi:10.3390/en13112756.
144. Angelescu, N.; Stanciu, D.; Barroso de Aguiar, J.; Abdelgader, H.S.; Bratu, V. Role of Superplasticizer Additives Upon Hydration Process of Cement Pastes. *Scientific Bulletin of Valahia University - Materials and Mechanics* **2016**, *14*, 23–26, doi:10.1515/bsmm-2016-0004.
145. Ifguis, O.; Moutcine, A.; Laghlimi, C.; Ziat, Y.; Bouhdadi, R.; Chtaini, A.; Moubarik, A.; Mbarki, M. Biopolymer-Modified Carbon Paste Electrode for the Electrochemical Detection of Pb(II) in Water. *J Anal Methods Chem* **2022**, *2022*, doi:10.1155/2022/5348246.
146. Mohsen, A.; Aiad, I.; El-Hossiny, F.I.; Habib, A.O. Evaluating the Mechanical Properties of Admixed Blended Cement Pastes and Estimating Its Kinetics of Hydration by Different Techniques. *Egyptian Journal of Petroleum* **2020**, *29*, 171–186, doi:10.1016/j.ejpe.2020.03.001.
147. Boualleg, S.; Bencheikh, M.; Belagraa, L.; Daoudi, A.; Chikouche, M.A. The Combined Effect of the Initial Cure and the Type of Cement on the Natural Carbonation, the Portlandite Content, and Nonevaporable Water in Blended Cement. *Advances in Materials Science and Engineering* **2017**, *2017*, doi:10.1155/2017/5634713.

148. Alonso, C.; Fernandez, L. Dehydration and Rehydration Processes of Cement Paste Exposed to High Temperature Environments. *J Mater Sci* **2004**, *39*, 3015–3024, doi:10.1023/B:JMSC.0000025827.65956.18.
149. Santos, T.A.; De Oliveira Silva, G.A.E.; Ribeiro, D.V. Mineralogical Analysis of Portland Cement Pastes Rehydrated. *Journal of Solid Waste Technology and Management* **2020**, *46*, 15–23, doi:10.5276/JSWTM/2020.15.
150. Habte, L.; Shiferaw, N.; Mulatu, D.; Thenepalli, T.; Chilakala, R.; Whan Ahn, J. Synthesis of Nano-Calcium Oxide from Waste Eggshell by Sol-Gel Method. *Sustainability* **2019**, *11*, 2–10.
151. Zhang, Z.; Scherer, G.W. Evaluation of Drying Methods by Nitrogen Adsorption. *Cem Concr Res* **2019**, *120*, 13–26, doi:10.1016/j.cemconres.2019.02.016.
152. Zhang, Q.; Ye, G. Dehydration Kinetics of Portland Cement Paste at High Temperature. *J Therm Anal Calorim* **2012**, *110*, 153–158, doi:10.1007/s10973-012-2303-9.
153. Lazău, I.; Păcurariu, C.; Ciobanu, C. The Use of Thermal Analysis to Investigate the Effects of Cellulose Ethers on the Portland Cement Hydration. *J Therm Anal Calorim* **2012**, *110*, 103–110, doi:10.1007/s10973-011-2091-7.
154. Ermilova, E.; Kamalova, Z.; Ravil, R. Influence of Clay Mineral Composition on Properties of Blended Portland Cement with Complex Additives of Clays and Carbonates. *IOP Conf Ser Mater Sci Eng* **2020**, *890*, doi:10.1088/1757-899X/890/1/012087.
155. epd-norge *Environmental Product Declaration*; 2024;
156. Zorica, J.; Sinka, M.; Sahmenko, G.; Vitola, L.; Korjakins, A.; Bajare, D. Hemp Biocomposite Boards Using Improved Magnesium Oxychloride Cement. *Energies (Basel)* **2022**, *15*, doi:10.3390/EN15197320.
157. ASTM International Standard Test Method for Sieve Analysis of Fine and Coarse Aggregates. *Annual Book of ASTM Standards* 2011, 5–9.
158. Smadi, E.; Jafarian, M.; Dally, B.; Nathan, G.J. Steam Calcination of Lime for CO2 Capture. *J Environ Chem Eng* **2023**, *11*, 109812, doi:10.1016/J.JECE.2023.109812.
159. Muñoz, I.; Cifrian, E.; Andrés, A.; Miguel, G.S.; Ruiz, D.; Viguri, J.R. Analysis of Environmental Benefits Associated with the Incorporation of Waelz Slag into Fired Bricks Using LCA. *Constr Build Mater* **2018**, *168*, 178–186, doi:10.1016/J.CONBUILDMAT.2018.02.108.
160. Georgiopoulou, M.; Lyberatos, G. Life Cycle Assessment of the Use of Alternative Fuels in Cement Kilns: A Case Study. *J Environ Manage* **2018**, *216*, 224–234, doi:10.1016/J.JENVMAN.2017.07.017.
161. Yüksek, İ.; Öztaş, S.K.; Tahtalı, G. The Evaluation of Fired Clay Brick Production in Terms of Energy Efficiency: A Case Study in Turkey. *Energy Effic* **2020**, *13*, 1473–1483, doi:10.1007/S12053-020-09896-Y/METRICS.
162. Wolde, M.G.; Khatiwada, D.; Bekele, G.; Palm, B. A Life Cycle Assessment of Clinker and Cement Production in Ethiopia. *Cleaner Environmental Systems* **2024**, *13*, 100180, doi:10.1016/J.CESYS.2024.100180.

163. Zhang, X.; Biswas, W.K. Development of Eco-Efficient Bricks – A Life Cycle Assessment Approach. *Journal of Building Engineering* **2021**, *42*, 102429, doi:10.1016/J.JOBE.2021.102429.
164. Galvez-Martos, J.L.; Schoenberger, H. An Analysis of the Use of Life Cycle Assessment for Waste Co-Incineration in Cement Kilns. *Resour Conserv Recycl* **2014**, *86*, 118–131, doi:10.1016/J.RESCONREC.2014.02.009.
165. Gopalraj, S.K.; Deviatkin, I.; Horttanainen, M.; Kärki, T. Life Cycle Assessment of a Thermal Recycling Process as an Alternative to Existing CFRP and GFRP Composite Wastes Management Options. *Polymers 2021, Vol. 13, Page 4430* **2021**, *13*, 4430, doi:10.3390/POLYM13244430.
166. Pedreño-Rojas, M.A.; Fořt, J.; Černý, R.; Rubio-de-Hita, P. Life Cycle Assessment of Natural and Recycled Gypsum Production in the Spanish Context. *J Clean Prod* **2020**, *253*, 120056, doi:10.1016/J.JCLEPRO.2020.120056.
167. Zimele, Z.; Sinka, M.; Bajare, D.; Jakovics, A. Life Cycle Assessment for Masonry Exterior Wall Assemblies Made of Traditional Building Materials. *IOP Conf Ser Mater Sci Eng* **2019**, *660*, doi:10.1088/1757-899X/660/1/012042.
168. Argalis, P.P.; Sinka, M.; Bajare, D. Recycling of Cement–Wood Board Production Waste into a Low-Strength Cementitious Binder. *Recycling* **2022**, *7*, doi:10.3390/recycling7050076.
169. López Turnes, E.; Professor María Teresa Da Cruz Carvalho Professor Ana Mª Méndez Lázaro, A.; Manuel Vaz Velho Barbosa Marques Supervisor, J.; María Teresa Da Cruz Carvalho, P. *A Study on the Relationship between Cement Particle Size Distribution and Strength Development Mining and Geological Engineering Examination Committee*; 2021;
170. Zoz, H.; Jaramillo, D.; Tian, Z.; Trindade, B.; Ren, H.; Chimal-V, O.; Diaz De La Torre, S. *High Performance Cements and Advanced Ordinary Portland Cement Manufacturing by HEM-Refinement and Activation*;
171. Wang, X.Y.; Park, K.B. Analysis of the Compressive Strength Development of Concrete Considering the Interactions between Hydration and Drying. *Cem Concr Res* **2017**, *102*, 1–15, doi:10.1016/J.CEMCONRES.2017.08.010.
172. Shi, Y.; Wang, T.; Li, H.; Wu, S. Exploring the Influence Factors of Early Hydration of Ultrafine Cement. *Materials* **2021**, *14*, 5677, doi:10.3390/MA14195677.
173. Lv, L.; Luo, S.; Šavija, B.; Zhang, H.; Li, L.; Ueda, T.; Xing, F. Effect of Particle Size Distribution on the Pre-Hydration, Hydration Kinetics, and Mechanical Properties of Calcium Sulfoaluminate Cement. *Constr Build Mater* **2023**, *398*, 132497, doi:10.1016/j.conbuildmat.2023.132497.
174. Rajczakowska, M.; Nilsson, L.; Habermehl-Cwirzen, K.; Hedlund, H.; Cwirzen, A. Does a High Amount of Unhydrated Portland Cement Ensure an Effective Autogenous Self-Healing of Mortar? *Materials 2019, Vol. 12, Page 3298* **2019**, *12*, 3298, doi:10.3390/MA12203298.
175. Semugaza, G. Reactivation of Hydrated Cement and Recycled Concrete Powders by Thermal Treatment for Partial Replacement of Virgin Cement. **2024**, doi:10.17185/DUEPUBLICO/81866.

176. Semugaza, G.; Mielke, T.; Castillo, M.E.; Gierth, A.Z.; Tam, J.X.; Nawrath, S.; Lupascu, D.C. Reactivation of Hydrated Cement Powder by Thermal Treatment for Partial Replacement of Ordinary Portland Cement. *Materials and Structures/Materiaux et Constructions* **2023**, *56*, 1–16, doi:10.1617/S11527-023-02133-9/FIGURES/8.
177. Gholizadeh-Vayghan, A.; Meza Hernandez, G.; Kingne, F.K.; Gu, J.; Dilissen, N.; El Kadi, M.; Tysmans, T.; Vleugels, J.; Rahier, H.; Snellings, R. Thermal Reactivation of Hydrated Cement Paste: Properties and Impact on Cement Hydration. *Materials* **2024**, *17*, 2659, doi:10.3390/ma17112659.
178. Shui, Z.; Xuan, D.; Wan, H.; Cao, B. Rehydration Reactivity of Recycled Mortar from Concrete Waste Experienced to Thermal Treatment. *Constr Build Mater* **2008**, *22*, 1723–1729, doi:10.1016/j.conbuildmat.2007.05.012.
179. Serpell, R.; Lopez, M. Reactivated Cementitious Materials from Hydrated Cement Paste Wastes. *Cem Concr Compos* **2013**, *39*, 104–114, doi:10.1016/J.CEMCONCOMP.2013.03.020.
180. Eštoková, A.; Palaščáková, L.; Singovszká, E.; Holub, M. Analysis of the Chromium Concentrations in Cement Materials. *Procedia Eng* **2012**, *42*, 123–130, doi:10.1016/J.PROENG.2012.07.402.
181. Soja, W.; Maraghechi, H.; Georget, F.; Scrivener, K. Changes of Microstructure and Diffusivity in Blended Cement Pastes Exposed to Natural Carbonation. *MATEC Web of Conferences* **2018**, *199*, doi:10.1051/MATECCONF/201819902009.
182. Elvatech Ltd. XRF Analysis of Cement - X-Ray Fluorescence Analysis in Cement Industry Available online: https://elvatech.com/applications/cement/ (accessed on 18 March 2025).
183. Vanoutrive, H.; Van den Heede, P.; Alderete, N.; Andrade, C.; Bansal, T.; Camões, A.; Cizer, Ö.; De Belie, N.; Ducman, V.; Etxeberria, M.; et al. Report of RILEM TC 281-CCC: Outcomes of a Round Robin on the Resistance to Accelerated Carbonation of Portland, Portland-Fly Ash and Blast-Furnace Blended Cements. *Materials and Structures/Materiaux et Constructions* **2022**, *55*, doi:10.1617/S11527-022-01927-7.
184. Jakob, C.; Jansen, D.; Ukrainczyk, N.; Koenders, E.; Pott, U.; Stephan, D.; Neubauer, J. Relating Ettringite Formation and Rheological Changes during the Initial Cement Hydration: A Comparative Study Applying XRD Analysis, Rheological Measurements and Modeling. *Materials* **2019**, *12*, doi:10.3390/MA12182957.
185. Tao, X.; Liu, J.; Wang, M. Effect of Heat-Treatment on Microstructure and Mechanical Properties of Magnesium Phosphate Cement. *Key Eng Mater* **2016**, *680*, 447–450, doi:10.4028/WWW.SCIENTIFIC.NET/KEM.680.447.
186. Pawluczuk, E.; Kalinowska-Wichrowska, K.; Bołtryk, M.; Jiménez, J.R.; Fernández, J.M. The Influence of Heat and Mechanical Treatment of Concrete Rubble on the Properties of Recycled Aggregate Concrete. *Materials 2019, Vol. 12, Page 367* **2019**, *12*, 367, doi:10.3390/MA12030367.

187. Taylor, H.F.W. *Cement Chemistry*; Thomas Telford Publishing, 1997; ISBN 0-7277-3945-X.
188. Scrivener, K.L.; Juilland, P.; Monteiro, P.J.M. Advances in Understanding Hydration of Portland Cement. *Cem Concr Res* **2015**, *78*, 38–56, doi:10.1016/J.CEMCONRES.2015.05.025.
189. Alonso, C.; Fernandez, L. Dehydration and Rehydration Processes of Cement Paste Exposed to High Temperature Environments. *J Mater Sci* **2004**, *39*, 3015–3024, doi:10.1023/B:JMSC.0000025827.65956.18.
190. Moropoulou, A.; Bakolas, A.; Aggelakopoulou, E. The Effects of Limestone Characteristics and Calcination Temperature to the Reactivity of the Quicklime. *Cem Concr Res* **2001**, *31*, 633–639, doi:10.1016/S0008-8846(00)00490-7.
191. Cuberos, A.J.M.; De la Torre, Á.G.; Martín-Sedeño, M.C.; Moreno-Real, L.; Merlini, M.; Ordónez, L.M.; Aranda, M.A.G. Phase Development in Conventional and Active Belite Cement Pastes by Rietveld Analysis and Chemical Constraints. *Cem Concr Res* **2009**, *39*, 833–842, doi:10.1016/J.CEMCONRES.2009.06.017.
192. Kurdowski, W. Cement and Concrete Chemistry. *Cement and Concrete Chemistry* **2014**, *9789400779457*, 1–700, doi:10.1007/978-94-007-7945-7.
193. Bullard, J.W.; Jennings, H.M.; Livingston, R.A.; Nonat, A.; Scherer, G.W.; Schweitzer, J.S.; Scrivener, K.L.; Thomas, J.J. Mechanisms of Cement Hydration. *Cem Concr Res* **2011**, *41*, 1208–1223, doi:10.1016/J.CEMCONRES.2010.09.011.
194. Barnes, P.; Bensted, J. Structure and Performance of Cements. *Structure and Performance of Cements* **2002**, doi:10.1201/9781482295016.
195. Hewlett, P.C. Lea's Chemistry of Cement and Concrete. *Lea's Chemistry of Cement and Concrete* **2003**, 1–1057, doi:10.1016/B978-0-7506-6256-7.X5007-3.
196. Gholizadeh-Vayghan, A.; Meza Hernandez, G.; Kingne, F.K.; Gu, J.; Dilissen, N.; El Kadi, M.; Tysmans, T.; Vleugels, J.; Rahier, H.; Snellings, R. Thermal Reactivation of Hydrated Cement Paste: Properties and Impact on Cement Hydration. *Materials 2024, Vol. 17, Page 2659* **2024**, *17*, 2659, doi:10.3390/MA17112659.
197. Poletto, M.; Zattera, A.J.; Santana, R.M.C. Thermal Decomposition of Wood: Kinetics and Degradation Mechanisms. *Bioresour Technol* **2012**, *126*, 7–12, doi:10.1016/J.BIORTECH.2012.08.133.
198. Brandt, A.M.; Marks, M. Optimization of the Material Structure and Composition of Cement Based Composites. *Cem Concr Compos* **1996**, *18*, 271–279, doi:10.1016/0958-9465(96)00018-2.
199. Scrivener, K.; Snellings, R.; Lothenbach, B. A Practical Guide to Microstructural Analysis of Cementitious Materials / Edited by Karen Scrivener, Ruben Snellings, Barbara Lothenbach. **2016**, 420–442.
200. Kim, H.S.; Kim, S.; Kim, H.J.; Yang, H.S. Thermal Properties of Bio-Flour-Filled Polyolefin Composites with Different Compatibilizing Agent Type and Content. *Thermochim Acta* **2006**, *451*, 181–188, doi:10.1016/J.TCA.2006.09.013.
201. Santhanam, M.; Cohen, M.D.; Olek, J. Sulfate Attack Research - Whither Now? *Cem Concr Res* **2001**, *31*, 845–851, doi:10.1016/S0008-8846(01)00510-5.

202. Shui, Z.; Xuan, D.; Chen, W.; Yu, R.; Zhang, R. Cementitious Characteristics of Hydrated Cement Paste Subjected to Various Dehydration Temperatures. *Constr Build Mater* **2009**, *23*, 531–537, doi:10.1016/J.CONBUILDMAT.2007.10.016.
203. Moropoulou, A.; Bakolas, A.; Aggelakopoulou, E. Evaluation of Pozzolanic Activity of Natural and Artificial Pozzolans by Thermal Analysis. *Thermochim Acta* **2004**, *420*, 135–140, doi:10.1016/J.TCA.2003.11.059.
204. Castellote, M.; Alonso, C.; Andrade, C.; Turrillas, X.; Campo, J. Composition and Microstructural Changes of Cement Pastes upon Heating, as Studied by Neutron Diffraction. *Cem Concr Res* **2004**, *34*, 1633–1644, doi:10.1016/S0008-8846(03)00229-1.
205. REAL, C. Hydration Products in Two Aged Cement Pastes. *J Therm Anal Calorim* **2005**.
206. A Study of Carbonation in Non-Hydraulic Lime Mortars — the University of Bath's Research Portal Available online: https://researchportal.bath.ac.uk/en/studentTheses/a-study-of-carbonation-in-non-hydraulic-lime-mortars (accessed on 22 October 2024).
207. Ji, X.; Ji, D.; Yang, Z.; Wang, G.; Huang, X.; Ma, S.; Li, W. Study on the Phase Composition and Structure of Hardened Cement Paste during Heat Treatment. *Constr Build Mater* **2021**, *310*, 125267, doi:10.1016/J.CONBUILDMAT.2021.125267.
208. Guzhan, O.˘; Glu, Ç.˘ Revealing the Dark Side of Portlandite Clusters in Cement Paste by Circular Polarization Microscopy. *Materials 2016, Vol. 9, Page 176* **2016**, *9*, 176, doi:10.3390/MA9030176.
209. Tosun, K. Effect of SO3 Content and Fineness on the Rate of Delayed Ettringite Formation in Heat Cured Portland Cement Mortars. *Cem Concr Compos* **2006**, *28*, 761–772, doi:10.1016/J.CEMCONCOMP.2006.06.003.
210. Tran, T.T.; Kwon, H.M. Influence of Activator Na2O Concentration on Residual Strengths of Alkali-Activated Slag Mortar upon Exposure to Elevated Temperatures. *Materials 2018, Vol. 11, Page 1296* **2018**, *11*, 1296, doi:10.3390/MA11081296.
211. Thiery, M.; Villain, G.; Dangla, P.; Platret, G. Investigation of the Carbonation Front Shape on Cementitious Materials: Effects of the Chemical Kinetics. *Cem Concr Res* **2007**, *37*, 1047–1058, doi:10.1016/J.CEMCONRES.2007.04.002.
212. Alarcon-Ruiz, L.; Platret, G.; Massieu, E.; Ehrlacher, A. The Use of Thermal Analysis in Assessing the Effect of Temperature on a Cement Paste. *Cem Concr Res* **2005**, *35*, 609–613, doi:10.1016/J.CEMCONRES.2004.06.015.
213. Moropoulou, A.; Bakolas, A.; Aggelakopoulou, E. The Effects of Limestone Characteristics and Calcination Temperature to the Reactivity of the Quicklime. *Cem Concr Res* **2001**, *31*, 633–639, doi:10.1016/S0008-8846(00)00490-7.
214. Ghosh, S.N.; Rao, P.B.; Paul, A.K.; Raina, K. The Chemistry of Dicalcium Silicate Mineral. *J Mater Sci* **1979**, *14*, 1554–1566, doi:10.1007/BF00569274/METRICS.
215. Jelenić, I.; Bezjak, A.; Bujan, M. Hydration of B2O3-Stabilized A′-and β-Modifications of Dicalcium Silicate. *Cem Concr Res* **1978**, *8*, 173–180, doi:10.1016/0008-8846(78)90006-6.

216. Rikoto II; Nuhu *Effect of Free Lime and Lime Saturation Factor on Grindability of Cement Clinker*; Vol. 7;.
217. Cruz, T.A.M. da; Henrique Geraldo, R.; Damasceno Costa, A.R.; Rândello Dantas Maciel, K.; Pereira Gonçalves, J.; Camarini, G. Microstructural and Mineralogical Compositions of Metakaolin-Lime-Recycled Gypsum Plaster Ternary Systems. *Journal of Building Engineering* **2022**, *47*, 103770, doi:10.1016/J.JOBE.2021.103770.
218. Xuan, D.; Molenaar, A.A.A.; Houben, L.J.M. Compressive and Indirect Tensile Strengths of Cement-Treated Mix Granulates with Recycled Masonry and Concrete Aggregates. *Journal of Materials in Civil Engineering* **2012**, *24*, 577–585, doi:10.1061/(ASCE)MT.1943-5533.0000401.
219. Sahmenko, G.; Sinka, M.; Namsone, E.; Korjakins, A.; Bajare, D. Sustainable Wall Solutions Using Foam Concrete and Hemp Composites. *Environmental and Climate Technologies* **2021**, *25*, 917–930, doi:10.2478/rtuect-2021-0069.
220. Bumanis, G.; Bajare, D. PCM Modified Gypsum Hempcrete with Increased Heat Capacity for Nearly Zero Energy Buildings. *Environmental and Climate Technologies* **2022**, *26*, 524–534, doi:10.2478/rtuect-2022-0040.
221. Bumanis, G.; Irbe, I.; Sinka, M.; Bajare, D. Biodeterioration of Sustainable Hemp Shive Biocomposite Based on Gypsum and Phosphogypsum. *Journal of Natural Fibers* **2022**, *19*, 10550–10563, doi:10.1080/15440478.2021.1997871.
222. Sinka, M.; Korjakins, A. Hemp Concrete Composite Panel, Its Environmental Impact 2019.
223. Walker, R.; Pavia, S.; Mitchell, R. Mechanical Properties and Durability of Hemp-Lime Concretes. *Constr Build Mater* **2014**, *61*, 340–348, doi:10.1016/j.conbuildmat.2014.02.065.
224. Dıker, B.; Yazicioğlu, F. A Research on Straw Bale and Traditional External Wall Systems: Energy and Cost-Efficiency Analysis. *A/Z ITU Journal of the Faculty of Architecture* **2020**, *17*, 95–103, doi:10.5505/itujfa.2019.65882.
225. Mehravar, M.; Veshkini, A.; Veiseh, S.; Fayaz, R. Physical Properties of Straw Bale and Its Effect on Building Energy Conservation and Carbon Emissions in Different Climatic Regions of Iran. *Energy Build* **2022**, *254*, 111559, doi:10.1016/J.ENBUILD.2021.111559.
226. Segovia, F.; Blanchet, P.; Auclair, N.; Essoua, G.G.E. Thermo-Mechanical Properties of a Wood Fiber Insulation Board Using a Bio-Based Adhesive as a Binder. *Buildings* **2020**, *10*, 1–15, doi:10.3390/BUILDINGS10090152.
227. Khabbazi, A.; Garoum, M.; Terhmina, O. Experimental Study of Thermal and Mechanical Properties of a New Insulating Material Based on Cork and Cement Mortar Available online: https://www.researchgate.net/publication/279591550_Experimental_study_of_thermal_and_mechanical_properties_of_a_new_insulating_material_based_on_cork_and_cement_mortar (accessed on 21 March 2023).
228. Collet, F.; Pretot, S. Thermal Conductivity of Hemp Concretes: Variation with Formulation, Density and Water Content. *Constr Build Mater* **2014**, *65*, 612–619, doi:10.1016/J.CONBUILDMAT.2014.05.039.

229. Gurunathan, T.; Mohanty, S.; Nayak, S.K. A Review of the Recent Developments in Biocomposites Based on Natural Fibres and Their Application Perspectives. *Compos Part A Appl Sci Manuf* **2015**, *77*, 1–25, doi:10.1016/J.COMPOSITESA.2015.06.007.
230. Ardanuy, M.; Claramunt, J.; Toledo Filho, R.D. Cellulosic Fiber Reinforced Cement-Based Composites: A Review of Recent Research. *Constr Build Mater* **2015**, *79*, 115–128, doi:10.1016/J.CONBUILDMAT.2015.01.035.
231. Kosiachevskyi, D.; Abahri, K.; Chaouche, M.; Prat, E.; Daubresse, A.; Bousquet, C. Risk Assessment of Mold Growth in Hemp Concrete. In Proceedings of the SynerCrete'18: Interdisciplinary Approaches for Cement-based Materials and Structural Concrete; SynerCrete'18: Funchal, Madeira Island, October 2018.
232. Collet, F.; Prétot, S.; Lanos, C. Hemp-Straw Composites: Thermal and Hygric Performances. *Energy Procedia* **2017**, *139*, 294–300, doi:10.1016/j.egypro.2017.11.211.
233. Brzyski, P.; Gładecki, M.; Rumińska, M.; Pietrak, K.; Kubiś, M.; Łapka, P. Influence of Hemp Shives Size on Hygro-Thermal and Mechanical Properties of a Hemp-Lime Composite. *Materials* **2020**, *13*, 1–17, doi:10.3390/MA13235383.
234. Abdellatef, Y.; Khan, M.A.; Khan, A.; Alam, M.I.; Kavgic, M. Mechanical, Thermal, and Moisture Buffering Properties of Novel Insulating Hemp-Lime Composite Building Materials. *Materials 2020, Vol. 13, Page 5000* **2020**, *13*, 5000, doi:10.3390/MA13215000.
235. Bumanis, G.; Sinka, M.; Irbe, I.; Bajare, D. *Physical, Mechanical and Biodeterioration Properties of Hempcrete Based on Gypsum and Phosphogypsum*;
236. Arnaud, L.; Gourlay, E. Experimental Study of Parameters Influencing Mechanical Properties of Hemp Concretes. *Constr Build Mater* **2012**, *28*, 50–56, doi:10.1016/J.CONBUILDMAT.2011.07.052.
237. Benfratello, S.; Capitano, C.; Peri, G.; Rizzo, G.; Scaccianoce, G.; Sorrentino, G. Thermal and Structural Properties of a Hemp–Lime Biocomposite. *Constr Build Mater* **2013**, *48*, 745–754, doi:10.1016/J.CONBUILDMAT.2013.07.096.
238. Diquélou, Y.; Gourlay, E.; Arnaud, L.; Kurek, B. Impact of Hemp Shiv on Cement Setting and Hardening: Influence of the Extracted Components from the Aggregates and Study of the Interfaces with the Inorganic Matrix. *Cem Concr Compos* **2015**, *55*, 112–121, doi:10.1016/J.CEMCONCOMP.2014.09.004.
239. Tefa, L.; Coppola, B.; Palmero, P.; Bassani, M. Mechanical Properties, Life-Cycle Assessment, and Costs of Alternative Sustainable Binders to Stabilise Recycled Aggregates. *Cleaner Materials* **2025**, *15*, 100302, doi:10.1016/J.CLEMA.2025.100302.
240. Sinka, M.; Van den Heede, P.; De Belie, N.; Bajare, D.; Sahmenko, G.; Korjakins, A. Comparative Life Cycle Assessment of Magnesium Binders as an Alternative for Hemp Concrete. *Resour Conserv Recycl* **2018**, *133*, 288–299, doi:10.1016/J.RESCONREC.2018.02.024.
241. Arrigoni, A.; Pelosato, R.; Melià, P.; Ruggieri, G.; Sabbadini, S.; Dotelli, G. Life Cycle Assessment of Natural Building Materials: The Role of Carbonation,

Mixture Components and Transport in the Environmental Impacts of Hempcrete Blocks. *J Clean Prod* **2017**, *149*, 1051–1061, doi:10.1016/j.jclepro.2017.02.161.

242. Bajare, D.; Puzule, L.; Sinka, M.; Tambovceva, T.; Bumanis, G. Life Cycle Assessment of the Lightweight Timber Structures with Bio-Based Aggregate Composites. *Lecture Notes in Civil Engineering* **2024**, *489 LNCE*, 582–591, doi:10.1007/978-3-031-57800-7_54/FIGURES/4.
243. Sinka, M.; Zorica, J.; Bajare, D.; Sahmenko, G.; Korjakins, A. Fast Setting Binders for Application in 3d Printing of Bio-Based Building Materials. *Sustainability (Switzerland)* **2020**, *12*, 1–12, doi:10.3390/SU12218838.
244. Hafner, A.; Özdemir, Ö. Comparative LCA Study of Wood and Mineral Non-Residential Buildings in Germany and Related Substitution Potential. *European Journal of Wood and Wood Products* **2023**, *81*, 251–266, doi:10.1007/S00107-022-01888-2/FIGURES/8.
245. Souza, E. What Is the Environmental Impact of Each Building Material? | ArchDaily 2022.

Pauls Pāvils Ārgalis was born in 1996 in Riga. He obtained a Bachelor of Engineering in Materials Science in 2018 and a Master of Engineering in Materials Science in 2021 from Riga Technical University. He has been working at Riga Technical University since 2020, initially as a scientific assistant in the Institute of General Chemical Engineering at the Faculty of Materials Science and Applied Chemistry, and currently as a researcher in the Institute of Sustainable Building Materials and Engineering Systems at the Faculty of Civil and Mechanical Engineering. He has worked as a project assistant in "KV Consulting" in the fields of GHG emission calculations and optimisation of biomethane production facilities. His scientific interests are related to the reactivation of cement binder, sustainable building material production and circular manufacturing.